(12) **LEVEL** Ⅲ

11

CHARACTERIZATION AND ANALYSIS OF INDIUM—DOPED SILICON EXTRINSIC DETECTOR MATERIAL

J. Baukus
Hughes Research Laboratories
3011 Malibu Canyon Road
Malibu, CA 90265

T. McGill
California Institute of Technology
Pasadena, CA 91125

June 1980

70

DAAK—77—C—0082

Final Technical Report

For period 31 March 1977 through 30 September 1979

DTIC
S ELECTE D
MAR 4 1981
B

81 3 3 052

SECURITY CLASSIFICATION OF THIS PAGE (When Data Entered)

REPORT DOCUMENTATION PAGE	READ INSTRUCTIONS BEFORE COMPLETING FORM

1. REPORT NUMBER	2. GOVT ACCESSION NO. AD-A095982	3. RECIPIENT'S CATALOG NUMBER

| 4. TITLE (and Subtitle) CHARACTERIZATION AND ANALYSIS OF INDIUM-DOPED SILICON EXTRINSIC DETECTOR MATERIAL. | 5. TYPE OF REPORT & PERIOD COVERED Final Report 31 Mar 1977 — 30 Sept 1979 |
| | 6. PERFORMING ORG. REPORT NUMBER |

| 7. AUTHOR(s) James Baukus and T. McGill | 8. CONTRACT OR GRANT NUMBER(s) DAAK70-77-C-0082, ARPA Order 3211 |

| 9. PERFORMING ORGANIZATION NAME AND ADDRESS Hughes Research Laboratories 3011 Malibu Canyon Road Malibu, CA 90265 | 10. PROGRAM ELEMENT, PROJECT, TASK AREA & WORK UNIT NUMBERS 145 |

| 11. CONTROLLING OFFICE NAME AND ADDRESS Defense Advanced Research Projects Agency Arlington, VA 22200 | 12. REPORT DATE June 1980 |
| | 13. NUMBER OF PAGES 144 |

| 14. MONITORING AGENCY NAME & ADDRESS(if different from Controlling Office) Philip R. Boyd Attn: DRSEL-NV-FIR Night Vision Laboratory Ft. Belvoir, VA 22060 | 15. SECURITY CLASS. (of this report) UNCLASSIFIED |
| | 15a. DECLASSIFICATION DOWNGRADING SCHEDULE |

16. DISTRIBUTION STATEMENT (of this Report)

Approved for public release; distribution unlimited.

17. DISTRIBUTION STATEMENT (of the abstract entered in Block 20, if different from Report)

18. SUPPLEMENTARY NOTES

19. KEY WORDS (Continue on reverse side if necessary and identify by block number)

Extrinsic silicon, Infrared detectors, SIMDEC program, Photoluminescence, Excitons, IR, Capture cross section

20. ABSTRACT (Continue on reverse side if necessary and identify by block number)

This final report of a two-year program describes progress made in analyzing Si:In detector material. Hall-effect, photoluminscence, and IR measurements were performed to characterize the X level and to determine its nature.

DD FORM 1 JAN 73 1473 EDITION OF 1 NOV 65 IS OBSOLETE

172600

JOB

TABLE OF CONTENTS

LIST OF ILLUSTRATIONS

LIST OF TABLES

7

SECTION 1

INTRODUCTION AND SUMMARY

The objective of the silicon indium material and detector
characterization (SIMDEC) program conducted by Hughes Research Labora-
tories (HRL) under contract DAAK70-77-C-0082 was to investigate the
nature of defects in indium-doped silicon detector material and to
develop techniques for the control of quality in the growth of extrinsic
and high-purity undoped silicon for IR detector monolithic chips. This,
the final report, was preceeded by three interim reports.[1,2,3] HRL was
the prime contractor for this program, with the California Institute of
Technology (CIT) and the University of California at Davis (UCD) as
subcontractors.

The discovery at Hughes[4] of a second, shallower acceptor level in
indium-doped silicon (Si:In), the so-called X level, demonstrated the
need for further research on Si:In. The X level has been observed in
measurements of Hall effect versus temperature and of IR photoconduc-
tivity[4,5,6] and absorption.[7] It is undesirable in extrinsic Si:In
photoconductors because its shallower energy level results in excess
thermally ionized carriers. These lower the maximum temerature at which
background-limited detectivities can be obtained. This can reduce the
operating temperature by as much as 10°K with a corresponding increase
in cooling power requirements.

The X level has an ionization energy of 0.11 eV and has a concen-
tration that increases as the concentration of the indium increases.
Different growth conditions can produce drastically different amounts
of X level in comparably indium doped material samples. These facts
indicate that the X level is likely to be a complex of indium and some
other crystalline defect or impurity. However, the exact physical nature
of the X level was unknown at the beginning of the program, as were the
growth and processing factors that determine its concentration. The pur-
pose, then, of the SIMDEC program has been to apply the appropriate
physical measurements to Si:In to identify the nature of the X level and
means of controlling it.

Numerous accomplishments were made during the SIMDEC program. The
major goal, the identification of the nature of the X level in Si:In,
was achieved. The structure and constituents of the X level were first
discovered at HRL.[8] This discovery was due in large part to the inter-
action with CIT. New knowledge of the energy structure of dopants in
silicon was obtained through photoluminescence studies at CIT. Finally,
several new research directions are indicated as a result of the SIMDEC
program.

The most significant result during this program was the discovery
of the nature of the X level in Si:In. The X level was found to be an
indium-carbon nearest-neighbor pair. This model was established on
the basis of X-level and In data (taken by Hall-effect measurements)
and carbon data (from IR transmission studies). The X-level concentra-
tion observed as a function of anneal temperature for Czochralski (Czo)
crystals is consistent with the mass-action law and yields a reasonable
In-C pair binding energy, as first observed and reported by our group.[8]

Photoluminescence (PL) experiments at CIT have yielded new informa-
tion about extrinsic silicon. The ground- and excited-state bound-
exciton spectra of deep acceptors in silicon have been identified. The
exciton capture cross sections and their temperature dependence for In-,
B-, and P-doped silicon have been determined. The splitting of the In
ground state due to Jahn-Teller distortion was discovered and quantified.
Extra PL lines in Si:In, some of which are very long-lived, were seen,
as was evidence for an exciton transfer mechanism.

The studies conducted under SIMDEC have raised some new questions
about defect complexes and diffusion mechanisms. The X level is a com-
plex. In addition, PL lines were observed which have tentatively been
attributed to In-B complexes. Thus, we have developed new techniques to
observe complexes that can be used to aid in the study of their effects
on device properties.

One very surprising result was the difference in anneal temperature
dependence between samples from floating zone (FZ) and Czo crystals. This
effect, discussed in Section 2, appears to be due to a difference in
diffusion mechanisms between the crystals. Although these results need

further study and verification, the implication of an unexpected, enhanced diffusion process in Czo silicon for future-generation sub-micrometer devices could be quite serious.

The HRL contribution to this program is summarized in Section 2. Twelve crystals were grown exclusively for this program, and 63 Hall-effect analyses and 24 IR spectra were reported on this material. Each Hall-effect analysis consists of an experimental run versus temperature, which takes 8 to 10 hr, several nonlinear curve fitting analyses, and interpretation of the results. In addition, the analyses of data from scores of other Hughes crystals were used to aid in the SIMDEC investigations. A list of Hughes publications directly related to this program is also included in Section 2.

Section 3 presents the major results obtained at CIT for the SIMDEC program, the conclusions drawn from the excitation transfer mechanism study, and a list of CIT publications that resulted from this program. Two recent CIT publications are included as appendices to this report.

As is the case for all experimental techniques, the PL method has advantages and disadvantages. The method requires virtually no sample preparation; a suitably s d piece of material is mounted on the cold finger of the dewar. Thus, results are not clouded by possible effects of device processing on material properties.

The technique is extremely sensitive; very small concentrations of impurities can be detected, and highly accurate energy determinations are possible since this is a spectroscopic technique. However, a large number of spectral lines result from the measurement, and the assignment of lines to specific transitions is not always a simple matter. The method is not absolute and a calibration for determining concentrations from observed line strength must be established.

A unique problem with the PL technique was discovered during this program. This is the quenching of the PL from a shallow acceptor (e.g., B) by a sufficiently large concentration of a deeper impurity (e.g., In); this problem is discussed in more detail in Section 3. Although this effect would not generally be of concern, it interfered with our study of the X level in Si:In.

11

In summary, PL is a sensitive, accurate method of determining semi-conductor impurity concentrations and one requiring almost no sample preparation. The technique is not yet suitable for routine evaluations by semiconductor device manufacturers since it requires cryogenic cooling of the samples and the development of standards and spectral interpretation techniques. However, with the evolution of cryogenic and computer-related technologies, these aspects of the PL method can be automated and this technique can be used for semiconductor processing evaluations.

Another semiconductor characterization technique studied under this contract was the application of the MOSFET device structure to measure the emission rates, capture cross sections, and ionization energies of In and X-level impurities in silicon. The technique involves fabricating a MOS structure and measuring transient responses to substrate bias pulses at cryogenic temperatures.

The method involves considerable sample preparation, and the electric field in the device is large and nonuniform. These conditions made interpretation of the measurements difficult. Large corrections for the Poole-Frenkel effect must be applied because of the high field in the device. To determine material parameters from the results requires carrier concentration data at the measurement temperatures. These data are obtained from Hall-effect measurements on companion samples that have undergone much more benign processing and are measured under low-field conditions. Thus, there is some question as to the compatibility of the results of these two techniques. Observations of the X level by the MOSFET method are based on relatively small transients which must be separated from the large In-related transients.

For these reasons, work on this technique was not continued into the second year of this program. A complete report on the MOSFET technique, which was written by Prof. Leonard Forbes, is included as Appendix C.

12

SECTION 2

CRYSTAL GROWTH AND CHARACTERIZATION

This section describes HRL's contribution to the program. Twelve crystals were grown exclusively for the SIMDeC program. Samples from these and many other crystals were provided to the subcontractors for their studies. All crystals were carefully analyzed using Hall-effect versus temperature measurements and/or IR spectroscopy. In all, 63 Hall analyses and 24 IR measurements were reported during this program. In addition, the analyses of data from scores of crystals grown for other programs as well as for HRL IR&D studies were used to aid in the investigations undertaken for SIMDEC.

The characterization of crystals by Hall effect involved fabricating samples from each crystal, measuring the Hall coefficient and resistivity as a function of temperature using computer-controlled equipment, and analyzing the data using a nonlinear least-squares computer curve-fitting procedure. The interstitial oxygen and substitutional carbon contents of the crystals were determined from IR transmission spectra. These spectra were obtained using the double-beam technique with a high-purity vacuum FZ sample as a reference. The samples were measured at liquid-nitrogen temperature. The reflectivities as well as the individual thicknesses of the reference and sample were accounted for in the impurity concentration calculations.

These analyses as well as anneal studies of the indium-doped crystals provided the data base for the indium-carbon nearest-neighbor pair model of the X level. The interaction with CIT was instrumental in developing this interpretation.

A. CRYSTAL GROWTH

1. HRL and IPD Growth Facilities

In all the Czo crystal growth done for the program, two HRL NRC Czo pullers were used. These machines are essentially standard manufacturing growers that have been outdated for commercial use because

13

the melt mass is limited (1 kg for one of them, 1.5 kg for the other). The 2-in.-diameter crystals nearly fill the aperture of the 3-in.-diameter crucible. This situation may significantly influence the axial distribution of volatile impurities in the crystals.

Under other programs, we have determined that Si:In crystals grown in the IPD Varian Model 2848A puller have significantly lower X-level concentrations than those grown in the NRC machines. The Varian grower is a modern, large-capacity machine that can accommodate either a 6- or an 8-kg melt. Either 6- or 8-in. o.d. crucibles can be used with it; obviously, there is much more free melt surface when a 2-in. crystal is grown in this grower rather than in the NRC machine.

We have also developed procedures for the FZ growth of 2-in. Si:In in an Ecco gas zoner. Crystals made by this procedure were studied on the SIMDEC program.

2. Expected Dopant Distribution in the HRL and IPD Pullers

The uniformity of the nonvolatile dopants between 2-in.-diameter crystals grown from 3-in.-diameter (NRC) and 6-in.-diameter (Varian) crucibles was expected to be drastically different because of the difference in the convection flow. The spreading resistance measurements on In-doped crystals showed, however, that the Varian-grown crystal was only slightly more uniform than the NRC; the forced convections caused by crystal and crucible rotation isolated the freezing interface, making it less sensitive to the fluctuations in the bulk convection flows. The radial uniformity of the Czo-grown crystals was generally very good.

The axial uniformity of the nonvolatile dopants was better for the Varian-grown crystal because of the larger melt volume. The axial dopant distribution can be altered by adjusting the growth parameters to achieve the optimum uniformity.

3. Growth and Analysis of SIMDEC Crystals

Twelve crystals were grown exclusively for the SIMDEC program. Growth conditions for these crystals are summarized in Table 1.

Three Si:Al and one Si:In ingot were grown at HRL early in the SIMDEC program. Hall-effect measurements were made on samples from slices adjacent to those sent to CIT and UCD. The results of the analyses are given in Tables 2 and 3. The values represent the best fit to the data of several trials using various numbers of acceptor levels and various random starting vectors. The degeneracy, g, was an adjustable parameter and not fixed at 4.

The results for the Si:Al ingots (Table 2) include the aluminum concentration, the concentration of a second acceptor level if observed, and that of the compensation level. This last value refers to the net donor level (the concentration of donors minus that of all shallow acceptors). The principal shallow acceptor is boron, and the usual interpretation is $N_{comp} = N_D - N_B$. Essentially, however, if the second acceptor level is actually boron, then N_{comp} is equal to N_D. Also included in the table are the activation energies of the acceptor levels and the rms percent error of the fit to the data.

Ingot C040Al was quite lightly doped. A second acceptor level was apparently present, as partly evidenced by the rather high error. But attempts to fit the data by including a second level were inconclusive.

A second, more heavily doped, Czo ingot showed a second acceptor level in the high 10^{14} concentration region. The energy level (about 50 meV) is midway between that of boron and that of the X level reported by Scott.[7] The concentration of this level was sufficiently below the donor level that its value and energy level could not be accurately determined.

15

Table 1. SIMDEC Crystal Growth Conditions

Crystal	Dopant	Initial Melt Concentration, cm^{-3}	Growth Rate, in./hr	Rotation, rpm		Atmosphere
				Seed	Crucible	
C040	Al	2.5×10^{17}	1.6	18	7	He
C041	Al	5.0×10^{18}	1.6	18	7	He
C042	In	6.3×10^{18}	1.6	18	7	He
Z047	Al	9.9×10^{19}	——	—	—	Ar
C055	In	2.8×10^{20}	1.6	18	8	Ar
C076	In	2.9×10^{20}	1.7	13	8	Ar
C078	None	—	1.6	20	8	Ar
C086	In	3.1×10^{20}	1.8	20	·5	Ar
F001	None	—	2.4	12	12	Ar
C112	In B	4.0×10^{20}	1.0	6	7	He
C117	In B	3.9×10^{19} 2.1×10^{18}	1.0	16	8	Ar
Z163	In B	2.0×10^{16} 2.8×10^{13}	——	—	—	Ar

Table 2. Hall-Effect Analyses of SIMDEC Si:Al Material

Parameter (units)	C040 Al	C041 Al			Z047 Al	
	Slice 4	Slice 1	Slice 4	Slice 4A	Seed	Tang
N_{Al} (cm^{-3})	1.4×10^{14}	1.34×10^{16}	1.35×10^{16}	7.41×10^{15}	4.85×10^{14}	9.66×10^{14}
N_2 (cm^{-3})	2.5×10^{13}	6.23×10^{14}	9.41×10^{14}		1.32×10^{14}	6.071×10^{13}
N_{comp} (cm^{-3})		1.18×10^{15}	1.80×10^{15}	5.56×10^{15}	5.56×10^{13}	6.104×10^{13}
ΔE_A (eV)	0.0707	0.0706	0.0706	0.0684	0.0692[a]	0.0704
ΔE_2 (eV)		0.0500	0.0514		0.0465	0.0472
RMS error (%)	5.0	0.32	1.04	1.22	1.24	1.86

[a]This value was held constant during the analysis.

5998

17

Table 3. Hall Analyses of SIMDEC Si:In Material C042IN

Parameter (units)	Slice S	Slice T	Slice TA
N_{In} (cm^{-3})	1.9×10^{15}	2.3×10^{15}	2.0×10^{15}
N_x (cm^{-3})	2.9×10^{13}	3.2×10^{13}	7.4×10^{13}
N_{comp} (cm^{-3})	6.7×10^{13}	6.7×10^{13}	7.8×10^{13}
ΔE_{In} (eV)	0.1572^a	0.1623	0.1623
ΔE_x (eV)	0.1244	0.1216	0.1237
RMS error (%)	0.66	0.91	0.62

[a] This value was held constant during the analysis.

The donor concentration in this crystal was considerably higher than would be predicted from the growth conditions; the sample was subsequently given an additional anneal at 650°C for 4 hr to reduce oxygen donors. The results of Hall-effect measurements made after this anneal are listed in Table 2 as slice 4A. The aluminum acceptor concentration decreased and the donor concentration increased. Thus, the second acceptor level could not be observed. A further anneal of 850°C for 1 hr changed the sample to n-type. This increase in donors with annealing is due to the formation of an aluminum-oxygen complex.[9]

An FZ Si:Al ingot, Z047Al, was also grown for this program to determine if a correlation exists between X-level concentration and growth conditions. The results from samples from seed and tang of this ingot are given in Table 2. A second level, which appears to be boron, is evident. However, this concentration of boron is much higher than would be expected from the growth conditions.

Thus, the existence of an X level in Si:Al cannot be confirmed or disproven. A second, shallower acceptor level can be seen; however, its concentration is sufficiently low that its energy level cannot be determined with confidence. Specifically, it cannot be conclusively shown that the level is not boron.

18

A lightly doped Czo Si:In ingot, C042In, was also grown for this program. Results of Hall evaluations of slices immediately adjacent to the seed and tang sides of the slices sent to CIT and UCD are shown in Table 3. The relatively low value of indium, which was desired for the CIT and UCD experiments, results in a value of X-level concentration that is barely discernible in the Hall-effect measurements. The sample labeled TA is sample T after it was further annealed at 850°C for 1 hr. For more heavily doped samples, this anneal generally reduces the X-level concentration. However, for this lightly doped sample, it is not clear whether there is an increase in X level or whether this is an artifact of the analysis technique.

Ingot C076 was grown in a 1-kg system as part of the SIMDEC program to produce a very lightly counterdoped crystal with a low boron concentration. The principal sources of boron in Czo-grown silicon are the starting polycrystalline silicon and the quartz crucible, which dissolves slowly in the melt during growth and releases its boron impurity. Low-boron starting material was used, and the growth was from a Suprasil-lined crucible. This type of container was used because Suprasil has a significantly lower boron content than does regular quartz, which is typically used for crucibles. Since B cannot be removed from Si during the growth process to any significant extent, care must be taken to minimize its introduction during growth. Although Suprasil has a higher dissolution rate into Si, the B buildup in the melt is considerably slower than for regular quartz. This results in a crystal with lower B concentration.

Since P must be added to compensate for the B, crystals grown with this type of crucible require less P to be added to ensure that $N_P > N_B$ throughout the ingot. Therefore, they will have a lower net compensation and a correspondingly higher detector responsivity. Since the values of N_P and N_B are lower, their difference can also be kept smaller.

No P was intentionally added during the growth of crystal C076. The major sources of P were the silicon starting material, which had an initial P concentration of 8×10^{12} cm^{-3}, and the crucible. Phosphorus tends to build up in the melt (and the crystal) during growth because

19

its segregation coefficient is less than one. The rate of this buildup is reduced by the evaporation of P from the melt under the low-pressure condition of the crystal growth. The overall result under these conditions is a net increase in B relative to P in the crystal from seed to tang due to the rate of B buildup from crucible dissolution.

Table 4 lists the results of Hall-effect versus temperature measurements on three samples from ingot C076. The samples labeled "A" are from the seed end of the crystal. The "M" sample is from about midway between the seed and tang. All samples are from the center of the wafer from which they were cut. Sample A20 received a 650°C anneal for 30 min to reduce the oxygen donor content. Samples A30 and M30 received an 850°C anneal for 60 min, which we have found reduces the X-level concentration and the oxygen-donor concentration.

The 850°C anneal reduced the X level, as can be seen by comparing samples A20 and A30. Samples A20 and A30, which were adjacent, differ by an order of magnitude in net compensation, $N_D - N_B$. This is apparently due to slight fluctuations in an extremely close balance between the P and B concentrations. Both B and P increased in concentration toward the center, axially, *of the ingot; B increased more rapidly*, as expected.

Table 4. Dopant Concentrations in Crystal C076IN

	A20	A30	M30
N_{In}, 10^{17} cm^{-3}	1.4	1.3	1.8
N_X, 10^{13} cm^{-3}	62-170	5.7	45
N_B, 10^{13} cm^{-3}			15
N_D, 10^{13} cm^{-3}			5.3
$N_D - N_B$, 10^{13} cm^{-3}	0.18	1.4	

6303

An analysis of the pickup of B and P in crystal C076 was made using a model developed by H. Kimura.[10] The dopant concentrations measured on the Hall samples were used as boundary conditions, and initial values of B and P in the melt were calculated to be 1.7×10^{14} B/cm^3 and 8×10^{14} P/cm^3. This amount of B far exceeds the amount possible due to crucible dissolution. However, it corresponds to 0.6 ppm in the indium material used for doping. This is within the manufacturer's specification for purity of 6-9's indium. Other Si:In crystals doped with this material were also doped with P and were grown in regular quartz crucibles; as a result, this amount of B pickup would not be observed.

Crystal C055 was an experiment to simulate, using a small (1 kg) grower at HRL, growth of Si:In cyrstals in the large crystal grower at IPD. The same polysilicon starting material and In and P dopant materials were used, and the gas overpressure and the pull and rotation rates were the same. The ratio of crystal diameter to crucible diameter was also identical. The object of this simulation was to determine if any of these growth parameters influenced the X level. The results of Hall-effect measurements of samples from the center of the seed end of this ingot are presented in Table 5. Sample A30 had a 650°C anneal for 30 min, and sample A40 had an 850°C anneal for 1 hr. The ingot has a rather high X-level concentration, one similar to the levels observed in crystals grown under the normal conditions for this machine. Since this crystal was grown under the same conditions as crystals at IPD that consistently exhibit X-level concentrations at or below 10^{14} cm^{-3}, it is unlikely that these growth parameters are influencing the X level.

The data for the next five crystals grown for this program are listed in Table 6, which also includes the IR spectroscopic results (which are discussed later).

Crystal C078, grown by the Czo method, was undoped. It was grown to determine if the C was introduced by the In dopant charge. Since no dopant was added in this growth, the amount of B and P picked up from this Suprasil-lined crucible could also be determined.

21

Table 5. Hall-Effect Results for the Seed End of Crystal CO55IN

Concentration	A30	A40
N_{IN}, 10^{17} cm^{-3}	1.6	1.8
N_X, 10^{14} cm^{-3}	30	5.8
$N_D - N_B$, 10^{14} cm^{-3}	2.7	2.4

6303

The crystal had a C concentration slightly above 10^{17} cm^{-3}, which ranked it with the more heavily C-contaminated crystals. Thus, the In charge was clearly not the source of the carbon associated with the X level in Si:In. The Hall results indicated P at 8.3×10^{13} cm^{-3} at the tang. The p-type compensation, presumably B, rose slightly from 5.0 to 5.4×10^{13} cm^{-3} from seed to tang. This increase corresponds to 3.3 ppb of B in the crucible. This is a rather low value, but within the lot-to-lot variation observed for the Suprasil crucible material.

An attempt was made to minimize C contamination from the grower components and dopant charge in crystal CO86. Before growth was initiated, the heater radiation shields, Suprasil-lined crucible, and crucible holder components were baked out under vacuum to remove any volatile contaminants. The In dopant charge was separately vacuum baked and then recleaned, as was the crucible.

The resulting ingot was lower in X level than were other comparably doped Si:In crystals grown in the small (1 kg) pullers, but it was still substantially higher than were crystals from the large (3 kg) grower. These experiments point very clearly to the graphite heater, radiation shields, and crucible holder as sources of the carbon. The definitive experiment would be to grow a Si:In crystal in a small grower with no graphite components. We attempted to procure tungsten components for use in our system, but the vendor was not willing to supply parts adapted to our grower.

22

Table 6. Results of Hall-Effect and IR Absorption
Measurements of SIMDEC-Related Crystals

Ingot	Position	N_{In}, cm^{-3}	N_X, cm^{-3}	N_B, cm^{-3}	N_D, cm^{-3}	α_{In}, cm^{-1}	σ_{In}, x 10^{-17} cm^2	N_O, cm^{-3}	N_C, cm^{-3}
C008	TANG	2.6×10^{17}	3.2×10^{15}	—	5.7×10^{19}	—	—	1.4×10^{18}	6.0×10^{16}
C014	SEED	1.2×10^{17}	4.7×10^{14}	—	4.6×10^{13}	9.6	8.0	1.4×10^{18}	1.9×10^{16}
C017	TANG	3.8×10^{17}	3.4×10^{15}	—	1.3×10^{14}	LARGE	—	1.4×10^{18}	4.8×10^{16}
C025	SEED	1.5×10^{17}	7.3×10^{14}	—	4.8×10^{13}	10.0	6.7	1.3×10^{18}	4.0×10^{16}
	MID	1.6×10^{17}	9.3×10^{14}	2.6×10^{13}	2.3×10^{13}	12.8	8.0	8.8×10^{17}	1.1×10^{17}
C039	SEED	8.8×10^{16}	1.2×10^{15}	—	1.3×10^{14}	8.1	9.2	1.4×10^{18}	1.1×10^{17}
C042	TANG	3.0×10^{15}	5.8×10^{13}	—	6.1×10^{13}	SMALL	—	1.3×10^{18}	3.6×10^{16}
C078	SEED			5.0×10^{13}	8.3×10^{13}		—	8.8×10^{17}	1.1×10^{17}
	TANG			5.4×10^{13}	1.1×10^{14}				
C086	SEED	1.1×10^{17}	3.2×10^{14}	—	1.3×10^{13}			3.0×10^{17}	3.0×10^{16}
	TANG	1.4×10^{17}	4.0×10^{14}	—	2.2×10^{13}				
C097	TANG			3.8×10^{14}	3.6×10^{14}			5.1×10^{17}	1.3×10^{17}
C112	MID	3.4×10^{17}	—	4.5×10^{15}	3.6×10^{14}			1.0×10^{18}	
C117	SEED	2.1×10^{16}	5.0×10^{14}	7.8×10^{13}	2.2×10^{13}	1.83	8.7	8.4×10^{17}	2.0×10^{17}
C20102A	650/60	6.0×10^{16}	5.2×10^{14}	—	9.0×10^{13}	6.6	11.0	1.0×10^{18}	3.4×10^{16}
C20102B	850/60	6.1×10^{16}	1.1×10^{14}	—	1.1×10^{14}	6.6	10.8	8.6×10^{17}	4.1×10^{16}
C70401	TANG	1.8×10^{17}	$<1 \times 10^{14}$	1.9×10^{14}	7.0×10^{13}	14.2	7.9	3.9×10^{17}	8.3×10^{15}
C71601	SEED	1.3×10^{17}	1.1×10^{14}	—	1.1×10^{14}	8.4	6.5	7.4×10^{17}	5.6×10^{15}
C74101	SEED			5.3×10^{13}	1.3×10^{13}			9.7×10^{17}	1.0×10^{16}
F001	TANG			1.1×10^{14}	2.6×10^{13}			6.7×10^{17}	1.6×10^{17}
Z008B	SEED	1.0×10^{17}	1.8×10^{14}	—	8.8×10^{12}			—	2.0×10^{16}
Z059	SEED	8.4×10^{14}	7.0×10^{11}	1.6×10^{13}	1.0×10^{13}				
Z074	SEED	1.7×10^{16}	4.2×10^{13}	3.9×10^{13}	2.0×10^{13}	1.9	11.6	—	6.8×10^{16}
Z076	MID			$\approx 4 \times 10^{12}$	2.1×10^{13}			—	2.7×10^{15}
Z111	SEED			5.0×10^{12}	3.1×10^{12}			—	1.6×10^{16}
Z7577								—	—

7024-R

23

An undoped crystal, F001, was grown in an rf-heated growth apparatus to avoid contamination from a graphite heater. However, the system required a graphite susceptor to initiate meltdown, and the resulting crystal had a high C content.

Three crystals were grown specifically for the CIT excitation transfer experiment. All were double doped with In and B. Crystals C112 and C117 were grown by Czo, while Z163 was a FZ pass given to a Si:In Czo crystal, C004. It was anticipated that this FZ pass would reduce the In concentration by more than three orders of magnitude and also greatly reduce the P concentration. The Hall-effect measurement results for both Z163 and C004 are listed in Table 7. The In concentration declined, as expected, while the B concentration, which had been expected to remain constant, increased slightly. The net donor concentration was reduced by less than a factor of 2. The resulting levels of B and donors are probably the result of contamination. However, these crystals were satisfactory for the CIT experiment.

In addition to samples from these crystals, samples from several crystals not grown specifically for the SIMDEC program were delivered to CIT for photoluminescence studies. Hall-effect versus temperature data were measured and analyzed so as to provide CIT with well-characterized samples. The Hall analyses for samples from crystals C71601, C008, C0141, C120, Z074, C7411, C025, and C20102 are given in Table 6.

Crystal	Position	N_{In}, cm^{-3}	N_X, cm^{-3}	N_B, cm^{-3}	N_D, cm^{-3}
C004	MIDDLE	2.0×10^{16}	2.9×10^{13}	2.8×10^{13}	1.5×10^{13}
Z163	SEED	6.8×10^{12}	–	3.5×10^{13}	8.8×10^{12}
	TANG	2.2×10^{13}	–	3.9×10^{13}	1.0×10^{13}

7024

24

B. IR SPECTROSCOPIC STUDIES

Several studies were undertaken at HRL to characterize various X-level properties; the purpose was to help determine the origin of the X level. A strong correlation between the X-level and indium concentrations had been observed,[4-8] which implied that an indium complex was most likely the impurity responsible for this level. However, FZ ingots and Czo ingots pulled at IPD tended to have significantly lower X-level concentrations.

As mentioned previously, the Czo Hall samples underwent a 650°C anneal before measurement to reduce the oxygen donors. Frequently, a subsequent 850°C anneal drastically reduced the X-level concentration, and another 650°C anneal returned the concentration to its former level. An 850°C anneal had no effect on those crystals that had initially had a low X-level concentration. To explain these results, we began studying the oxygen concentration of these crystals using IR transmission measurements.

We also attempted to make direct absorption (transmission) measurements of our Czo Si:In crystals to determine the X-level concentration. This was to be a verification of Scott's work,[7] an independent measurement of the concentration, and a lead-in to a symmetry study of this defect. However, since the absorption was below the noise level of our Beckman IR-12 spectrometer, we could not observe this level. Increasing the sample thickness would not improve the situation because this absorption is in a region of lattice absorption.

A sample of Si:In was sent to Sandia Laboratories for electron paramagnetic resonance (EPR) measurements. The X level was not observed under either no excitation or photon excitation. Thus, the X level was indistinguishable from the usual p-type dopants, which are not observed under these conditions.

The experimental apparatus for the IR spectral measurements consisted of two liquid-nitrogen dewars designed and fabricated at HRL; the dewars are compact enough to fit into the sample and reference compartments of the Beckman IR-12 spectrometer. The double-beam-difference

method was used to obtain the absorption spectrum of the sample. An oxygen- and carbon-free sample of undoped, zone-refined Si (furnished by John Baker, Dow Corning) was mounted in the reference dewar, and the sample to be tested was mounted in the matching dewar in the sample beam. Both dewars have CsI windows that allow measurements to be made to 30 μm. The double-beam-difference method cancelled the lattice absorptions that appear near both the oxygen and carbon impurity center peaks. Because of the lattice absorption interference, care was taken to assure that both the unknown and the reference samples were of nearly the same thickness. (This measurement technique and others are described in Refs. 11 and 12.) There has traditionally been disagreement among experimenters as to the correct calibration factor to use to convert optical data to oxygen and carbon concentrations.[13] The relationships used in this study between the peak absorption coefficients at liquid nitrogen temperature (α_0 and α_C) and concentrations (atoms/cm^3) are

$$[0] = (1.43 \times 10^{17})\alpha_0$$

$$[C] = (3.1 \times 10^{16})\alpha_C \quad .$$

The oxygen calibration is derived from Refs. 11 and 12 scaled to 77 K, and the carbon calibration is from ASTM F123-74 corrected for a different baseline. The limits of sensitivity for measuring oxygen and carbon concentrations are 1×10^{15} atoms/cm^3 and 2×10^{15} atoms/cm^3, respectively.

The results were also plotted in terms of the peak-half-width product, which approximates the area of the absorption line. The data were consistent; thus, we have continued to use the peak value since the same instrument slit program is used for all these measurements, and the measured resolutions of the lines were always very nearly the same.

The measurements are summarized in Table 6, which contains the O and C concentrations calculated from the IR as well as the In, X-level, B, and donor concentrations as appropriate when these values could be calculated from Hall-effect data on adjacent samples. The Czo Hall-effect samples were annealed at 650°C for 30 min to reduce the O donor concentration; the optical samples were not annealed. The samples measured represent a range of In concentrations of two orders of magnitude, X-level concentrations of about one order, and C concentrations of about two orders. The O concentration was either near 1.0×10^{18} cm^{-3} or below the detection limit of 1.0×10^{15} cm^{-3}, depending on whether the sample was from a Czo or an FZ crystal.

Table 6 also contains the In absorption coefficient as calculated from the IR spectra and the absorption cross section based on the corresponding N_{In} value. Also included are O and C concentrations for several undoped crystals, also measured by IR transmission.

Figure 1 is a plot of the X to In concentration ratio versus N_O and N_C. The plot shows a correlation with the C data and clearly no correlation with O; note that the FZ N_O values are less than 1.0×10^{15} cm^{-3}. The curve in the figure is a unit-slope straight line, as predicted by the mass action law. This gives a reasonably good fit considering the uncertainties in determining the three concentrations involved over this wide a range of parameters.

C.   CHARGED-PARTICLE ACTIVATION ANALYSES FOR O AND C

A separate IR&D study was performed, under contract with HRL by Prof. R. Hart at Texas A&M University, to investigate a new method of analysis for O and C in Si. This work is described here because correlations were made with samples measured by IR absorption in the SIMDEC program and because this technique holds out the promise of better sensitivity for detecting O and C.

Charged-particle activation analysis (CPAA) involves bombarding the Si sample with high-energy ^{3}He and D beams for O and C, respectively. The reactions are $^{16}O(^3He,n)^{18}F$ and $^{12}C(D,n)^{13}N$. The activities of the
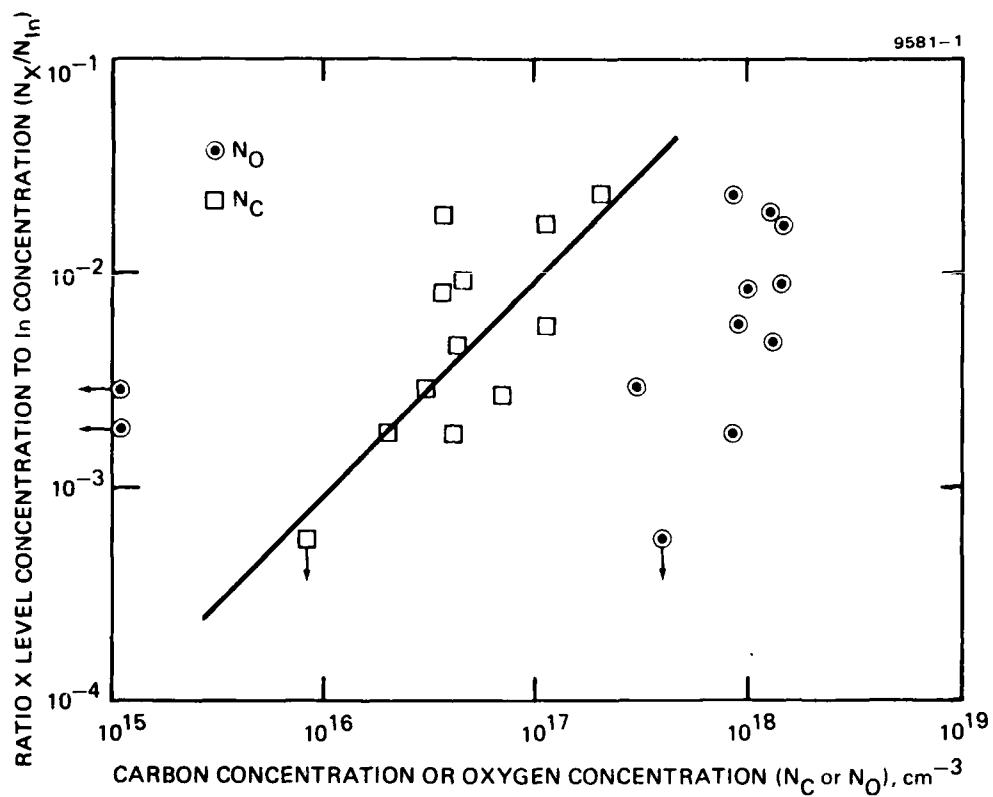
27

Figure 1. The ratio of X-level concentration to In concentration versus the O and C concentrations.

isotopes of F or N are then analyzed to determine the amount of O or C present in the sample. This work is in its early stages, and thus improvements are still being made in beam current magnitude and its measurement, sample mounting procedure, counting technique, and the development of calibration standards. Initial studies used an IR-measured sample as the calibrating standard, while more recent work is using graphite and oxidized aluminum.

The results obtained at this stage of the study are listed in Table 8. The agreement is extremely good in most cases, well within the confidence limits of the IR measurements. The generally higher CPAA results obtained for the lower O and C concentrations and for the polycrystalline sample may in fact be real, since the IR method measures only those O and C atoms in their respective interstitial and substitutional positions. The CPAA method, on the other hand, measures the total O or C content. The very high concentration of C measured by CPAA in polycrystalline Si may reflect segregation of C at grain boundaries. The CPAA results indicate sensitivities for O of 10^{14} cm^{-3} and for C of 10^{15} cm^{-3}.

D.   ION IMPLANTATION OF In AND C

An experiment was performed to produce controlled amounts of X in Hall-effect samples by ion implanting controlled doses of In and C. The implants were done in four steps for each impurity so as to give a flat carrier concentration profile to a depth of about 0.25 μm. Implant concentrations of In ranged from 3×10^{15} cm^{-3} to 1×10^{17} cm^{-3}; concentrations of C ranged from 1×10^{16} cm^{-3} to 1×10^{18} cm^{-3}. Permutations in the order of species and implant energies were performed. All implants were done into n-type wafers that had a P concentration of about 2.5×10^{12} cm^{-3}.

Hall samples were fabricated and were heated to 900°C for 30 min to anneal the implant damage; then the temperature was reduced to 650°C and held there for 30 min to produce high X-level concentrations.

29

Hall-effect measurements were made as a function of temperature and the results analyzed to determine the In, X, and net donor concentrations.

The In concentrations thus obtained were in agreement with the values expected on the basis of the implant parameters. However, a large net donor concentration was observed in all cases. This value was in the range from 5×10^{15} cm^{-3} to 10×10^{15} cm^{-3}, which is several orders of magnitude higher than the residual P content of the wafers. This donor concentration was higher than the predicted X-level concentration and made its quantitative evaluation impossible.

The most likely cause of this high a net donor concentration was unannealed implantation damage. Further annealing to remove or reduce this damage is clearly indicated.

Table 8. Comparison of O and C in Si Determined by IR and CPAA

Sample	N_O (IR)	N_O (CPAA)	N_C (IR)	N_C (CPAA)
C74101UD	9.7×10^{17}	(Standard)	3.2×10^{17}	3.5×10^{17}
C017IN (Poly)	1.45×10^{18}	1.37×10^{18}	4.8×10^{16}	1.6×10^{19}
C014IN	1.3×10^{18}	9.9×10^{17}		
C70401IN	3.9×10^{17}	4.0×10^{17}		
Z111UD	$<10^{15}$	3.2×10^{16}		
Z008IN	$<10^{15}$	7.9×10^{15}	2.0×10^{16}	2.2×10^{16}
Z7577UD	$<10^{15}$	6.8×10^{15}	$<2 \times 10^{15}$	4.7×10^{15}
C71601IN			7.7×10^{15}	9.0×10^{15}

All units are cm^{-3}

7024

30

E.   FZ AND Czo ANNEAL STUDIES

Samples from FZ refined and Czo crystals were given a sequence of anneals at various temperatures, and Hall-effect measurements versus temperature were made between each anneal. The purpose of this study was to determine the thermal equilibrium X-level concentration as a function of anneal temperature and to compare it with the relationship predicted by the mass-action law.

The anneal condition and the X-level and net donor concentrations are given in Tables 9 and 10 for samples from the FZ ingot Z008IN and Czo ingot C019IN, respectively. Six different samples from Z008IN were studied: Z2, M6, D1, D2, D3, and D4. The third digit in the sample designation indicates the anneal state. In the cases of Z2 and M6, 0 in this position indicates unannealed or as-grown material (these samples had only a 650°C heat treatment for a few minutes to alloy the evaporated Al contacts). The samples were then sequentially annealed as indicated by the increasing letter designation. Most of the samples received 1-hr anneals, and all were quenched after annealing. Thus, sample Z2 was first measured before anneal, annealed at 850°C for 1 hr, measured, annealed at 650°C for 1 hr, measured, etc. The samples designated D were separate samples from the same wafer and had the indicated anneals. The sample M came from the middle of the ingot and had higher In and X concentrations than samples Z and D, which came from nearer to the seed end of the crystal. The Czo sample M3 had an anneal sequence analogous to sample Z2. Sample M3B was a rerun of M3A two years later with no intervening high-temperature anneal.

Two sets of results are presented for the anneal temperatures around 850°C. The analysis of the Hall-effect data involves the minimization of the sum of the squares of the errors between the data and the value predicted by the model at each temperature. Since the equations generated by the model are nonlinear in the parameters, an iterative approach is taken using several sets of randomly chosen initial parameters. Generally, the various sets either diverge or all converge to one

Table 9. Anneal Sequence Results for Ingot Z008IN

Sample Designation	Anneal Temperature, °C	N_X, 10^{14} cm^{-3}	$N_D - N_B$, 10^{14} cm^{-3}
Z20	As grown	2.39	0.120
Z2A	850	0.405, 7.13	0.384, 0.356
Z2B	650	2.26	0.109
Z2C	850	0.34, 5.21	0.230, 0.289
Z2D	750	2.57	0.137
Z2E	700	1.96	0.109
Z2F	650	2.25	0.112
Z2G	600	1.95	0.105
Z2H	550/2 hr	1.84	0.098
Z2I	1000	3.74	2.25
Z2J	1000	5.12	3.42
M60	As grown	7.47	0.160
M6A	450/72 hr	No change	No change
M6B	650/30 min	No change	No change
M6C	850/15 min	8.67	0.202
M6D	900/3 hr	6.31	0.359
M6E	1000	1.58	1.49
D10	1000	3.04	3.14
D20	500	2.40	0.119
D30	650/30 min	2.27	0.121
D40	850	0.354, 5.74	0.336, 0.305

All anneals are for 1 hr unless otherwise indicated.

7024

32

Table 10. Anneal Sequence Results for Ingot C019IN

Sample Designation	Anneal Temperature, °C	N_X, 10^{14} cm^{-3}	$N_D - N_B$, 10^{14} cm^{-3}
M30	650/30 min	19.5	1.94
M3A	850	2.15, 44.4	2.06, 2.02
M3B	Retake data	2.13, 48.3	2.05, 2.04
M3C	800	1.15, 14.4	1.05, 0.774
M3D	750	12.0	0.650
M3E	700	13.3	0.812
M3F	650	20.1	1.64
M3G	600	24.5	2.79
M3H	600	28.9	3.65
M3I	550/2 hr	13.0	13.2
M3J	550	14.9	15.3
M3K	500	15.7	16.2
M3L	500/3 hr	Not detected	172
M3M	850	3.94	4.45

All anneals are for 1 hr unless otherwise indicated.

7024

33

solution. However, in the case of Si:In annealed near 850°C, two or more solutions often emerge from this procedure. The principal difference is in the X-level concentration and energy level obtained.

Thus, two sets of values are given for the anneal temperatues in this range. The explanation of this effect continues to elude us and there is no way to determine, a priori, which solution is correct. To resolve this dilemma, a spectral photoconductive measurement was made on the sample from CO19IN. No X level was observed. Since our limit of detectability was 1×10^{15} cm^{-3}, it can be concluded that the lower X-level value is correct.

These results are plotted versus the reciprocal of the anneal temperature in Figures 2 and 3 for crystals Z008IN and CO19IN, respectively. Several trends can be seen in the data. The donor concentration of the Czo samples increases with decreasing anneal temperature at the lower temperatures, while the FZ samples do not show this effect. This increase has been determined to result from the formation of oxygen donors.[14] The donor concentration tends to increase at the highest anneal temperatures for both the Czo and FZ crystals. This unexpected result has not been explained. Oxygen-donor complexes must be ruled out as the cause since this effect is seen in the FZ crystal, which did not exhibit the low-temperature oxygen-related behavior.

An attempt was made to getter possible defect complexes in sample Z008IN.Z2J. A heavy dose of phosphorus was implanted into the back of this sample so as to create considerable lattice damage. The sample was then annealed for an additional hour at 1000°C, after which the damaged implanted layer was removed by etching. The subsequent Hall analysis showed that both donor and X concentrations went up. Thus, either no gettering took place (which is unlikely) or the increase in donors is not defect related. It was also observed that the surface morphology of the sample after the etch was extremely bad.

The most striking result of this anneal study, as revealed in Figures 2 and 3, is that the X-level concentration in the FZ samples is anneal independent! The Czo sample exhibits the inverse temperature relationship that is predicted by the mass-action law, but the FZ samples
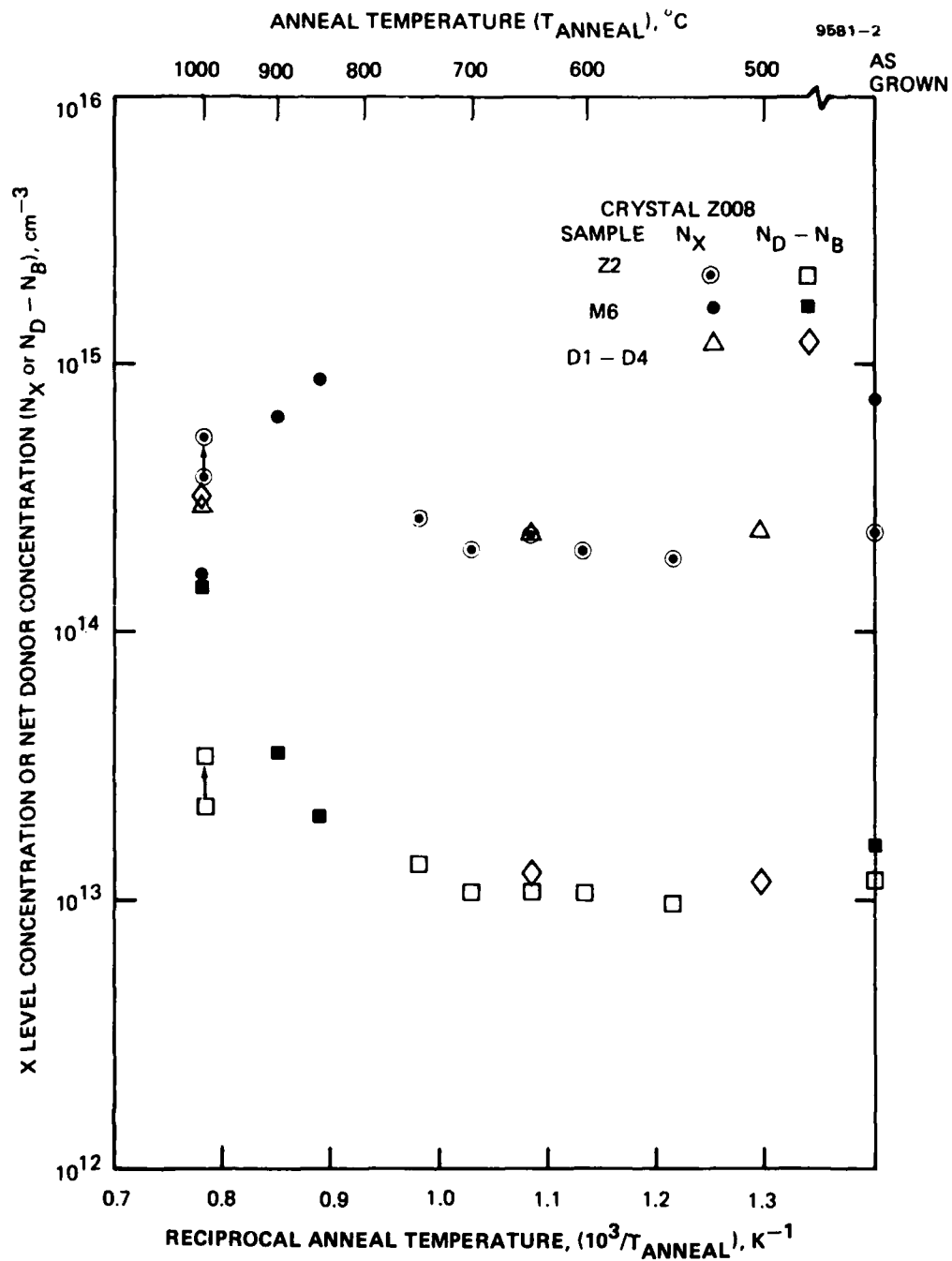
34

Figure 2. X-level and donor concentrations as functions of anneal temperature for crystal Z008IN.
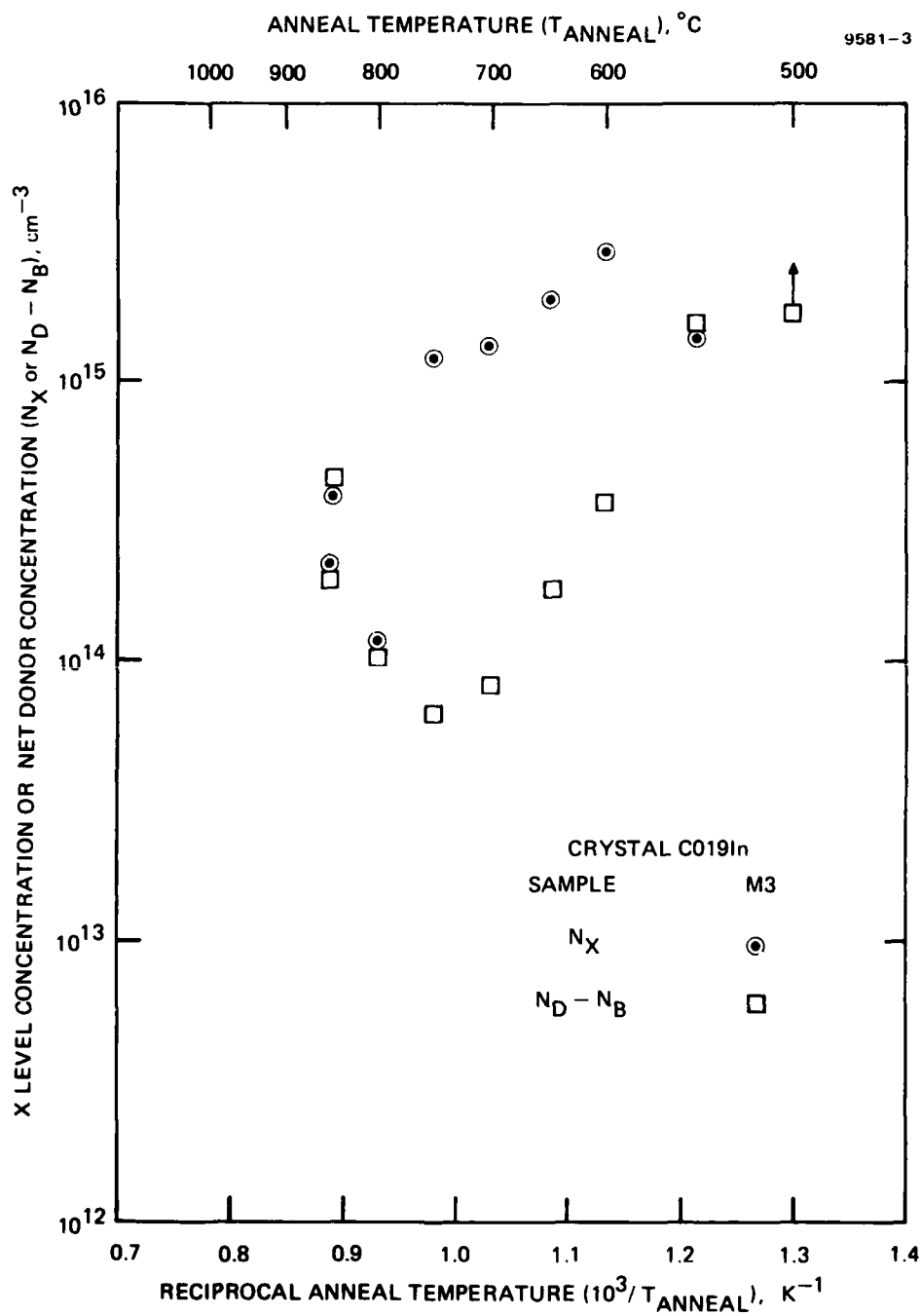
35

Figure 3.   X-level and donor concentrations as functions
of anneal temperature for crystal C019IN.

appear to be in violation. Thus, whatever the X-level model, there clearly is a significant difference between FZ and Czo samples in the way they respond to heat treatment. We believe that this fact has serious implications for the processing of high-speed large-scale-integration (LSI) devices.

In the present case, we believe that the FZ data result from the In-C pairs not reaching their thermal equilibrium distribution. Extrapolation of In and C diffusion data indicate that thermal equilibrium of In-C pairs should not be obtained in this material. We believe that the diffusion of C in Czo material is greatly enhanced, perhaps by the presence of O.

F. LIST OF PUBLICATIONS

1. R. Baron, M.H. Young, J.P. Baukus, O.J. Marsh, and M.J. Sheets, Properties of Indium-Doped Silicon as an Extrinsic Detector Material, Proc. of the IRIS Specialty Group on Infrared Detectors, 1977 (Infrared Information and Analysis Center, Ann Arbor, 1977) Vol. I, p. 23.

2. J.P. Baukus, M.H. Young, R. Baron, M.J. Sheets, and O.J. Marsh, Characterization of Gallium and Aluminum Doped Silicon Detectors, Proc. of the IRIS Specialty Group on Infrared Detectors, 1977 (Infrared Information and Analysis Center, Ann Arbor, 1977) Vol. I, p. 35.

3. J.P. Baukus, R. Baron, M.J. Sheets, and O.J. Marsh, Photoconductive Properties of Indium-Doped Silicon, Proc. of the Joint Meeting of the IRIS Specialty Groups on Infrared Detectors and Imaging, 1978 (Infrared Information and Analysis Center, Ann Arbor, 1978) Vol. I, p. 263.

4. R. Baron, M.H. Young, J.P. Baukus, O.J. Marsh, and T.C. McGill, Structure in the Photoconductive Spectra of P-Type Silicon, Proc. of the Joint Meeting of the IRIS Specialty Groups on Infrared Detectors and Imaging, 1978 (Infrared Information and Analysis Center, Ann Arbor, 1978) Vol. I, p. 281.

5. R. Baron, J.P. Baukus, S.D. Allen, T.C. McGill, M.H. Young, H. Kimura, H.V. Winston, and O.J. Marsh, Nature of the 0.111 eV Acceptor Level in Indium-Doped Silicon, Appl. Phys. Lett. 34, 257 (1979).

SECTION 3

PHOTOLUMINESCENCE STUDIES IN EXTRINSIC SILICON

This section, which describes work done at CIT during this program, was written by Professor T.C. McGill.

The primary goals of the program at the California Institute of Technology were to develop photoluminescence as a diagnostic tool for measuring the relative concentrations of various defects and impurities in In-doped Si and to develop as much understanding as possible of the properties of In-doped Si. This section summarizes the major results obtained at CIT during this program, discusses the exciton transfer mechanism, and lists publications from our group that were a direct result of this contract.

A. MAJOR RESULTS

During this program, several major advances were made:

- The ground state and excited state spectra of the bound exciton for the deeper acceptors (Al, Ga, In, and Tl) in Si were determined. Knowledge of these spectra made it possible for us to identify the lines associated with certain known impurities. The results are reported in the first two entries in the publication list.

- The value and temperature dependence of the capture cross section for excitons on In, B, and P were determined. These cross sections make it possible for us to model in detail the photoluminescence process for samples with various centers present. The results are reported in the third and fourth entries (the fourth is also presented in Appendix A).

- We obtained evidence that strongly suggests that In undergoes a Jahn-Teller distortion in Si. That is, the four-fold degeneracy of the ground state of the In acceptor is lifted by moving the In atom slightly off the substitutional site. The splitting between the ground state and the first excited state is 4 meV. This observation is reported in the fifth publication.

39

- Extra lines were observed in the Si:In samples. These included some lines that had lifetimes on the order of 200 μsec. These lifetimes are very long for Si, where the line related to boron has a lifetimes of 2 μsec. These lines are likely to be due to donor-acceptor complexes of some type. The observation of these lines marks the first time that anyone has observed such long-lived lines in Si. The results of this study are reported in the sixth publication.

- Evidence for a new exciton transfer mechanism was found in samples doped moderately with In ($N_{In} >$ 10^{15} cm^{-3}). This effect shows up in that the ratio of the ratio of the photoluminescence line intensities to the ratio of the impurity concentrations for B and In is not a constant. This effect has rather important implications for the use of photoluminescence as a method for detecting small concentrations of impurities in the presence of a much larger background concentration. This result is expanded on in Section 3.B and explained in more detail in Appendix B.

B. EXCITON TRANSFER MECHANISM

In the third interim report,[3] we indicated that we believed that the measurement of relative impurity concentrations using photoluminescence line intensities could be difficult because of excitation transfer. Excitation transfer is a process in which an exciton originally captured on one center is transferred to a second center via a tunneling process. Although it seemed very likely that processes like this would occur, and exciton transfor has in fact been observed in the silver halides, the concentration at which these kinds of processes would occur in the semiconductor had not been determined. We chose to study the variation of the photoluminescence intensity with concentration in specially prepared B and In samples. The ratio

$$R = (I_B/I_{In})/(N_B/N_{In}) \quad ,$$

where I_B and I_{In} are the intensities of the B and In photoluminescence lines, respectively, and N_B and N_{In} are the concentration of B and In as determined by Hall-effect measurements, respectively. This ratio

40

should be independent of concentration. The variation of R with N_{In} is shown in Figure 4. This figure shows R to be independent of N_{In} for $N_{In} < 10^{15}$ cm^{-3}. However, for $N_{In} > 10^{15}$ cm^{-3}, a variation of R is observed. For $N_{In} \sim 2 \times 10^{16}$ cm^{-3}, we have been unable to observe the photoluminescence due to the B at all, and hence we are unable to assign values to R. These data strongly suggest that, for $N_{In} > 10^{15}$ cm^{-3}, excitons are being transferred from the B to the In, where they decay rapidly. The variation in the ratio can be accounted for in a model in which an additional term is added to the rate equations. This additional term accounts for transfer of excitons from the B to the In and is assumed to take the form $A \exp(-r/z)$, where r is the spacing between B and In atoms, and A and z are constants. The impurities are assumed to be randomly distributed, and the appropriate averages over r are taken. For $A = 10^{-13}$ sec^{-1} and z = 18 to 28 Å, the fit between experiment and theory is quite good. The value of A is taken from observations of exciton transfer in GaP:N.[15] The value of z was varied to obtain the best fit and is in the range expected given the size of the electron and hole orbits in the bound exciton. These results are explored and explained in more detail in Appendix B. These results on Si:(In,B) suggest that it is impossible to see the photoluminescence from shallower impurities in the presence of a moderately heavy concentration of deep dopant ($N > 10^{15}$ cm^{-3} in the case of In). These results indicate that it will be difficult to use phosoluminescence as a tool to study the X level, whose concentration is always substantially less than that of indium.

C.   LIST OF CIT PUBLICATIONS

1.   K.R. Elliott, G.C. Osbourn, D.L. Smith, and T.C. McGill, "Bound Exciton Absorption in Si:Al, Si:Ga, and Si:In," Phys. Rev. B17, 1808 (1978).

2.   K.R. Elliott, D.L. Smith, and T.C. McGill, "Absorption and Luminescence of the Bound Exciton in Thallium Doped Silicon," Solid State Comm. 27, 317 (1978).
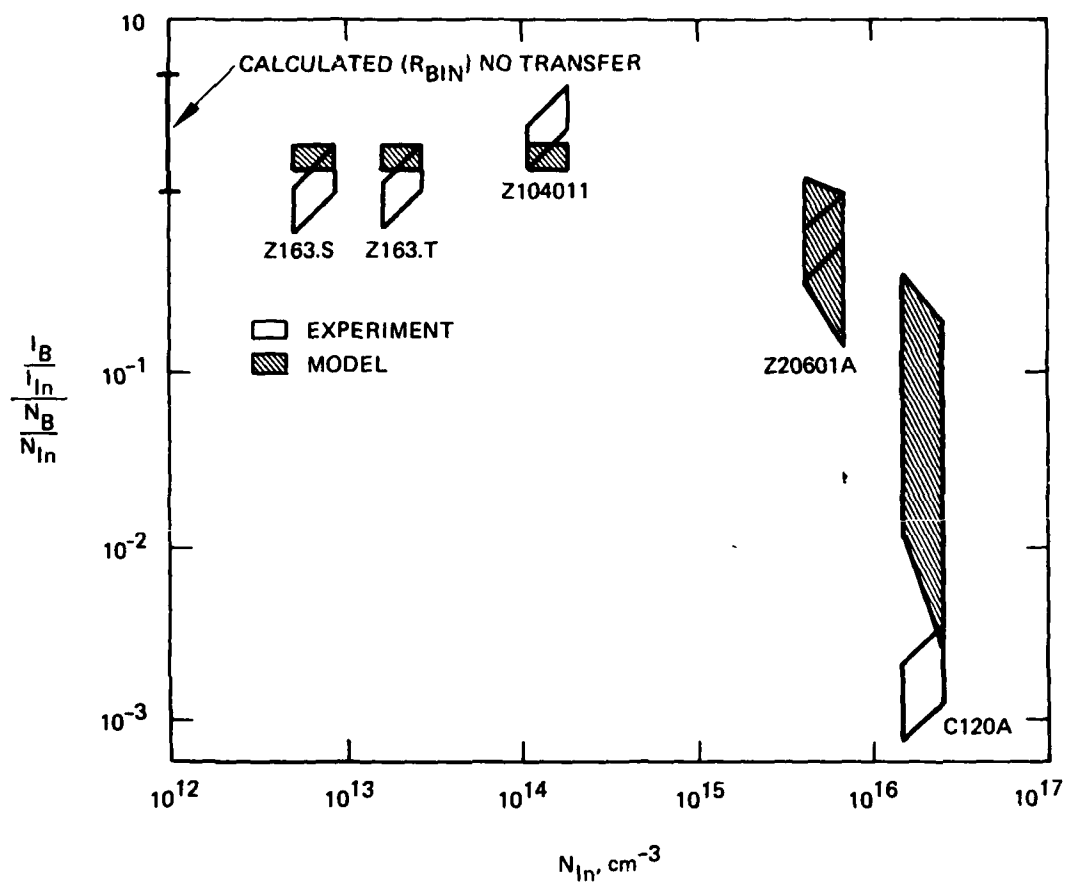
Figure 4.
The ratio R as a function of the N_{In}. The open boxes are the experimental
data. The cross-hatched boxes are the theoretical points obtained from
a simple excitation transfer model. The size of the boxes representing
the experimental data indicates the errors in determining N_{In}, N_B, I_B,
and I_{In}. The size of the boxes representing the theory is a result of
the uncertainty in the ratio without excitation transfer and the vari-
ation in z from 10 to 28 Å.

C. LIST OF CIT PUBLICATIONS (Cont.)

3. K.R. Elliott, D.L. Smith, and T.C. McGill, "Capture Cross Section of Excitons on Neutral Indium Impurities in Silicon," Solid State Comm. 24, 461 (1977).

4. R.F. Feenstra and T.C. McGill, "Exciton Capture Cross Sections of Indium and Boron Impurities in Silicon," Solid State Comm. (submitted for publication). A preprint is presented in Appendix A.

5. K.R. Elliott, S.A. Lyon, D.L. Smith, and T.C. McGill," Evidence for an Excited Level of the Neutral Indium Acceptor in Si," Phys. Letters 70A, 52 (1979).

6. G.S. Mitchard, S.A. Lyon, K.R. Elliott, and T.C. McGill, "Observation of Long Lifetime Lines in Photoluminescence for Si:In," Solid State Comm., 29, 425 (1979).

7. A.T. Hunter, S.A. Lyon, D.L. Smith, and T.C. McGill, "Transient Decay of Satellite Lines of the Bound Exciton in Si:P," Phys. Rev. B20, 2431 (1979).

8. S.A. Lyon, K.R. Elliott, G.S. Mitchard, D.L. Smith, T.C. McGill, J.P. Baukus, R. Baron, M. Young, and O.J. Marsh, "Photoluminescence Studies of Acceptors in Silicon," Proc. of the Joint Meeting of the IRIS Specialty Groups on Infrared Detectors and Imaging, 1978 (Infrared Information and Analysis Center, Ann Arbor, 1978) Vol. I, p. 273.

9. G.S. Mitchard and T.C. McGill, "Determination of the Relative Impurity Concentrations Using Photoluminescence: — A Case Study of Si:(B,In)," Appl. Phys. Lett., 37, 959 (1980). A reprint is presented in Appendix B.

REFERENCES

1. J. Baukus, T. McGill, and L. Forbes, Interim Technical Report 1, Contract DAAK-77-C-0082 (Army Night Vision and Electro-Optics Laboratory, Fort Belvoir, VA), 1977.

2. J. Baukus and T. McGill, Interim Technical Report 2, Contract DAAK-77-C-0082 (Army Night Vision and Electro-Optics Laboratory, Fort Belvoir, VA), 1978.

3. J. Baukus and T. McGill, Interim Technical Report 3, Contract DAAK-77-C-0082 (Army Night Vision and Electro-Optics Laboratory, Fort Belvoir, VA), 1980.

4. R. Baron, M.H. Young, J.K. Neeland, and O.J. Marsh, Appl. Phys. Lett. 30, 594 (1977).

5. R.N. Thomas, T.T. Brﾐggins, H.M. Hobgood, and W.J. Takei, J. Appl. Phys. 49, 2811 (1978).

6. R.D. Larrabee, Semiconductor Characterization Techniques. Edited by P.A. Barnes and G.A. Rozgonyi (Electrochemical Society, Princeton, 1978), p. 71.

7. M. Scott, Appl. Phys. Lett. 32, 540 (1978).

8. R. Baron et al., Appl. Phys. Lett. 34, 257 (1979).

9. C.S. Fuller, F.H. Doleiden, and K. Wolfstirn, J. Phys. Chem. Solids 13, 187 (1960).

10. CCD-Squared Final Report, Contract DAAH01-75-C-0276, Hughes Aircraft Co. (1978).

11. NBS Technical Note 529.

12. ASTM Bulletin F121-76.

13. Patel, J.R., Semiconductor Silicon 1977, edited by H.R. Huff and E. Sirtl (The Electrochemical Society, Princeton, N.J., 1977) p. 521.

14. A. Kanamori, Appl. Phys. Lett. 34, 287, (1979).

15. P.J. Wiesner, R.A. Street, H.D. Wolf, Phys. Rev. Lett. 35, 1366 (1975).

APPENDIX A

EXCITON CAPTURE CROSS SECTIONS OF INDIUM AND BORON

IMPURITIES IN SILICON [*]

R. M. Feenstra[†] and T. C. McGill
California Institute of Technology
Pasadena, California 91125

ABSTRACT

Measurements have been made of the decay rates and intensity ratios of photoluminescence lines from Si:In, B. We deduce values for the In and B exciton capture cross sections in the temperature range 3.6 - 5.9 K. The large difference between the In and B cross sections is discussed in terms of excited states of the In bound exciton.

47

During the past several years studies have been made on the process by which free excitons (FE) in a semiconductor crystal are captured on impurity sites to form bound excitons (BE). The luminescence resulting from radiative recombination of a bound exciton in silicon was first observed about twenty years ago [1], but only recently have attempts been made to measure the cross section (which characterizes the capture rate) for FE capture. Knowledge of the capture cross sections for many impurities is necessary in order to use exciton photoluminescence as a quantitative tool for determining impurity concentrations in semiconductors [2,27].

To date, capture processes have been studied in detail only in silicon. Elliott, et al [3] observed the In BE lifetime in the temperature range 10-30 K and deduced values for the In cross section (σ_{In}) which have a temperature dependence of roughly T^{-4} with $\sigma_{In} \approx 10^{-13} cm^2$ at 10 K. Hammond and Silver [4] assume a cross section of $(10^{-12} cm^2 K)/T$ for B and P impurities in silicon, and show that this value is consistent with their observations of the FE lifetime and BE to FE intensity ratios, in the temperature range 2-16 K. Nakayama, et al [27] report a value of $1.51 \times 10^{-14} cm^2$ for the B cross section at 4.2 K. In the present work, measurements are reported for the BE decay rates and intensity ratios for silicon doped with In and B. From this data values are deduced for the exciton capture cross sections of In and B in the temperature range 3.6 - 5.9 K. The impurity concentrations of the sample used in these experiments were suitable to permit cross section measurements in the above stated temperature range.

48

The results indicate that the In cross section continues to show a strong temperature dependence below 10 K, increasing to greater than $10^{-12}cm^2$ at 3.6 K. The B cross section is found to be about $10^{-13}cm^2$ for T ≃ 5 K, in agreement with the Hammond and Silver results. The ratio of B BE release rate to capture rate is shown to agree with simple detailed balance results using a ground state binding energy of 3.3 ± 0.2 meV. The role of BE excited states in the temperature dependence of the cross section is examined.

Measurements were made on a single crystal float-zoned silicon sample doped with In and B. Concentrations were determined by Hall effect measurements [5] to be $6.8x10^{12}cm^{-3}$ and $3.5x10^{13}cm^{-3}$, respectively. The residual P concentration was determined to be $0.9x10^{13}cm^{-3}$. The sample was mounted in a Janis variable temperature dewar. Optical excitation was provided by an Ar^{+} laser with an opto-acoustic coupler to provide pulses of variable width. The beam was unfocussed with a diameter of approximately 2 mm. Observations of the B BE decay rate were usually made using 2 μs pulses with a 10% duty cycle, and the In BE decay was observed using 20 ns pulses with a 0.2% duty cycle. Average power levels were always less than 5 mW which was determined to result in less than 0.1 K sample heating. Continuous mode laser operation was used for observations of the intensity ratios. The luminescence wavelength was selected with a SPEX 1269 single-pass spectrometer and photon counting was accomplished with a cooled S-1 photomultiplier. A time-to-pulse-height converter was used for decay rate measurements. The photomultiplier response as a function of wavelength was calibrated using a 1500 K black body source. All data were acquired on a Nuclear Data ND-60 multichannel analyzer and then passed to a PDP 11/34 computer for storage on floppy disk.

Figure 1 shows a typical photoluminescence spectrum, taken at 4.2 K with a pump power of 3 mW. The B(TO) line at 1.0928 eV and the In(NP) line at 1.1409 eV were used for the decay time observations. We note that, using a

B(TO) oscillator strength of 2.8×10^{-5} [6] along with the measured ratio of B(TO) to B(NP) lines (corrected for photomultiplier response) of 67 ± 5, gives a B(NP) oscillator strength of $4.2 \times 10^{-7} \pm 7\%$, in disagreement with previously reported values [7].

Fig. 2 shows the observed decay rates of the BE luminescence lines. For $T \lesssim 7$ K the In and B BE decay curves (intensity vs. time) appear to be single exponentials (as opposed to the sum of several exponentials). Roughly speaking, the In BE decay rate equals the capture rate of FE on In sites, and the B BE decay rate is the sum of the Auger decay rate (zero temperature limit of the observed rate) and the release rate of the BE. As the temperature increases the FE population increases (relative to the BE) and the decay curves of the In BE, B BE, and FE all start to resemble each other. The major component of the resulting decay curve is due to FE recombination, which does not contain any information about the cross sections. For $T \leq 3$ K the B BE decay rate equals (within experimental error) the Auger decay rate, so that the B BE release rate is too small to measure and the associated cross section cannot be calculated. Thus, only for $3 \lesssim T \lesssim 7$ K do the observed decay rates yield the kinetic information required for computation of the cross sections.

Let us now investigate how the cross sections can be calculated from the observed decay rates of the luminescence lines. The observed intensity, I, of the luminescence arising from a particular exciton state is linearly related to the concentration of occupied states, n, by

$$I \propto Rfn$$

where R is the collection efficiency (determined by the sample characteristics and the efficiency of the photon collection system), and f is the oscillator strength of the transition. The occupation of the exciton states is determined by a set of coupled kinetic equations[4] which describe the effect of exciton capture, release and recombination at neutral impurities. In the limit of low FE concentrations (low pump power) the role of bound multiple exciton complexes can be neglected and the resulting equation for the FE (subscript o) is

$$\frac{dn_o}{dt} = g - \frac{n_o}{\tau_o} - n_o \sum_i C_i (N_i - n_i) + \sum_i R_i n_i \quad , \qquad (1a)$$

where n_o is the FE concentration, n_i is the concentration of excitons bound on impurity type (i), N_i is the concentration of impurity type (i), g is the FE generation rate, C_i and R_i are the capture and release rates of excitons on impurity type (i), and τ_o is the FE recombination lifetime. For BE of concentration n_i (i = 1,2,...), the rate equations are

$$\frac{dn_i}{dt} = - \frac{n_i}{\tau_i} + n_o C_i (N_i - n_i) - R_i n_i \quad , \qquad (1b)$$

where τ_i is the BE recombination lifetime. For BE in silicon, Auger decay is the dominant recombination mechanism. For low exciton concentrations (i.e., when the impurities are far from saturation) these equations may be linearized by taking the concentration of unoccupied impurites, $(N_i - n_i)$, to be equal to the total concentration of impurities, N_i. For the case of interest, viz., decay following an optical pulse, g=0 in (1a). With these two simplifications, the solution of Eqn. (1), for the case of m impurity types, is

51

$$\underset{\sim}{n} = \sum_{i=0}^{m} a_i \, \underset{\sim}{\xi_i} \, e^{\lambda_i t} \quad , \tag{2}$$

where

$$\underset{\sim}{n} = \begin{bmatrix} n_o \\ n_1 \\ \cdot \\ \cdot \\ \cdot \\ n_m \end{bmatrix} \quad . \qquad ,$$

$\underset{\sim}{\xi_i}$ are the eigenvectors and λ_i the eigenvalues of the fundamental matrix, A, formed from the coefficients of the concentrations in (1). The a_i are constants determined by the initial conditions. For the case of two impurity types and the FE,

$$A = \begin{bmatrix} -\dfrac{1}{\tau_o} - C_1 N_1 - C_2 N_2 & R_1 & R_2 \\ C_1 N_1 & -\dfrac{1}{\tau_1} - R_1 & 0 \\ C_2 N_2 & 0 & -\dfrac{1}{\tau_2} - R_2 \end{bmatrix} \tag{3}$$

and the exciton concentrations will be composed of three decaying exponentials. The initial amplitudes of the exponentials are determined by the initial conditions, which for the case of decay following a long optical pulse will be the steady-state solutions of (1).

Once the fundamental matrix (3) is known it is straightforward to calculate its eigenvalues, which are equal to the experimentally observed decay times. For the case of In (subscript 1) and B (subscript 2) impurities, let us examine which parameters in (3) are known. The FE recombination time, τ_o, is not very well known and could be spatially dependent. Since these experiments were con-

52

ducted at relatively low temperatures the results were not very dependent on τ_o, and in all calculations τ_o was varied in the range 2-1000 µs. The In BE Auger time, τ_1, was taken to be 3 ns [25] but the results are in-sensitive to this value (one of the eigenvalues of A is always very close to - (3 ns)$^{-1}$ and contains no useful kinetic information). The B BE Auger time, τ_2, has been extrapolated from low temperature measurements (see Figure 2) and is $1/\tau_2 = 0.91 \pm 0.02$ µs^{-1} [8]. The T = 3.6 K results to be presented later in this work are somewhat sensitive to this Auger rate, although the higher temperature results are not. The capture rates, C_i, are related to the capture cross sections, σ_i, by

$$C_i = \sigma_i \, v_{th} \quad , \tag{4}$$

where v_{th} is the FE thermal velocity (the mean velocity is used here),

$$v_{th} = \left(\frac{8 \, kT}{\pi m_{ex}}\right)^{1/2} \quad , \tag{5}$$

where m_{ex} is the FE mass (0.6 m_o) [3]. Using detailed balance the release rates, R_i, can be related to the capture rates through an equilibrium constant, K_i, defined as,

$$K_i(T) = \frac{R_i}{C_i} \quad . \tag{6}$$

Using spherical FE bands and an acceptor BE ground state split by the J-J coupling of the holes, the equilibrium constant is computed to be,

$$K_i = \frac{4 \cdot 24(1 + e^{-\Delta E_o/kT})}{12 + 60 \, e^{-\Delta E_i/kT}} \left(\frac{m_{ex} kT}{2\pi\hbar^2}\right)^{3/2} e^{-E_i/kT} \tag{7}$$

where ΔE_o = 0.31 meV is the splitting of the FE ground state[9,10] (degeneracy of

53

24 in each of the upper and lower states), ΔE_i is the J-J splitting of the BE ground state (degeneracy of 12 and 60 in the lower and upper states respectively), and E_i is the BE binding energy. For In, $E_1 = 13.7$ meV, and for the temperature range used in these experiments the In release rate is negligibly small. The reported values of the B BE binding energy are 4.2 ± 0.2 [11], 3.8 ± 0.2 [12], 3.9 ± 0.3 [13], and 3.6 ± 0.5 meV [13]. For discussion we will use the value $E_2 = 3.9 \pm 0.3$ meV. The 8% error in E_2 results in almost an order of magnitude uncertainty in the factor $e^{-E_2/kT}$ (for $3 < T < 7$ K). For this reason, the value of E_2 (and then of K_2) is treated as an unknown in the calculations.

In summary, the fundamental matrix (3) contains three unknowns; the In cross section σ_1, the B cross section σ_2, and the B equilibrium constant K_2. The purpose of these experiments is to determine these three parameters, as a function of temperature, based on measurements of the decay times and intensity ratios of various luminescence lines. In particular, the quantities which are measured are two eigenvalues of the matrix (3) and the intensity ratio, I_B/I_{In}, of the B(TO) line to the In(NP) line. The observed values of I_B/I_{In} were corrected for photomultiplier response, and were related to a concentration ratio using a B(TO) oscillator strength of $2.8 \times 10^{-5} \pm 10\%$ [6] and an In(NP) oscillator strength of $8.5 \times 10^{-5} \pm 10\%$ [7]. This concentration ratio is related to the unknowns through the eigenvectors of (3) and the steady-state solutions of (1). The procedure used to analyze the data was to calculate as a function of K_2, values for σ_1, σ_2 and I_B/I_{In} based on the observed decay rates. The observed value of I_B/I_{In} was then used to determine the appropriate range of K_2 consistent with experiment, and using these K_2 values the cross sections were determined. This procedure was repeated at each temperature.

The results for the B equilibrium constant, K_2, are in agreement with the theoretical predictions of Eqn. 7 using a binding energy $E_2=3.3\pm0.2$ meV and a splitting $\Delta E_2=0$. This binding energy is about 20% lower than the values observed by other authors. Most of these other values were obtained using spectroscopic line positions, and do not rely on Eqn. (7). One possible source of the observed 20% discrepancy is that Eqn. (7) is too simple, since it neglects effects such as anisotropic FE bands and excited states of the BE resonant with FE states.

Shown in Fig. 3 are the cross sections measured in these experiments, along with previously reported values [3,4,27]. The error bars on the cross sections are the result of uncertainties in the various quantities used in the calculations, and include possible errors due to the residual P in the sample. We see that the In cross section continues to show a strong temperature dependence down to $T \approx 5$ K, in contrast with the mild temperature dependence of the B cross section. The B cross section measured here appears to be somewhat smaller than the Hammond and Silver results, although the difference is not significant within experimental error. It is surprising to see that for $T \approx 5$ K, the B cross section is an order of magnitude less than the In cross section. This is opposite to what is expected from consideration of the BE ground state binding energy, since the In BE is more tightly bound than the B BE and hence should have a smaller capture cross section.

In an effort to explain these large differences between the In and B cross sections, let us consider excited states of the BE and what effect these states may have on the results presented here. The BE spectrum for Si:In and Si:B has been previously investigated using both luminescence and absorption [6,11,14-16]. For Si:In a low energy triplet structure (ground state plus two excited states) has been observed as well as two highly excited states [14]. For Si:B the ground state appears to be split into a triplet [16], and no other

excited states have been observed. Calculations by Chang, et al [17] indicate

that the excitation energy of the 2s excited state of the outer particle, for

the case of Si:In, is comparable to the BE binding energy so that the state

might be bound. For Si:B the calculations indicate that this state is

definitely not bound. Inner particle excitations and multiple-particle

excitations may provide bound excited states.

It is straightforward to incorporate excited states into the rate equations

(1). One simply writes an equation for each state, the population of the

states being related by the transition rates between bound states and

the transition rates from bound to free states.————————————

———— A more common procedure (especially for the case of electron-donor capture)

is to analyze the decay rates (eigenvalues) on the basis of a single-level model

with one rate equation for the free species and one rate equation for each bound

species. The resulting capture cross sections are then interpreted as total

cross sections and are compared with that computed from the theory of cascade

capture, first developed by Lax [18], and extended by many authors [19-23].

Roughly speaking, the theory of cascade capture says that those levels bound

by energies greater than kT (lower levels) will contribute to the capture

process whereas those levels bound by energies less than kT (upper levels) do

not contribute to the total capture cross section. Particles captured in lower

levels are seen as rapidly losing their energy via phonon emission and moving

down to the ground state. Particles captured in upper states are quickly

ejected into the free states via phonon absorption. The total cross section,

σ_t, is computed from the cross sections of the individual levels, σ_j, by

$$\sigma_t = \sum_j S_j \, \sigma_j \qquad\qquad (8)$$

where S_j is the sticking probability of the jth level, defined as the probability

that a particle captured in the jth level will reach the ground state before being ejected into the free states. S_j is close to unity for the lower levels and close to zero for the upper levels.

It is clear that the total cross section defined by (8) is in no way rigorously related to that computed from experiment. As was originally pointed out by Lax, the very concept of a sticking probability implicitly makes some assumptions about the transition rates in the system, such that the captured particle reaches the ground state, or escapes, in a time that is small compared to the decay times in the experiment [18]. The validity of replacing a complete set of rate equations with just a single equation (for each impurity type) has been examined by Pickin [23] for the case of electron-donor capture. He shows that if the impurity concentration is low enough then the single rate equation is valid, with the capture rate being interpreted as a total capture rate (due to cascade capture) and the release rate as a total release rate (due to inverse-cascade). Direct calculation indicates that these total capture and release rates are related by detailed balance, using the ground state binding energy [24]. The reason that the ground state plays such an important role, even if most capture and release is via excited states, is that most of the population of the bound species resides in the ground state. Thus, when analyzing data in order to produce cross sections, it is only necessary to use one rate equation for each impurity type and one equation for the free species (e.g., as done in Eqn. (1)) even if there are excited states in the spectrum. Also, detailed balance (using ground-state energies) can be used to relate release and capture rates. The resulting cross sections must be interpreted as total cross sections (in the sense of Eqn. (8)) and may contain

small dependences on seemingly unrelated parameters, due to the approximations involved in defining a total cross section.

Now let us consider the case of interest, namely, acceptor bound excitons in silicon. The cross section of a single level, σ_j, is the integral over occupied FE states of the cross section for capture of a FE of energy ε into the jth level, $\sigma_{j\varepsilon}$;

$$\sigma_j(T) = \int_0^\infty f(\varepsilon,T) \, \sigma_{j\varepsilon} \, N(\varepsilon)d\varepsilon , \qquad (9)$$

where $f(\varepsilon,T)$ is the occupation of FE states and $N(\varepsilon)d\varepsilon$ is the density of FE states. Clearly Eqn. (9) will result in some temperature dependence of the σ_j, although $\sigma_{j\varepsilon}$ is not temperature dependent and is related to the matrix element of the electron-phonon interaction between neutral acceptor with FE state and the BE state. It seems reasonable that the temperature dependence expressed by (9) could account for the observed temperature dependence of the B cross section (see Fig. 3). However, the rapid variation with temperature of the In cross section must be due to highly excited states whose sticking probabilities contain the temperature dependence. The fact that σ_1 still varies rapidly at temperatures as low as 5 K suggests that the relevant excited states are bound by energies as small as about 1 meV. The 1.1544 eV line observed by Elliott, et al [14] for Si:In could play an important role in determining the magnitude of the capture cross section.

In conclusion, we have measured the boron BE equilibrium constant (ratio of release to capture rates) and the boron and indium FE capture cross sections, in silicon, for the temperature range 3.6 - 5.9 K. The B BE equilibrium constant is shown to agree with detailed balance results using a ground state binding energy of 3.3 ± 0.2 meV. The strong temperature dependence of the In cross

section, compared to that of B, probably results from highly excited states of the In BE. The concept of total cross sections and the effect of excited states in the temperature dependence of the total cross sections is discussed.

Scholar.

1. J. R. Haynes, Phys. Rev. Lett. **4**, 361 (1960).

2. M. Tajima, Appl. Phys. Lett. **32**, 719 (1978).

3. K. R. Elliott, D. L. Smith, and T. C. McGill, Solid State Comm. **24**, 461 (1978).

4. R. B. Hammond and R. N. Silver, Appl. Phys. Lett. **36**, 68 (1980).

5. Hall effect measurements were performed at Hughes Research Laboratories.

6. P. J. Dean, W. F. Flood, and G. Kaminsky, Phys. Rev. **163**, 721 (1967).

7. G. C. Osbourn and D. L. Smith, Phys. Rev. **B16**, 5426 (1977). The experimental value reported by Osbourn for the B(NP) oscillator strength is deduced from data in Ref. 6 and Ref. 26.

8. The uncertainty in the Auger rate, $1/\tau_2$, is estimated by calculating the difference between the decay rate, r_2, and the Auger rate for a very large range of capture cross sections and BE binding energies. The results demonstrate that $|r_2 - 1/\tau_2| < 0.005\ \mu s^{-1}$ for $T < 2.2$ K.

9. R. B. Hammond and R. N. Silver, Solid State Comm. **28**, 993 (1978).

10. J. C. Merle, M. Capizzi, P. Fiorini, and A. Frova, Phys. Rev. **B17**, 4821 (1978).

11. M. A. Vouk and E. C. Lightowlers, J. of Luminescence **15**, 357 (1977).

12. M. L. W. Thewalt, G. Kirczenow, R. R. Parsons, and R. Barrie, Can. J. Phys. **54**, 1728 (1976).

13. S. A. Lyon, D. L. Smith, and T. C. McGill, Phys. Rev. Lett. **41**, 56 (1978).

14. K. R. Elliott, G. C. Osbourn, D. L. Smith, and T. C. McGill, Phys. Rev. **B17**, 1808 (1978).

15. P. J. Dean, J. R. Haynes, and W. F. Flood, Phys. Rev. **161**, 711 (1967).

16. M. L. W. Thewalt, Can. J. Phys. 55, 1463 (1977).

17. Y. C. Chang and T. C. McGill, Solid State Comm. 32, 319 (1979).

18. M. Lax, Phys. REv. 119, 1502 (1960).

19. G. Ascarelli and S. Rodriguez, Phys. Rev. 124, 1321 (1961).

20. R. A. Brown and S. Rodriguez, Phys. Rev. 153, 890 (1967).

21. F. Belezany and G. Pataki, Phys. Stat. Sol. 13, 499 (1966).

22. W. Pickin, Solid State Elec. 21, 309 (1978).

23. W. Pickin, Solid State Elec. 21, 1299 (1978).

24. D. L. Smith, unpublished. For the case of several closely spaced states near the ground state the concept of a sticking probability must be generalized to include capture into such states as a "true capture event", and these states are assumed to be in thermal equilibrium with themselves.

25. W. Schmid, Phys. Stat, Sol(b) 84, 529 (1977).

26. R. Sauer and J. Weber, Phys. Rev. Lett. 36, 48 (1976).

27. H. Nakayama, T. Nishino and Y. Hamakawa, Jap. J. of Appl. Phys. 19, 501 (1980).

FIGURE CAPTIONS

Figure 1.   A typical luminescence spectra taken at 4.2 K of Si:In, B. An Ar$^+$ laser on all lines was used for optical excitation. The beam was unfocussed with a diameter of about 2 mm and a 3 mW power level.

Figure 2.   Decay rates of the In(NP) and B(TO) luminescence lines. Below 5 K the observed decays were exponential and the error bars are too small to show. Above 5 K the observed decays appeared to be the sum of several exponentials, with decay rates in the indicated range.

Figure 3.   The observed capture cross sections of free excitons on indium and boron impurities in silicon, as a function of temperature. The In cross section has roughly a T^{-4} temperature dependence, whereas the B cross section has a T^{-1} dependence.

PHOTOLUMINESCENCE SPECTRUM OF Si : In,B

$N_{In} = 6.8 \times 10^{12} \ cm^{-3}$
$N_B = 3.5 \times 10^{13} \ cm^{-3}$

$T = 4.2 K$

PUMP POWER = 3 mW CW

10× SLIT WIDTH

INTENSITY (arbitrary units)

ENERGY (meV)

B(TO)

P(TO)
B(LO)
FE(TO)
FE(LO)
B(TA)
In(NP)
P(NP)
B(NP)

Fig. 1
Feenstra,
et al

DECAY RATE OF THE Si:In AND Si:B BOUND EXCITONS AS A FUNCTION OF TEMPERATURE

EXTRAPOLATED Si:B BOUND EXCITON AUGER DECAY RATE

■ In (NP) 1.1409 eV
● B (TO) 1.0928 eV

65

Fig. 2
Feenstra
et al

EXCITON CAPTURE CROSS SECTIONS OF INDIUM AND BORON IMPURITIES IN SILICON

THIS WORK
HAMMOND, et al. (B)
ELLIOTT, et al. (In)
NAKAYAMA, et al. (B)

66

Fig. 3
Feenstra,
et al

APPENDIX B

DETERMINATION OF RELATIVE IMPURITY CONCENTRATIONS USING
PHOTOLUMINESCENCE: A CASE STUDY OF THE Si:(B, In) SYSTEM

Determination of relative impurity concentrations using photoluminescence: A case study of the Si: (B, In) system

G. S. Mitchard and T. C. McGill

California Institute of Technology, Pasadena, California 91125

We report on a systematic study of the use of photoluminescence for the determination of relative impurity concentrations. The system chosen for the study was Si with a shallow level, B, in the presence of a deeper level, In. The results show that, at sufficiently low concentrations, the photoluminescence intensities can be used to determine the relative impurity concentrations. At higher In concentrations ($N_{In} \gtrsim 10^{15}$ cm^{-3}) we find that exciton transfer from B to In results in a quenching of the B photoluminescence intensity. For $N_{In} > 2 \times 10^{16}$ cm^{-3}, B photoluminescence was not observed in any sample studied.

The development of photoluminescence as a method for evaluating semiconductor materials has been of interest for some time, mainly as a result of the convenience of the technique and its sensitivity to low impurity concentrations. Recently, attempts have been made to use photoluminescence as a quantitative tool for measuring impurity concentrations. At this point, only the Si:B, Si:P, and Si:(B,P) systems have been investigated, and only the low-concentration regime has been considered. Tajima[1] attempted an empirical calibration but failed to account for saturation effects, and as a result achieved only limited success. Nakayama *et al.*[2] considered low-level saturation effects (that is, creation of bound-multiexciton complexes) and produced a set of rate equations which were successfully used to model these systems in the low-concentration regime.

Often, however, it is necessary to determine concentrations of background impurities and defects at levels substantially below that of some majority dopant present at high concentration. The present work reveals that while the low-impurity-concentration case is well understood, effects resulting from multiple impurities at high concentrations lead to luminescence spectra which are much more difficult to interpret quantitatively in terms of impurity concentrations. Indeed, in the worst-case situation, the results indicate that it may not be possible to use photoluminescence in the evaluation of some semiconductor materials.

To systematically investigate the effects of high impurity concentrations in a multiple-impurity system, we undertook a careful study of one particularly interesting system: Si doped with B and In. Si: (B, In) was chosen as a model system for the study because heavily doped Si:In is a very important material for detector applications, and because the low-concentration photoluminescence properties of the Si:B and Si:In subsystems are relatively well understood. First, both B and In bound-exciton luminescence has been studied extensively, and the spectra are well characterized.[3,4] Also the decay mechanisms for excitons on B and In have been identified[5] and the decay rates have been measured.[6,7] Finally, the capture cross sections for excitons on B[8,9] and on In[9,10] have been determined as a function of temperature. In addition, the Si:In and Si:(B, In) systems are of current interest. Recently, very long-lived lines have been observed in the heavily doped Si:In spectrum,[11] and a multitude of low-energy lines have been observed in the heavily doped Si:(B, In) spectrum.[12] In the latter investigation, the anomalous absence of B luminescence in the Si:(B, In) spectrum was also reported, and was attributed to interaction between dissimilar acceptor bound-exciton states.

Measurements were made on crystals grown by the Czochralski and float-zone techniques. Impurity concentrations were determined from Hall-effect measurements performed at Hughes Research Laboratories, where the sam-

TABLE I. Samples of Si doped with In and B studied using photolumines-cence. The numbers identifying the samples correspond to the ingot number at Hughes Research Laboratories. All the concentrations were measured using the Hall experiment at Hughes Research Laboratories. The estimated accuracy is ± 25%.

Sample	N_B (cm^{-3})	N_{In} (cm^{-3})	N_B/N_{In}
Z20601	5.2×10^{12}	1.0×10^{17}	5.2×10^{-5}
C11204.T	1.4×10^{14}	1.3×10^{17}	1.1×10^{-3}
C11204.M	1.0×10^{14}	3.4×10^{16}	3.0×10^{-3}
Z20601R	9.8×10^{13}	4.3×10^{16}	2.3×10^{-3}
Z074	3.9×10^{13}	1.7×10^{16}	2.3×10^{-3}
C117	7.8×10^{13}	2.1×10^{16}	3.7×10^{-3}
C11204.S	6.3×10^{13}	1.3×10^{16}	4.8×10^{-3}
C112.M	4.2×10^{15}	2.4×10^{17}	1.8×10^{-2}
Z20601A	1.9×10^{14}	5.5×10^{15}	3.5×10^{-2}
Z104011	2.7×10^{13}	2.0×10^{14}	1.1×10^{-1}
Z163.T	3.9×10^{13}	2.2×10^{13}	1.8
C120A	8.2×10^{16}	2.0×10^{16}	4.1
Z163.S	3.5×10^{13}	6.8×10^{12}	5.1

ples were grown. The samples studied and their impurity concentrations are given in Table I. The crystals were me-chanically lapped and chemically etched, and then mounted in a Janis variable-temperature cryostat. The luminescence resulted from optical excitation by a Spectra-Physics model 166 Ar$^+$ laser operated in the cw mode. The output was varied from 1 mW–2 W depending on the details of the mea-surement being made. The laser spot size was estimated to be about 3 mm in diameter. The luminescence was collected from the edge of the sample, wavelength analyzed with a Spex model 1269 spectrometer, and detected with an RCA S-1 photomultiplier cooled to liquid-nitrogen temperature. The photomultiplier output was processed with standard photon counting electronics acquired on a Nuclear Data ND-60 multichannel analyzer, and finally passed to a PDP 11/34 computer for analysis and storage.

Typical spectra obtained in this manner are shown in Fig. 1. Figure 1(a) is a spectrum of sample Z163.S, the most lightly doped sample studied, and Fig. 1(b) is a spectrum of sample C120A, the most heavily doped sample from which B bound-exciton luminescence could still be observed. Lu-minescence lines due to free-exciton (FE) and B, P, and In bound-exciton recombination are visible in the no-phonon (NP), transverse-acoustic-phonon (TA), longitudinal-opti-cal- phonon (LO), and/or transverse-optical-phonon (TO) replicas. In addition, the first B bound multiexciton complex b_1 is visible in the TA and TO replicas. Finally, the previous-ly reported[11,13] long-lived luminescence line "P" and the lower-energy In luminescence line U 1 can be seen in the NP region.

To isolate the effects of impurity concentration and simplify the subsequent analysis, it was necessary to elimi-nate saturation effects from the luminescence intensity mea-surements. The initial investigations were designed to deter-mine the experimental conditions under which the assumption of no saturation effects is justified. Simple con-siderations indicate that bound-exciton luminescence inten-sity varies linearly with pump power when saturation effects are absent. Therefore measurements of the pump-power de-

pendence of the integrated luminescence intensity of the TO replica of the B bound exciton ($I_{B^{TO}}$) and the NP replica of the In bound exciton ($I_{In^{NP}}$) were made on each sample stud-ies. This determined the range of pump powers for which linear luminescence response and therefore absence of satu-ration effects could be expected. Care was then taken to en-sure that subsequent measurements were made under pump-power conditions for which there were no saturation effects.

Once the correct pump-power range was established for each sample, the dependence of the ratio

$$R_{BIn} = \left(\frac{I_{B^{TO}}}{I_{In^{NP}}}\right)\left(\frac{N_{In}}{N_B}\right) \qquad (1)$$

on the B concentration (N_B) and In concentration (N_{In}) was investigated. Measurements of R_{BIn} were made at 4.2 K for all the samples given in Table I. The results are summarized in Fig. 2, which is a plot of R_{BIn} vs N_{In}. As can be seen from Fig. 2, within experimental error R_{BIn} is independent of N_{In} for N_{In} between 6×10^{12} and about 10^{15} cm^{-3}. However, for $N_{In} > 10^{15}$ cm^{-3}, we observe that R_{BIn} decreases with in-creasing N_{In}. For $N_{In} > 2 \times 10^{16}$ cm^{-3}, we were not able to observe B^{TO} luminescence in any of our samples, and there-for no points are plotted in Fig. 2.

To explain this behavior, we propose that some direct interaction between the B and In impurities begins to occur in the high-concentration regime, which probably takes the
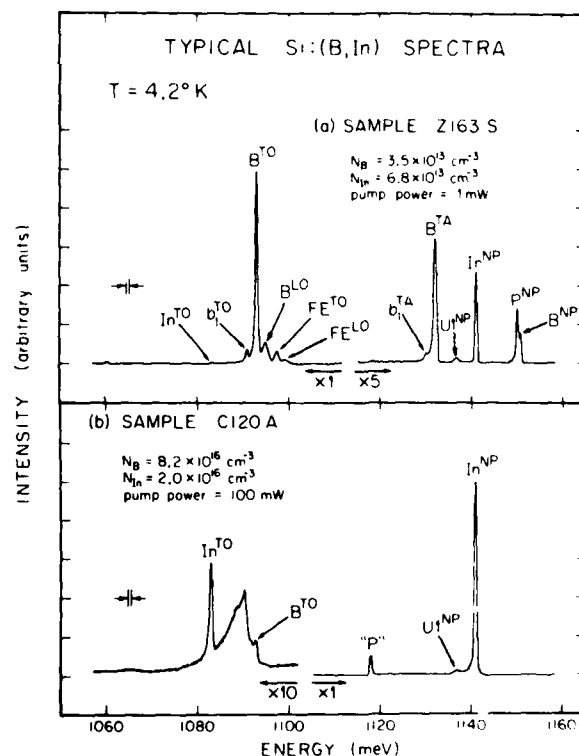

FIG. 1. Spectra of two Si:(B, In) samples included in this study. (a) Sample Z163.S, the most lightly doped sample. (b) Sample C120A, the most heavily doped sample from which B luminescence could still be observed. Refer to the text for an explanation of the line assignments.
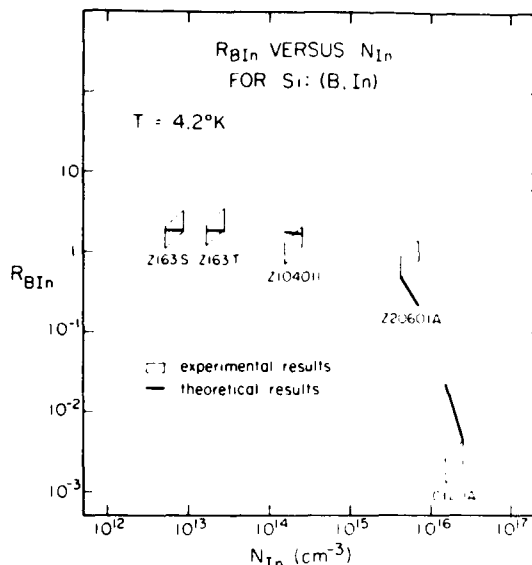
70

R_BIn VERSUS N_In
FOR Si: (B, In)

T = 4.2°K

FIG. 2. Ratio $R_{BIn} = (I_{B}.../I_{IN}\cdot)(N_{In}/N_{B})$ as a funtion of N_{In}. Experimental and theoretical results are shown. The parameters for the various samples are given in Table I. For $N_{In} > 2 \times 10^{16}$ cm^{-3}, B luminescence was not observed, and hence no points are plotted. The error regions for the experimental points are based on estimated of the error in N_{B}, N_{In}, I_{B}, and I_{In}. The variation in the calculated theoretical result for each sample is primarily a result of the uncertainty in N_{In}.

form of an exciton transfer process between a B bound exciton and a nearest-neighbor In. We include this process in a set of rate equations which describe the system in the absence of saturation. The steady-state result is

$$R_{BIn} = \int_0^\infty \frac{P(r)}{1 + w(r)} dr$$
$$\times \left(1 + \frac{\sigma_B}{\sigma_{In}} \frac{N_B}{N_{In}} \int_0^\infty \frac{w(r)P(r)}{1 + w(r)} dr\right)^{-1} R_{BIn}^0, \qquad (2)$$

where R_{BIn}^0 is the value R_{BIn} in the absence of transfer, the σ are free-exciton capture cross sections, $P(r)dr$ is the probability that the nearest neighbor In from a given B is between r and $r + dr$, and $w(r)$ is the ratio of the transfer rate to the total B bound-exciton decay rate. We take $\sigma_B/\sigma_{In} \approx 0.1$ at 4.2 K,[9]

$$P(r)dr = 4\pi r^2 dr N_{In} \exp(-\tfrac{4}{3}\pi r^3 N_{In}), \qquad (3)$$

(Ref. 14) and assume

$$w(r) = 10^7 e^{-r/r_o}, \qquad (4)$$

which is consistent with observations of exciton transfer in GaP:N.[15] Then Eq. (2) is fit to the data to obtain r_0 and R_{BIn}^0.

Good agreement has been obtained for $r_0 = 27$ Å and $R_{BIn}^0 = 1.8$. These results are also shown in Fig. 2.

In conclusion, we have attempted a quantitative analysis of the Si:(B, In) photoluminescence spectrum in the high In concentration regime. The results demonstrate that above In concentrations of about 10^{-15} cm^{-3} direct interimpurity interactions become important. A model based on exciton transfer from B to In is consistent with the experiment data. Of course another possibility is an interaction which results in the formation of (B, In) impurity complexes. We are currently investigating this process. In any event, the result is a quenching of the B luminescence at high concentrations. Consequently, it appears that photoluminescence may not be particularly useful for measuring concentrations of a second impurity in the presence of another dopant at much higher concentrations.

[1] M. Tajima, Appl. Phys. Lett. 32, 719 (1978).
[2] H. Nakayama, T. Nishino, and Y. Hamakawa, Jpn. J. Appl. Phys. 19, 501 (1980).
[3] See, for example, K. Kosai, and M. Gershenzon, Phys. Rev. B 9, 723 (1974).
[4] See, for example, S. A. Lyon, D. L. Smith, and T. C. McGill, Phys. Rev. B 17, 2620 (1978); K. R. Elliott, G. C. Osbourn, D. L. Smith, and T. C. McGill, ibid. 17, 1808 (1978).
[5] G. C. Osbourn and D. L. Smith, Phys. Rev. B 16, 5426 (1977).
[6] S. A. Lyon, G. C. Osbourn, D. L. Smith, and T. C. McGill, Solid-State Commun. 23, 425 (1978).
[7] W. Schmid, Phys. Status Solidi B 84, 529 (1977).
[8] R. B. Hammond and R. N. Silver, Appl. Phys. Lett. 36, 68 (1980).
[9] R. M. Feenstra and T. C. McGill, Solid-State Commun. (in press).
[10] K. R. Elliott, D. L. Smith, and T. C. McGill. Solid-State Commun. 24, 461 (1977).
[11] G. S. Mitchard, S. A. Lyon, K. R. Elliott, and T. C. McGill, Solid-State Commun. 29, 425 (1979).
[12] U. O. Ziemelis, R. R. Parsons, and M. Voos, Solid-State Commun. 32, 445 (1979).
[13] K. R. Elliott, S. A. Lyon, D. L. Smith, and T. C. McGill, Phys. Lett. A 70, 52 (1979).
[14] P. Hertz, Math. Ann. 67, 387 (1909).
[15] P. J. Wisner, R. A. Street, and H. D. Wolf, Phys. Rev. Lett. 35, 1366 (1975).

APPENDIX C

APPLICATION OF THE MOSFET DEVICE STRUCTURE IN
CHARACTERIZING INDIUM-DOPED SILICON

by

Dr. Leonard (Len) Forbes
Department of Electrical Engineering
University of California at Davis
Davis, California 95616

Abstract

C. T. Sah has published a review article demonstrating the appli-
cation of high-frequency small signal capacitance and current tran-
sients of a space charge layer which is depleted of carriers as a
powerful technique in characterizing deep level imperfection center
concentrations, energy levels, thermal and optical emission rates, and
thermal capture cross sections. Extensions of this work have also
led to the development of semi-automated "deep level transient spec-
troscopy techniques" by D. V. Lang et al., again based on capacitance
transients.

This report describes an extension of these techniques in using
the MOSFET device structure in performing the same characterizations
and extension of these techniques to shallower levels. The MOSFET
device structure is particularly convenient for low temperature mea-
surements of shallower levels where deionization occurs and the substrate
becomes highly resistive, seriously limiting capacitance transient
techniques. Examples are given by results on indium-doped silicon,
such as employed in extrinsic infrared detectors.

The indium concentration was found by variation of the MOSFET
threshold voltage with substrate bias, (4 to $6 \times 10^{16}/cm^3$) reverse
bias junction capacitance measurements, (5 to $7 \times 10^{16}/cm^3$) and resis-
tance versus temperature (6 to $8 \times 10^{16}/cm^3$). The indium concentrations
found were typically a factor of two less than concentrations found
using Hall measurements (1 to $2 \times 10^{17}/cm^3$). This difference in con-
centrations obtained is explained by Schroder as due to an unknown factor in
determining the scattering factor, r used in the Hall calculations.

The emission time constant of holes from the neutral indium center has been found to depend on the indium doping. Measurements on lightly doped samples yield a value for the emission rate, $1/e_p$, of 6.0 miliseconds at 77°K and a thermal activation energy of 0.15eV. These results correspond well with those previously published for the indium center in silicon. Measurements on heavily doped samples yield values of $1/e_p$ of 20 microseconds at 77°K and an activation energy of 0.117eV. All of the indium centers in the heavily doped samples decay with the 0.117eV energy indicating the 0.117eV is associated with all indium centers, not a small fraction of the centers. These results are consistent with the Poole-Frenkel effect describing field enhanced thermal emission of holes from the indium center.

Measurements of the hole capture coefficient at 77°K yields values for, c_p, of 3.7×10^{-7} cm^3/sec where the hole concentration as determined by resistance of the sample is used. These measurements have been made on the heavily doped samples, however, because of the particular technique used the capture coefficient measured is the zero field or quasi-equilibrium value. Measurements by Blakemore in 1956 gave a value for c_p of 1.0×10^{-6} cm^3/sec. The temperature dependence of the hole capture coefficient has also been found to be T^{-4}.

Small transients in the thermal emission rate measurements have been observed. These transients have associated with them, thermal 0.11eV level as reported by Hughes Research Labs after accounting for barrier lowering by the Poole-Frenkel effect. This level has been found to have a capture coefficient of around 1.5×10^{-6} cm^3/sec at 35K.

Applications of the results are shown in calculating and determining experimentally the frequency response of indium-doped silicon photoconductive infrared detectors.

Table of Contents

77

I. Introduction

Indium [1] is being used as a deep impurity in silicon devices
for use as infrared detectors. An accurate description of the
effects of indium in silicon is necessary for designing these
devices and predicting their performance. This report discusses and
presents work done to determine the characteristics of indium-doped
silicon. The properties that have been examined are the impurity
concentration, the thermal emission time constant of holes from the
impurity, the capture time constant of holes, the capture coefficient
and its temperature dependence, and a unique determination of the energy
levels of the impurity indium in silicon, including an investigation
of the "x-level" or 0.11eV level in indium doped silicon.

Particular attention in this work at the University of California
at Davis has been given to the application of the MOSFET device structure
in characterizing impurity levels in indium-doped silicon.

The indium center exists in two distinct charge states. The
neutral charge state occurs when the indium center is occupied by a
hole. The loss of a hole to the valence band corresponds to ionization
of the indium or emission of a hole from the indium. This process
leaves the indium center in a negative charge state. This ionization
will occur as a result of any photo or thermal excitation of sufficient

energy. Within a depletion region only the emission of holes from the impurity is possible, since no free holes are present for recapture. Since thermal emission is a strong function of temperature, it can be eliminated by adequate cooling. Optical emission can be eliminated by proper shielding.

This work demonstrates the utility of the MOSFET structure as a tool for characterizing deep impurity centers in silicon. This technique, along with capacitance methods, are more fully discussed in separate references by Sah, Schulz and Lang [2,3,4,5,6,7,8]. Results presented probably represent the most extensive treatment to date of indium-doped silicon. Energy level lowering was found in the samples as a result of the Poole-Frenkel effect. The new .11eV level reported by Hughes is believed to be present but modified by the Poole-Frenkel effect. [22]

Indium-doped silicon wafers were supplied by Hughes Research Labs (HRL) and Westinghouse. The MOSFET and resistor structures were designed and fabricated in the University of California, Davis, Solid State Devices Laboratory. The work was sponsored by the Defense Advanced Research Projects Agency, through HRL who provided materials and Hall characterizations.

II. Characterization Method

A. Theory of Operation

Characterization of deep level impurity centers in semiconductor material is done using many different methods. Techniques employed involve Hall measurements, optical absorption measurements, and conductivity measurements. The techniques or methods for measuring the properties of deep level impurities employed in this research are relatively

new [2]. These techniques were first developed in 1970 [9] and have
been developed extensively [11,2]. These methods are extremely
sensitive and the experimental data can be unambiguously interpreted.
Considerable simplification of the experimantal instrumentation can
be achieved by using these methods. These new techniques involve
electron and hole interaction in depletion charge regions at impurity
centers in semiconductors. C. T. Sah [2] has written an extensive
discussion of these new techniques.

The region of fixed ionic charges which consist of bound impurity
atoms in a semiconductor crystal lattice is known as the space-charge
or depletion region. The depletion region has no free charges within
it. Charges can only be found at impurity or trapping centers other-
wise they are swept out by the electric field which is always present
in the depletion regions. The space-charge region associated with a
MOSFET can be used for the characterization of impurity centers in
silicon. The MOSFET has been shown to be very useful for the charac-
terization of impurities in silicon [12,13,14].

The MOSFET structure shown in Figure 1 has been employed for many
of the experiments presented in this thesis to characterize the indium
impurity in silicon. The resistor structure shown in Figure 1, along
with the Infrared Field Effect Transistor (Irfet) device is used to
characterize the doping concentration of the impurity indium in silicon.

There are four basic transitions possible in a single energy level
impurity center: electron emission e_n, electron capture c_n, hole
emission e_p, and hole capture c_p. These four processes for the indium
center in silicon are shown in Figure 2. The Schockley, Read, Hall,
model equations describe the rates of these transitions with respect to
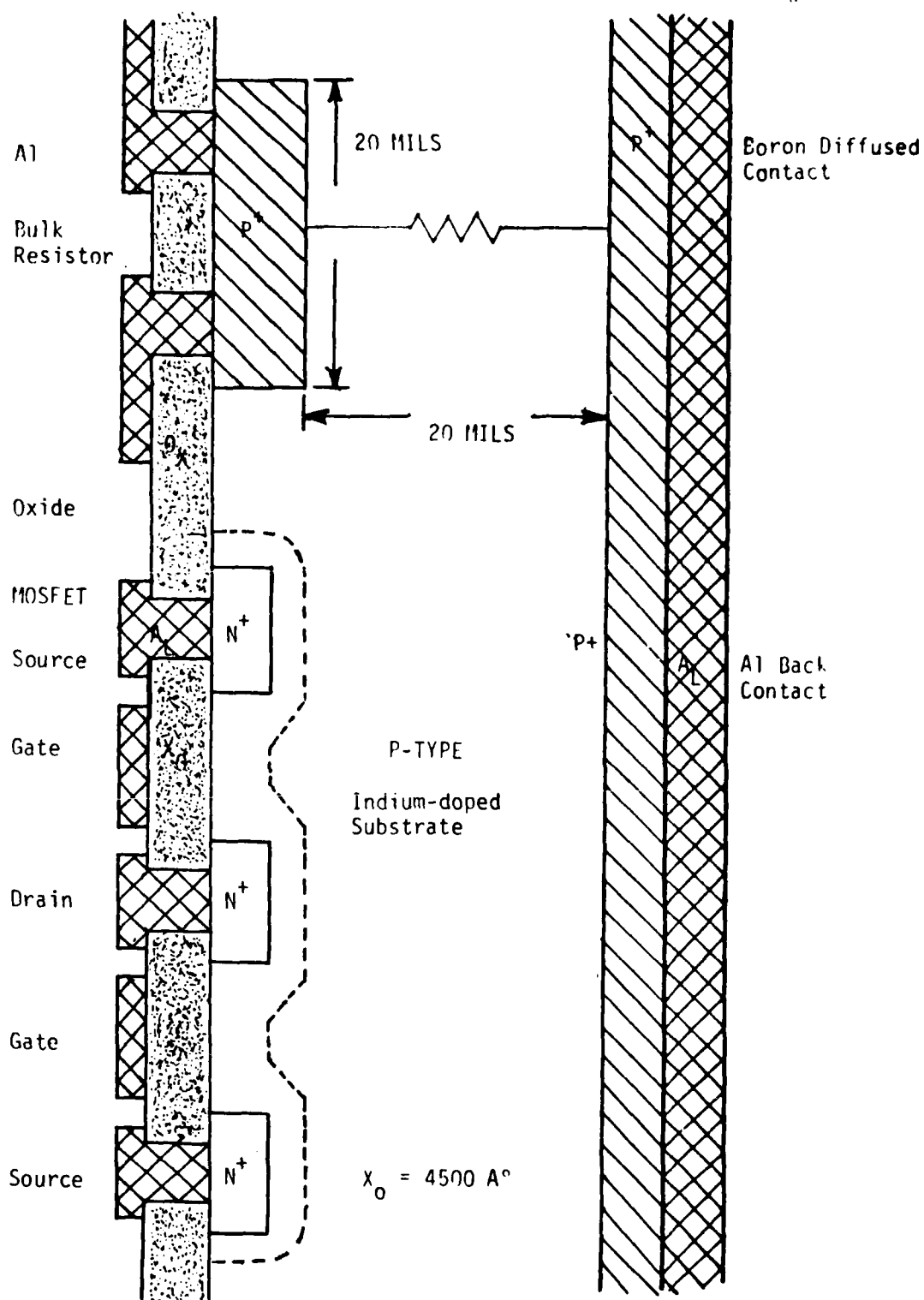time [15]. Energy sufficient to cause these transitions to occur can
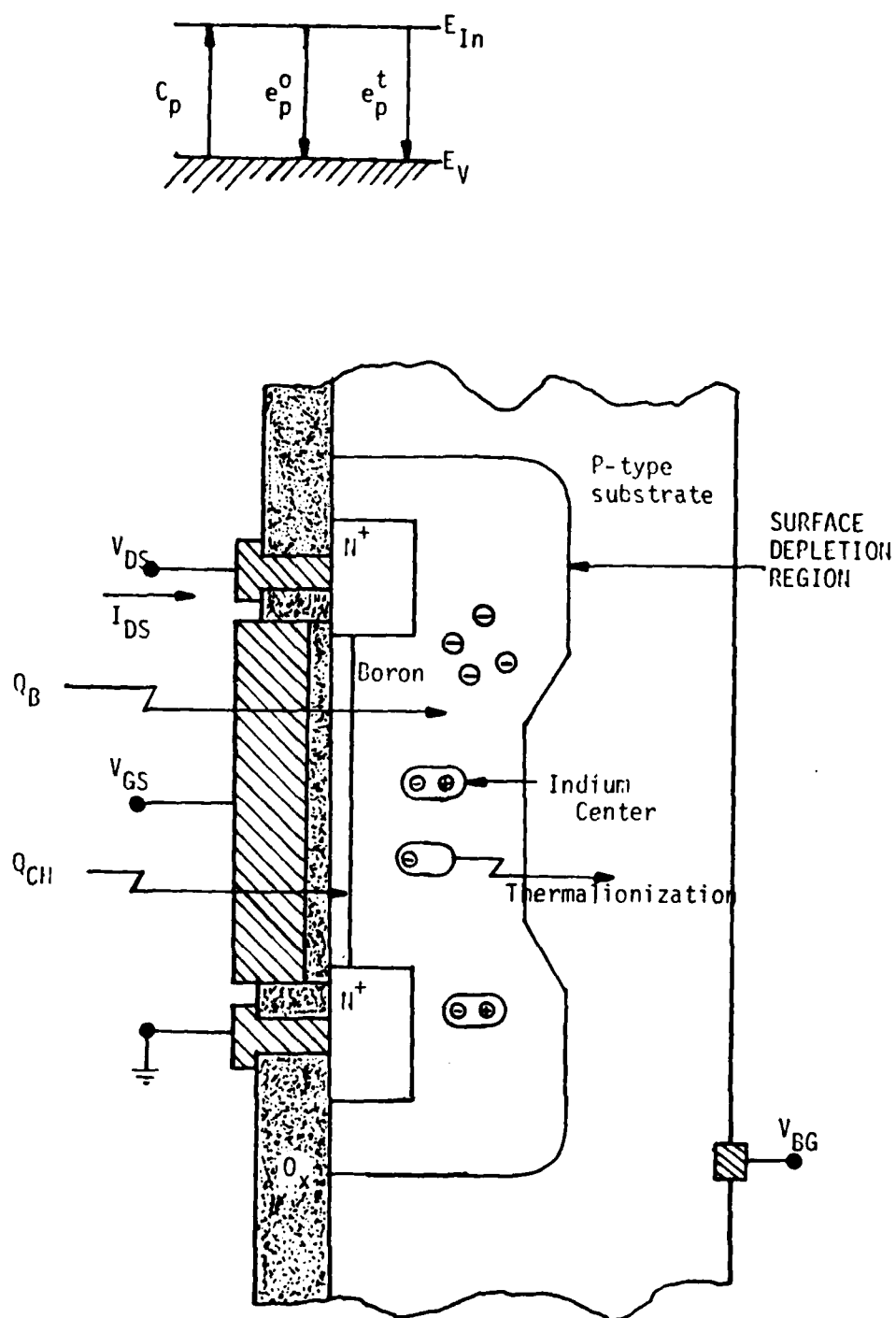
Fig. 1. Illustration of Device Cross Sections

Fig. 2   Illustration of Thermalionization of Indium

Centers in Depletion Region of MOSFET

come from optical or thermal energy sources. Since indium exists as an acceptor site in silicon the dominant transitions will be hole capture and hole emission to the valence band.

Methods of measuring capture and emission rate coefficients using this new method can be developed from a simplified expression of the rate equations [2]. That is, the change in the total number of ionized impurity states with respect to time is

$$\frac{dn_T}{dt} = -(c_n n + e_n + c_p p + e_p)n_T + (c_n n + e_p)N_{TT} , \qquad (1)$$

where N_{TT} is total concentration of the impurity in the sample. This rate equation can be linearized if the electron and hole concentrations are zero or constant. This condition exists in the depletion region of a MOSFET, Schockley barrier junction, or a p-n junction. The linear system is most accurate for measuring fundamental kinetic parameters. This is true because a linear system can exhibit exponential decay with time from any initial perturbation. Some unique features of this technique are that decay time constants are independent of the hole concentration, and the system decay is a true exponential. Thus, the reciprocal of the decay time is [2]

$$\frac{1}{\tau} = c_n n + e_n + c_p p + e_p . \qquad (2)$$

Certain transitions dominate depending upon the temperature of the sample, the relative position of the energy level, the electric field and the optical excitation. Careful selection of the operating conditions allows values for each of the terms in eqn. (2) to be determined.

Two types of transients are caused by changing of the charge state of the impurity center in the depletion region. The first is a current
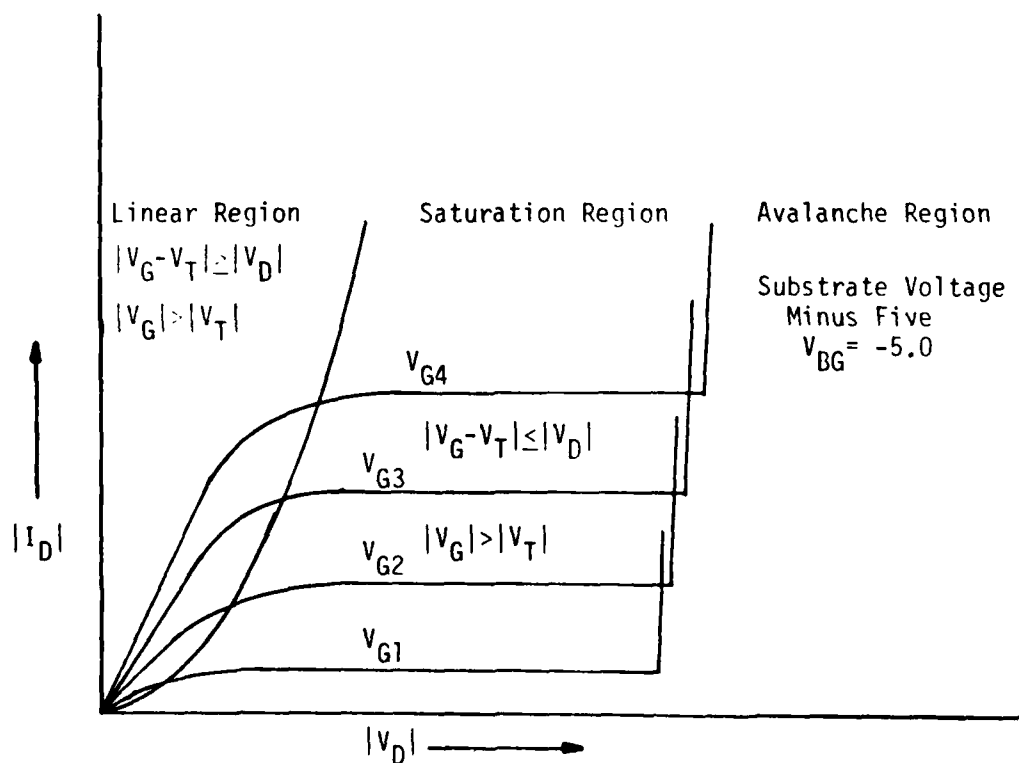
transient due to the loss or the increase of the number of free
carriers available for conduction. The second is a small-signal high
frequency change in the capacitance. We will indirectly measure the
change in charge state by measuring the change in channel conductance
with reference to the indium impurity in silicon.

If a MOSFET is initially biased off by the application of a large
reverse bias substrate voltage, then the indium center will be negative-
ly charged. The indium center in a negative charge state corresponds
to the emission of a hole into the valence band of silicon. A deep
depletion region will exist with a large reverse bias voltage. The
indium centers in this depletion region are initially negatively
charged. The reverse voltage is now reduced by several volts. As the
depletion region collapses, the negative indium centers capture holes
from the valence band and become neutrally charged. The time for the
depletion region to reach a new equilibrium will be limited by the
time constant of capture of holes by the indium center. The change in
charge state of the indium center will change the threshold voltage of
the MOSFET and thus change the conductance of the channel.

If the reverse bias voltage is increased again, the reverse process
will occur. The trapped holes are emitted by thermal excitation of the
indium impurity level to the valence band of the silicon. Thermal ion-
ization will be dominant if the sample is shielded from optical excita-
tion. The time for all the indium centers to emit a hole is limited by
the hole emission time constant for the indium centers. The neutral
indium centers will emit holes until the deep depletion region is formed
to balance the electric field created by the increase of the reverse
bias voltage. An examination of the MOSFET device equations is necessary
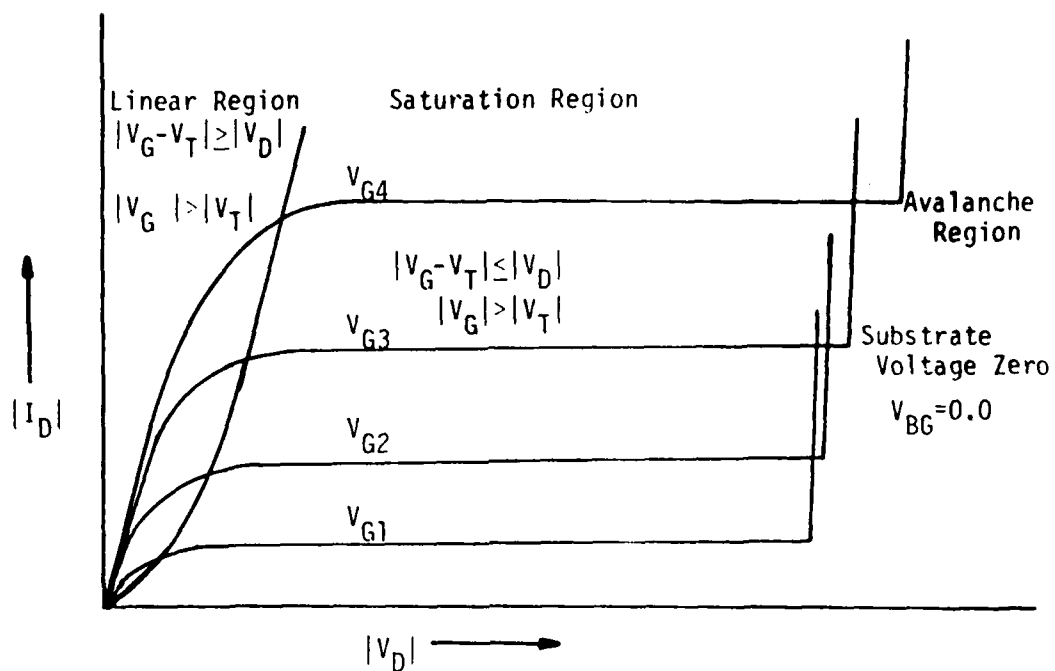
a) Fig. 3 I,V Characteristics of MOSFET with Zero Substrate Voltage

Linear Region   Saturation Region

$|V_G-V_T|\geq|V_D|$

$|V_G|>|V_T|$

$|V_G-V_T|\leq|V_D|$
$|V_G|>|V_T|$

V_{G4}

V_{G3}

V_{G2}

V_{G1}

Avalanche Region

Substrate Voltage Zero
$V_{BG}=0.0$

$|I_D|$

$|V_D|$

b) Fig. 3 I,V Characteristics of MOSFET with -5 Volt Substrate Voltage

Linear Region   Saturation Region   Avalanche Region

$|V_G-V_T|\geq|V_D|$

$|V_G|>|V_T|$

Substrate Voltage
Minus Five
$V_{BG}=-5.0$

V_{G4}

$|V_G-V_T|\leq|V_D|$

V_{G3}

V_{G2} $|V_G|>|V_T|$

V_{G1}

$|I_D|$

$|V_D|$

to explain how the indium charge state effects channel conductance.

B. Device Equations

The two basic operating regions of the MOSFET are the linear and saturation regions. Figure 3 shows typical characteristic curves of a MOSFET and points out the operating regions. Equations relating drain to source current to drain voltage and gate voltage are well-known. These equations are found in many solid-state device books [16,17,18,19].

In the linear region of operation, $V_{GS}-V_T > V_{DS}$, the device equation is expressed as

$$I_{DS} = \beta V_{DS}(V_{GS}-V_T-V_{DS}/2) \quad , \qquad (3)$$

where $\beta = \mu C_0 W/L$ and μ is the effective surface electron mobility in an n-channel device. The geometric width to length ratio is W/L. The gate oxide capacitance per unit area C_0 can be calculated from $C_0 = k_{OX} \varepsilon_0/X_0$ where k_{OX} is the relative dielectric constant of silicon dioxide and x_0 is the oxide thickness. Since the linear region is simplest to employ it will be used to characterize the impurity centers.

The saturation region of operation, $V_{GS} - V_T \leq V_{DS}$ and $V_{GS} > V_T$ can be described by the following equation

$$I_{DS} = \beta(V_{GS}-V_T)^2/2 \quad . \qquad (4)$$

There will be a greater change in the conductance with the change of impurity charge states in the saturation region because, the terms that cause this change are squared. Since greater response is desired in the operation of the infrared detector further emphasis would be placed on this equation, in such applications but not here.
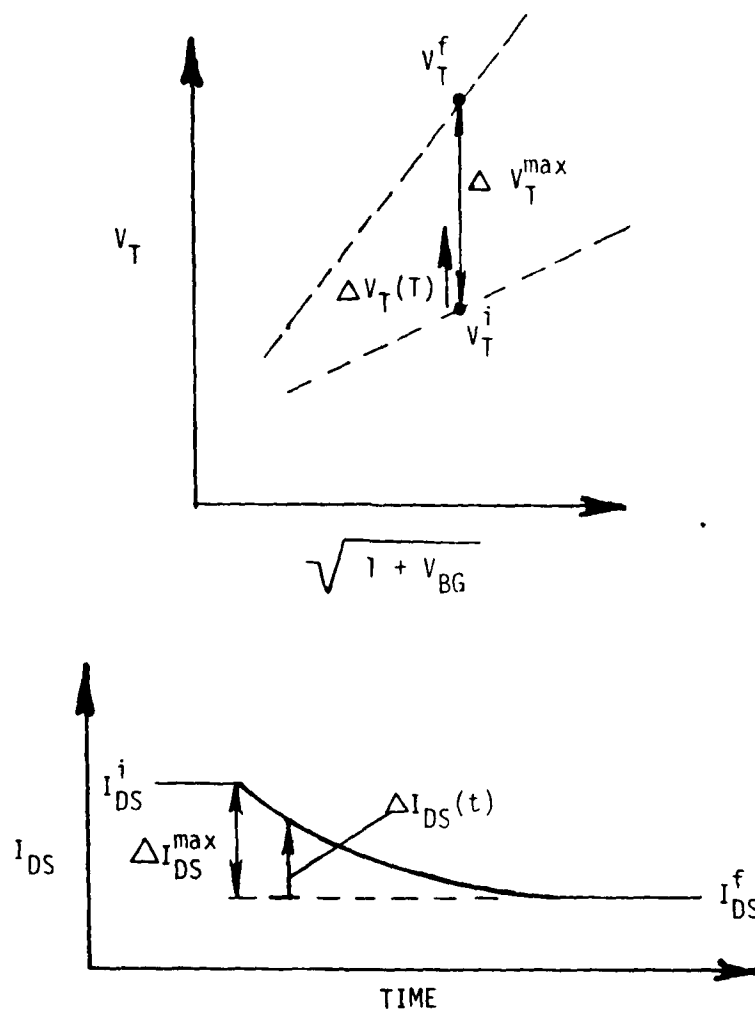
Fig. 4. Illustration of the change in threshold voltage and drain current of the MOSFET device due to the emission of holes from initially neutral centers in the surface depletion region.

The third equation describing MOSFET operation and the most important for demonstrating the effect of the change in charge state describes the threshold voltage,

$$V_T = A + B(1-V_{BG})^{1/2}[N_B]^{1/2} \tag{5}$$

$$A = V_{FB} + 2\emptyset_f \quad . \tag{6}$$

V_T is the threshold voltage and A and B are parameters which depend upon the design and processing of the MOSFET. Application of a voltage through the backgate V_{BG} or substrate causes a change in the threshold voltage and the channel current. The number of ionized impurity centers in the surface space charge or depletion region N_B can change the threshold voltage and finally the device current.

In the case of indium doped devices operated at low temperatures, N_B is time dependent with the applied voltage conditions. N_B is the, combination of the number of shallow level impurity centers N_A, for instance boron, and ionized deep level centers N_I where

$$N_B = N_A + N_I[1-\exp(^{-t}/\tau)] \quad . \tag{7}$$

Thus, if the indium centers are neutral initially, then $N_B = N_A$ at $t = 0$. If the indium centers are now all thermally or optically ionized, then $N_B = N_A + N_I$. The time constant depends upon the dominant excitation process.

A static change in the threshold voltage, ΔV_T, caused by the change in the indium charge state is

$$\Delta V_T = V_T{}^f - V_T{}^i = B(\sqrt{N_a + N_{IN}} - \sqrt{N_a}) \quad , \tag{8}$$

88

where V_T^i is the initial threshold voltage and V_T^f the final threshold voltage. A time dependent expression for the threshold voltage can now be written by use of the preceding equations.

$$V_T(t) = V_T^i + \Delta V_T(t) = A + B(1-V_{BG})^{1/2}[N_A]^{1/2}$$
$$+ B\left(\left|N_A+N_I[1-\exp(^{-t}/\tau)]\right|^{1/2} - [N_A]^{1/2}\right) \quad . \tag{9}$$

Finally, an equation can be developed relating the time dependent change of the indium charge state in the depletion region to the drain to source current [20],

$$I_{DS}(t) = I_{DS}^f + \Delta I_{DS}(t) \tag{10}$$

$$I_{DS}^f = \beta V_{DS}(V_{GS}-V_T^f-V_{DS}/2) \tag{11}$$

$$\Delta I_{DS}(t) = (\mu C_0(W/L)V_{DS}\Delta V_T^{max}(1-[1-\exp(t/\tau)]^{1/2}) \quad . \tag{12}$$

The equation for current in the linear region has been employed since this is the region of operation most appropriate to characterization of the impurity center [13]. Figure 4 illustrates the change of device current and the change of the threshold voltage due to the change of the impurity charge state in the depletion region.

C. The MOSFET Structure

Consideration should be given now to the MOSFET device and its characteristics that affect impurity characterization. The MOSFET structure shown in Figure 1 is a three terminal device (exclusive of the gate) where the surface conductivity between source and drain is measured. The substrate contact serves only to establish the substrate voltage bias or potential at low temperatures. The leakage current

drawn through the substrate is immeasurably small due to the high substrate impedance at low temperatures. Thus, measurements can be made with the MOSFET structure even though the substrate is deionized and has a high impedance. The MOSFET structure is ideally suited for measurements on single impurity material such as indium or gallium doped silicon with only residual impurity dopings of shallow level acceptors. Residual impurities such as boron and other imperfection centers have been observed in the extrinsic silicon photoconductive detectors. In fact, the concentration of such residual impurities can be easily determined as has been demonstrated [13].

The resistance of the sample can be calculated by using the detailed balance relationship to obtain the hole concentration

$$c_p p \, N_T = e_p P_T , \qquad (13)$$

where N_T is the number of ionized indium centers; P_T the number of neutral indium centers; $P_T + N_T = N_{TT}$ the total number of indium centers; p, the hole concentration; c_p, the hole capture coefficient at neutral centers; and e_p, the hole emission rate [2]. The assumption has been made that no other impurity except indium is present. Since charge neutrality requires

$$p = N_T , \qquad (14)$$

then it can be shown for low temperatures where only a fraction of the indium is ionized, p is approximately

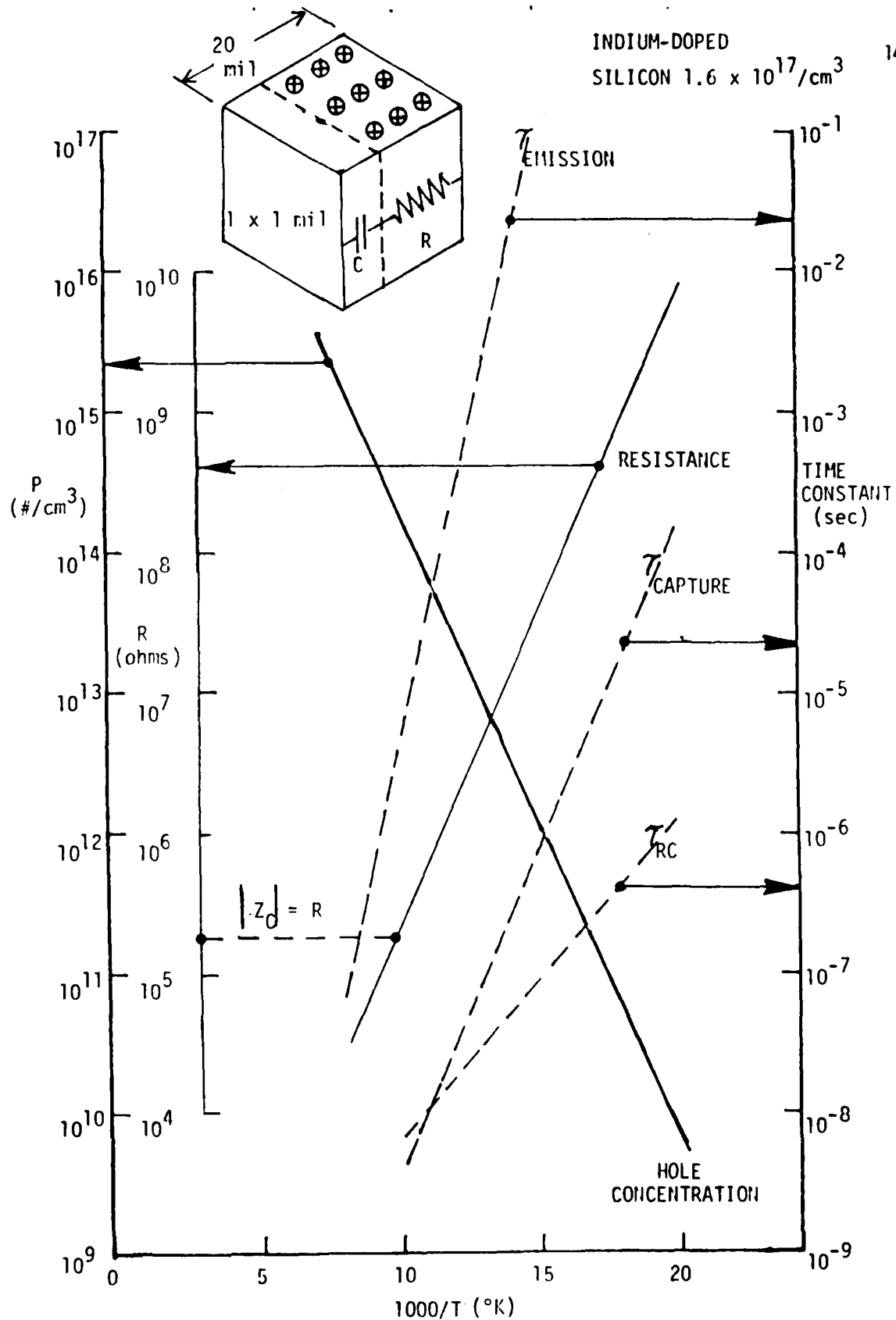$$p \cong (e_p N_{TT}/c_p)^{1/2} . \qquad (15)$$

Fig. 5. Calculated hole concentration and resistance of an indium-doped silicon sample and illustrations of the emission, capture, and RC time constants as a function of temperature.

The calculated resistance of an indium doped sample with $N_{TT} = 1.6 \times 10^{17}/cm$, with an area of 1.0 square mil, 20 mil thickness and assuming a mobility of 1000 cm^2/V sec is shown in Figure 5. The emission rate has been taken from an extrapolation in the literature [13] and the capture coefficient taken to be $10^{-6} cm^3/sec$ [21]. It is clear that the sample becomes highly resistive at low temperatures.

Figure 5 also demonstrates the temperature at which the magnitude of the 1.0 MHz impedance of the capacitance of a zero biased junction at room temperature, Z_c, becomes equal to the substrate impedance. At this temperature, 100°K, most high frequency capacitance techniques would become difficult to employ, thus, limiting their usefulness in characterizing a single energy level doped sample.

The emission time constant [13] is also shown in Figure 5

$$\tau \text{ emission} = {}^1/e_p \qquad (16)$$

and the capture time constant [2] assuming $c_p = 10^{-6} cm^3/sec$

$$\tau \text{ capture} = 1/(c_p p + e_p) . \qquad (17)$$

In addition to these time constants there is an RC time constant in the MOSFET device structure (and p-n junctions) associated with the capacitance of the depletion region and the resistance of the substrate. This time constant is shown in Figure 5 for the indium doped sample with an applied bias of 9 volts and using the initial value of N_T.

The capacitance of a depletion region initially formed on a de-ionized substrate will be

$$C = (qN_T/[K_s\varepsilon_0]2(V_0 + V_{RB}))^{1/2} \qquad (18)$$

where q is electronic charge, $K_s\varepsilon_0$ the electric permitivity and

$(V_0 + V_{RB})$ is the total potential drop. After initial formation of the depletion region neutral indium will become ionized in the depletion region due to the thermal emission of holes resulting in a collapse of the initially very wide depletion region. This will cause a large increase in the capacitance and the RC time constant. In order to observe capture by using pulse techniques one must have

$$\tau_{RC} \ll \tau_{capture} \tag{19}$$

or

$$K_s \epsilon_0 \, {}^d\!/q \, \mu \, W_d N_T \ll {}^1\!/c_p \quad , \tag{20}$$

where d is the thickness of the sample and W_d is the depletion region width. While this can be insured at low temperatures on reverse biased junctions with wide depletion regions it cannot be insured for narrow depletion regions at high temperatures.
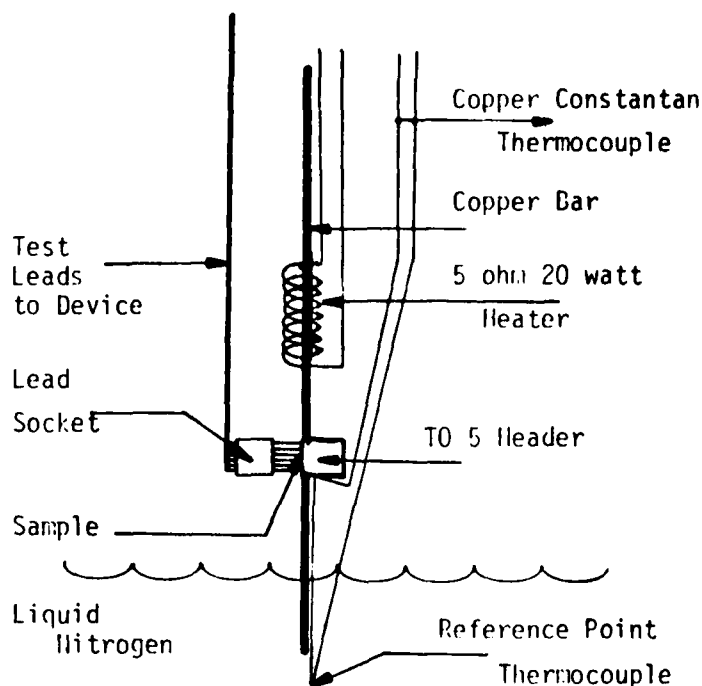
III. Experimental Methods and Techniques

Measurements were made on specially doped indium wafers prepared by Hughes Research Lab., Malibu, CA and on wafers supplied by Westinghouse Research Labs., Pittsburgh, Pennsylvania and compared with data obtained on a General diode sample [13]. The wafers supplied by Hughes were both heavily and lightly doped samples. These samples were 20 mils thick and had a (111) and (100) surface orientations. The heavily-doped wafers had an indium concentration of $3 \times 10^{17}/cm^3$ as determined by Hall measurements. These same wafers were compensated with phosphorus to an impurity concentration of $3 \times 10^{13}/cm^3$ as is required in making very responsive photoconductive detectors. The lightly doped wafers
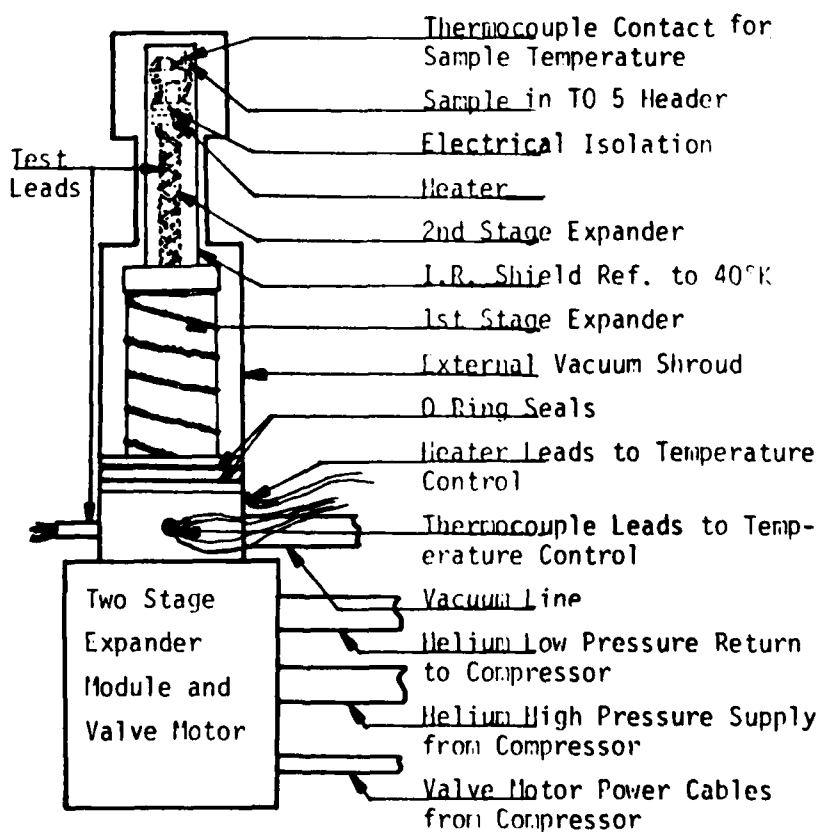
had an indium concentration of $5x10^{15}/cm^3$ as determined by Hall

measurements. These wafers were compensated with phosphorus. The

wafers supplied by Westinghouse Research Labs were doped to a concen-

tration of about $5x10^{15}/cm^3$. Measurements by Hughes Research Labs

using the Hall effect also indicate a concentration of the new .11eV

acceptor level [22] in these samples of $8x10^{14}/cm^3$, an undesirable

but unavoidable feature.

Two different low temperature set-ups were used. For measure-

ments above 77°K, a simple cold finger was cooled by liquid nitrogen.

The cold finger consisted of a copper bar upon which the MOSFET device

was mounted securely for good thermal contact. The copper bar is

equipped with a heater and a copper-constantan thermocouple.

A temperature gradient was established across the copper bar by

placing a heater at one end and liquid nitrogen at the other. As

the liquid nitrogen is boiled off, the temperature on the sample can

be made to increase very slowly from 77°K to 300°K. Measurements

over a wider range of 25°K to 100°K were made using the second tempera-

ture set-up. A closed cycle refrigeration system using helium as a

working gas was employed for these measurements. This system has a

capability of 10°K and is able to hold any specified temperature in

its working range. The system employed two gold-chromel thermocouples

which allowed for proper determination of temperature at all times.

The reference temperature employed was a 273°K or 0°C ice junction in

an oil bath. The closed cycle refrigeration system manufactured by

Air Products does not use any liquified or compressed bottles of gas

and allows a very quick recycling time in making measurements on dif-

ferent devices. The sample tip is electrically isolated from the

Copper Constantan
Thermocouple

Copper Bar

Test
Leads
to Device

5 ohm 20 watt
Heater

Lead
Socket

TO 5 Header

Sample

Liquid
Nitrogen

Reference Point
Thermocouple

a) Fig. 6 Simple Cold Finger Temperature Set up

Thermocouple Contact for
Sample Temperature

Sample in TO 5 Header

Electrical Isolation

Test
Leads

Heater

2nd Stage Expander

I.R. Shield Ref. to 40°K

1st Stage Expander

External Vacuum Shroud

O Ring Seals

Heater Leads to Temperature
Control

Thermocouple Leads to Temp-
erature Control

Vacuum Line

Two Stage

Expander

Module and

Valve Motor

Helium Low Pressure Return
to Compressor

Helium High Pressure Supply
from Compressor

Valve Motor Power Cables
from Compressor

b) Fig. 6 Air Products 10°K Low Temperature Chamber with
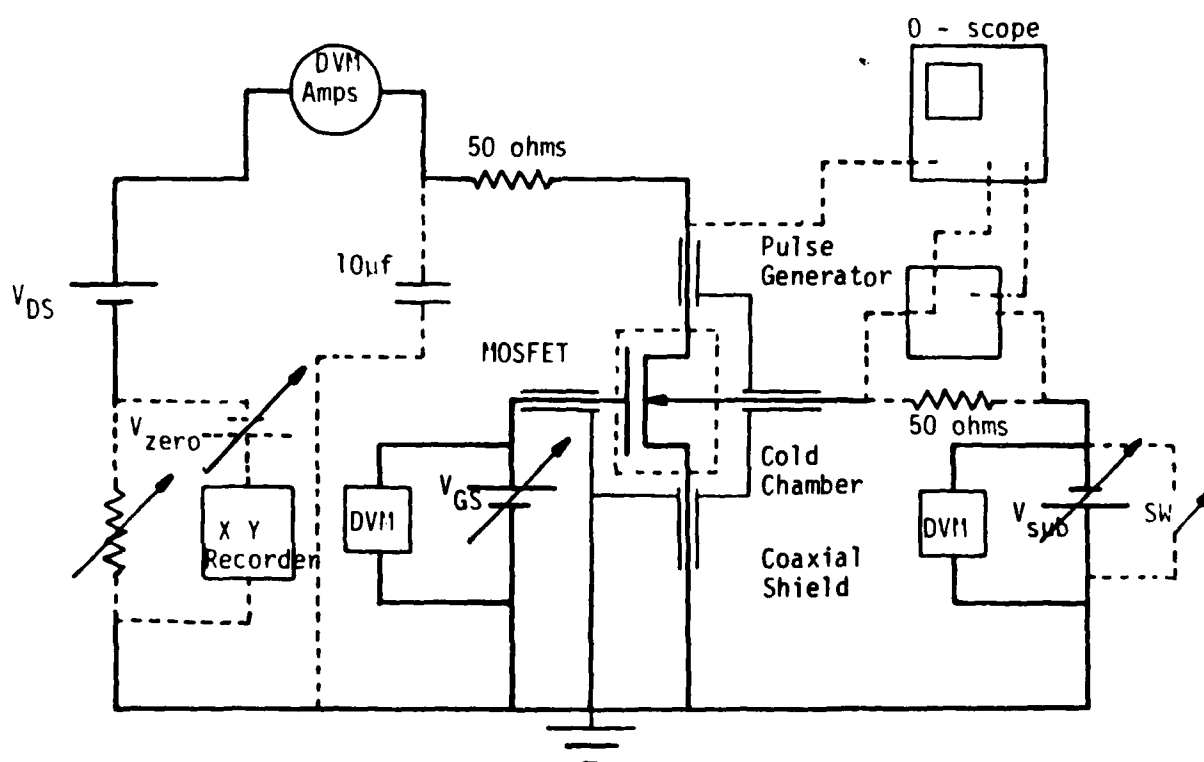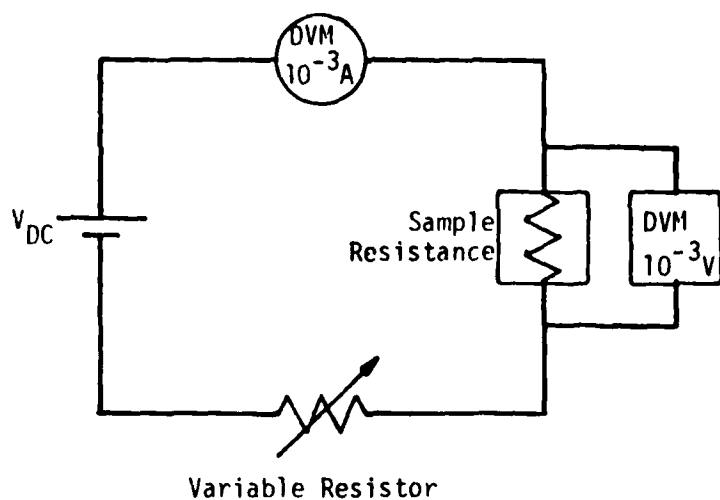Temperature Control

Fig. 7 Measurement Set ups for Various Test Measurements

cold tip but still maintains good thermal contact. Additional equip-
ment required are a vacuum system to evacuate the sample chamber and
a DVM to read the thermocouple voltage to determine temperature.
Both set-ups are shown in Figure 6.

Resistance of the sample substrate versus temperature was measured
using both temperature set-ups. Current through the substrate and
voltage across the substrate were the parameters measured to determine
resistance. Two Fluke 8000A Digital Multimeters were employed as well
as a Hewlett-Packard Power Supply and a variable resistance box to
obtain these measurements. By employing two different temperature set-
ups, results could be cross checked for greater accuracy. Refer to
Figure 7 for explanatory diagram of experiment.

Hole emission and hole capture were done using both temperature
set-ups. Such an arrangement allowed for transient measurements to be
conveniently made over the range of 10^{-7} sec to 10^{+3} sec or ten orders
of magnitude. At higher temperatures, the transients are relatively
fast. This allows the use of an oscilloscope to display the drain
voltage waveforms. An explanatory diagram of the measurement set-up
used in both the hole emission and capture is found in Figure 7. The
circuit was matched as close as possible to a 50 ohm system so that
sub-microsecond transients could be measured. Input and output wave-
forms were displayed alternately on a dual trace oscilloscope. Photo-
graphs were made of the traces and analized to determine data of
interest.

At lower temperatures, transients are very slow, therefore, the
results are recorded using an x-y chart recorder. Use was made of a
1000 ohm resistor in the drain circuit to develop a large enough voltage
variation to be amplified and recorded on the chart recorder.

Boron Diffusion Mask

Phosphorus Diffusion Mask
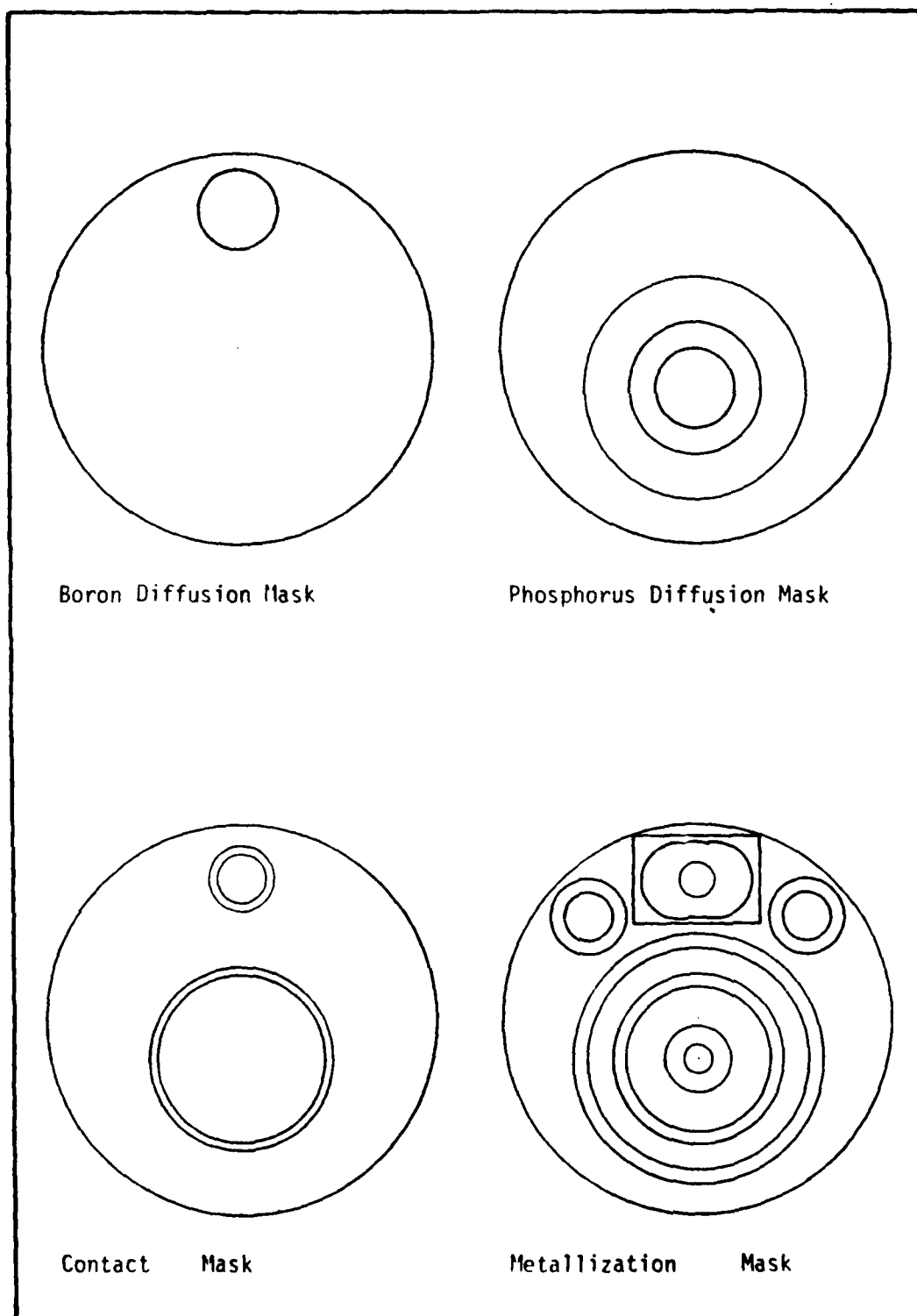
Contact   Mask

Metallization   Mask

Fig. 8 Mask Layout for MOSFET and Resistor Devices Fabricated on
    Indium Wafers

Calibration was provided for the time base by using a Hewlett-Packard swept function generator. Using appropriate shielding and grounding, the small transient signal is easily observed. Therefore, concern for noise sources in either the device or the circuit was at a minimum. Additional equipment required for these tests were power supplies, voltmeters, milli-amp meters and a pulse generator.

Devices were fabricated on these wafers such as shown in Figure 8 using standard silicon processing techniques. Individual MOSFET's are separated and mounted on TO5 headers using conductive epoxy. Wire bonds are made using aluminum wire and an ultra sonic bonder. The devices are tested and characterized using a curve tracer at room temperature. Part of the wafer which has been subjected to high temperature processing is returned to Hughes Research Laboratory for another Hall measurement. This check is made to insure that the processing has not significantly changed the characteristics of the sample.

Procedures for the measurement of threshold voltage as a function of backgate bias are done at room temperature using a curve tracer, variable power supplies and voltmeters. The measurement of the n+, p junction high frequency capacitance as a function of junction voltage is also made at room temperature using a Boonton Capacitance meter, variable power supply, and voltmeters. Standard 4-point probe measurements at temperatures above 300°K were also made on the indium doped sample wafers.

IV. Results and Discussion

    A. Determination of the Impurity Doping

        (a) Threshold Voltage versus Backgate Bias

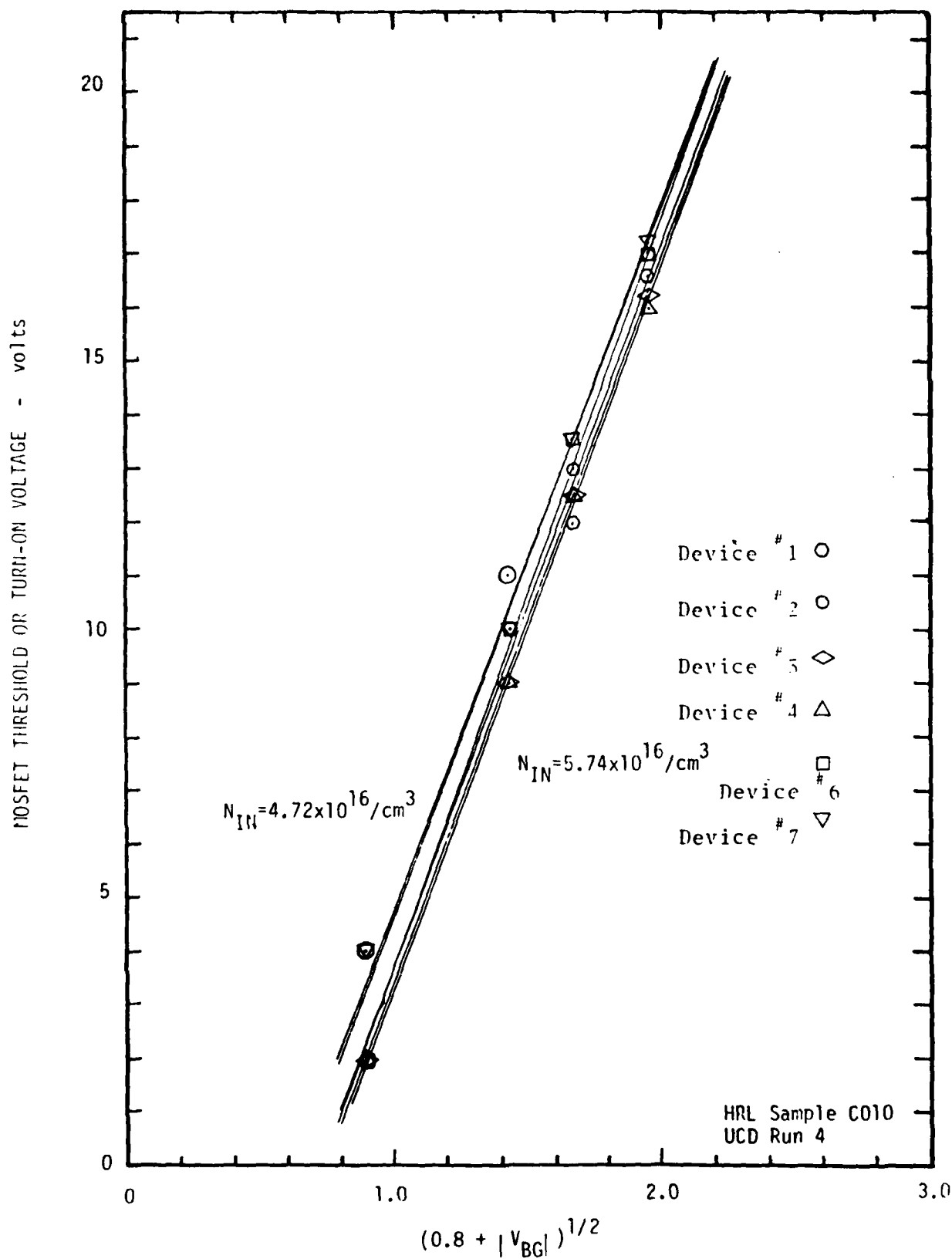   Data curves of threshold voltage versus backgate or substrate

Fig. 9 Threshold Voltage versus $(.8 + |V_{BG}|)^{1/2}$ Showing Calculated Indium Concentrations

voltage are shown in Figure 9. In this case the temperature during measurement was 300°K. The plot is actually of threshold voltage versus the square root of the quantity ϕ_f, taken to be .8V plus the absolute value of the backgate voltage. The relative doping concentration can be determined if we recall the equation for the threshold voltage,

$$V_T = A + \frac{t_{ox}}{\varepsilon_{ox}\varepsilon_o}\sqrt{qN_a\varepsilon_{si}\varepsilon_o(.8+|V_{BG}|)} \quad . \tag{21}$$

Taking the derivative of V_T with respect to $\sqrt{.8+|V_{BG}|}$ gives

$$\frac{dV_T}{d(\sqrt{.8+|V_{BG}|})} = \frac{t_{ox}}{\varepsilon_{ox}\varepsilon_o}\sqrt{q\varepsilon_{si}\varepsilon_o N_a} \quad . \tag{22}$$

Rearranging equation (22) and solving for N_a, we obtain

$$N_A = \left\{\left[\frac{dV_T}{d(\sqrt{.8+|V_{BG}|})}\right]\left[\frac{\varepsilon_{ox}\varepsilon_o}{t_{ox}}\sqrt{\frac{1}{q\varepsilon_{si}\varepsilon_o}}\right]\right\}^2 \quad . \tag{23}$$

Making an approximation of the derivative as the slope of the line

$$N_A = \left\{\left(\frac{\Delta(V_T)}{\Delta(\sqrt{.8+V_{BG}})}\right)\left(\frac{\varepsilon_{ox}\varepsilon_o}{t_{ox}}\sqrt{\frac{1}{q\varepsilon_{si}\varepsilon_o}}\right)\right\}^2 \quad . \tag{24}$$

The relative concentration of acceptors should correspond to the number of indium impurities in the sample assuming ionization of all the indium and existence of only one acceptor level for indium. Calculations from the plot give the concentration as shown in Figure 9, to be roughly $4\text{-}6\times10^{16}/cm^3$. All other contributions are assumed to be negligible. These measurements can be done for the indium impurity either ionized or neutral to accurately determine the indium concentration, and the concentration of the residual boron in the wafer as demonstrated in the literature [13].

The impurity concentration of the indium obtained in these experiments is less than those obtained by Hughes Research Labs using Hall-effect measurements. Measurements recently done at Westinghouse Research Center show that the Hall concentrations are typically twice those determined by C-V and junction breakdown techniques. Schroder attributes this discrepancy in the Hall concentrations due to the Hall scattering factor, r [30]. How this discrepancy leads to errors in determining the indium concentration in silicon is discussed in the reference by Schroder [30]. The results obtained for the indium concentration in silicon in these experiments are a factor of two less than the indium concentration obtained by HRL using Hall-effect measurements.

(b) Reverse Voltage Junction Capacitance

The junction capacitance of a standard n+, p junction can be used to determine the doping of the lightly doped p region [23,26]. For a n+, p junction the relation between junction capacitance and the reverse bias voltage is

$$C_j = \epsilon A \left| \frac{q \, N_d N_a}{2\epsilon (V_0 - V_{RB})(N_d + N_a)} \right|^{1/2} . \qquad (25)$$

Because the donor concentration N_d is much larger than the acceptor concentration N_a $(N_d + N_a) \cong N_d$, and, equation [25] becomes

$$C_j = \epsilon A \left| \frac{q \, N_a}{2 \, (V_0 - V_{RB})} \right|^{1/2} . \qquad (26)$$

Rearranging in terms of N_a gives the result

$$N_a = \left| \frac{C_j}{\epsilon A} \right|^2 \frac{2\epsilon (V_0 - V_{RB})}{q} . \qquad (27)$$

For large reverse bias voltage we can neglect V_0 and obtain

$$N_a = \frac{-2(V_{RB})C_j^2}{q\epsilon A^2} \quad . \tag{28}$$

Figure 10 is a plot of $\dfrac{1}{(C_{HF})^2}$ versus the reverse bias junction

voltage, the slope of the line at higher reverse voltages being an

accurate determination of the indium concentration. The accuracy of

this result depends upon an accurate knowledge of the junction area.

All other doping concentrations have been assumed to be negligible.

The indium concentration obtained yield values of 5 to $7 \times 10^{16}/cm^3$.

These measurements were done at room temperature 300°K, so this value

represents the total number of ionized impurities in a depletion region.

Since all the indium is ionized at 300°K and the number of other

impurities are negligible this is then the concentration of indium

centers in the sample. These results compare favorably with those

obtained in section IV(a) by measurement of threshold voltage versus

backgate bias voltage.

(c) High Temperature Four-Point Probe Resistivity

Resistance versus temperature using the four-point probe

technique is another standard technique [10]. These measurements have

been made at temperatures above room temperature to investigate the

partial ionization of the indium center at room temperature. Variation

of resistivity of an indium doped sample and a standard boron doped

sample versus temperature °K is shown plotted in Figure 11.

The indium concentration has been calculated by a least squares

fit of the single parameter charge balance equation [22];

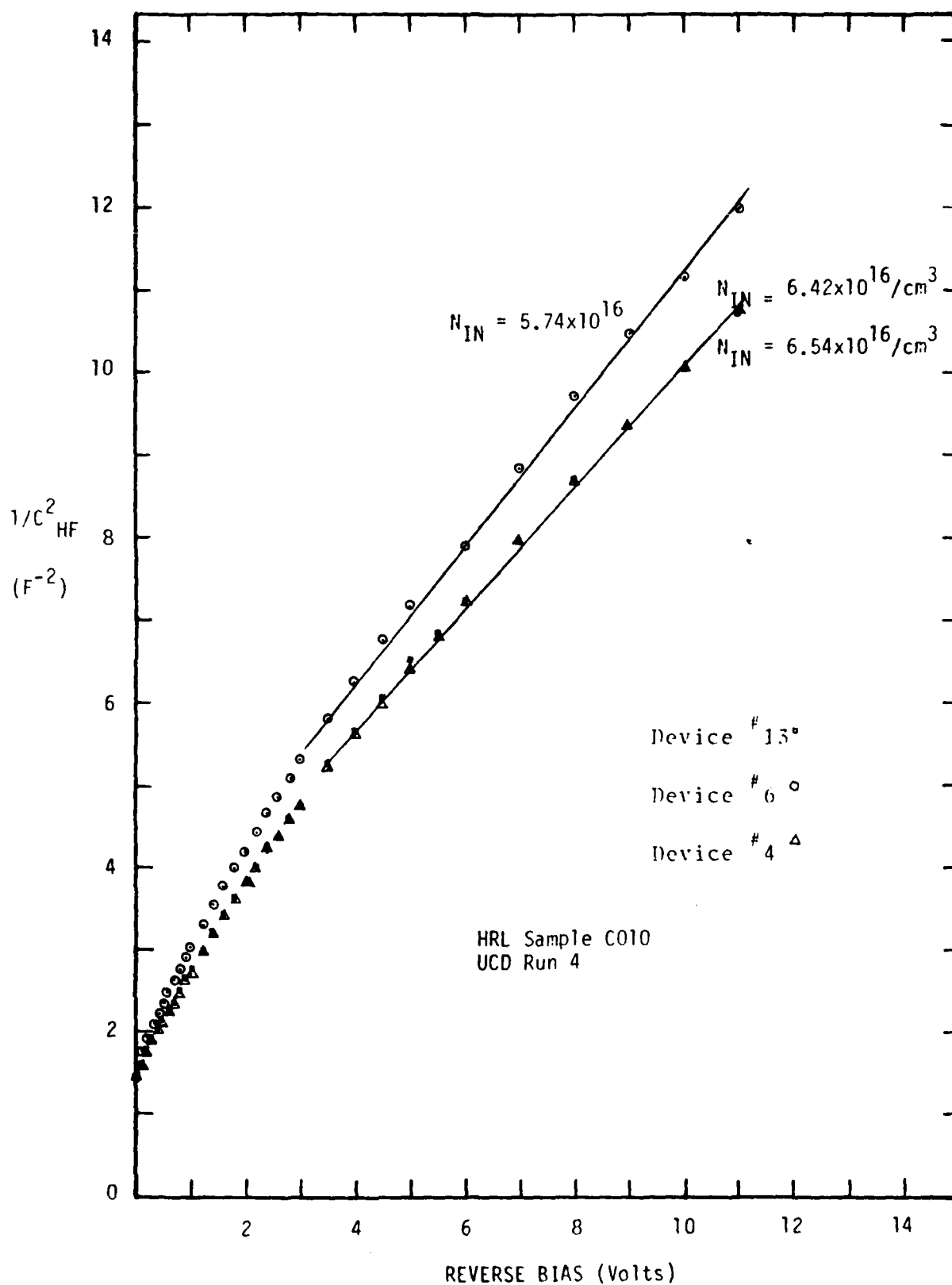$$p = N_{IN}\left\{(1+pq_{IN}\exp(E_{IN}/KT))\right\}N_V \quad . \tag{29}$$

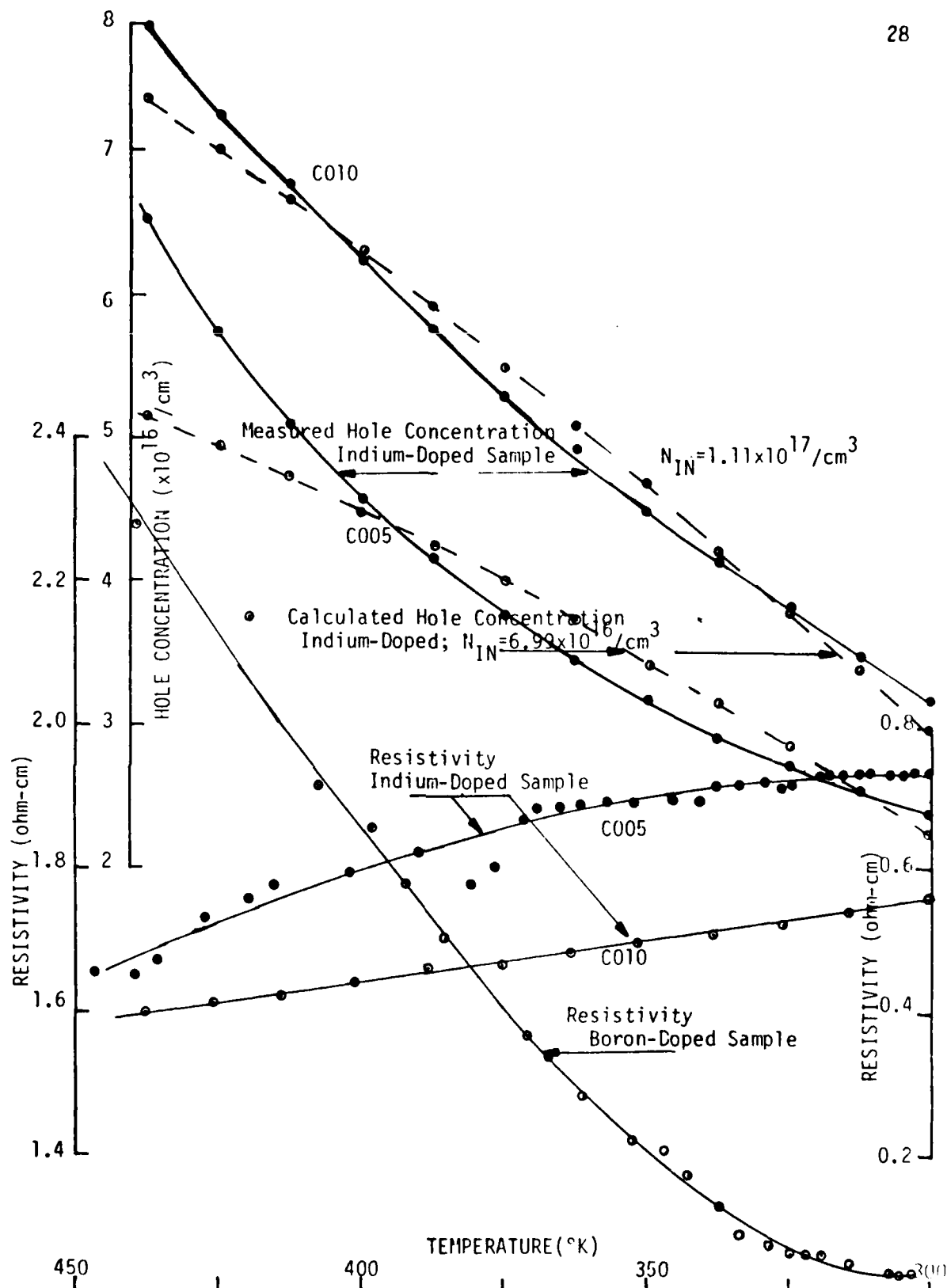Fig. 10 Plot of $(1/C^2_{HF})$ versus Reverse Voltage Showing Calculated Indium Concentration

Fig. 11 4 Point Probe Resistivity plots for two different samples with mobility proportional to $T^{-1.5}$ plotted versus temperature.

At high temperatures a large fraction of the indium is ionized so that one can neglect the concentrations of the other levels and their contributions to the charge balance equation. A mobility variation of $T^{-1.5}$ gives an indium concentration of $6.99 \times 10^{16}/cm^3$ for HRL samples C005 with an RMS error of 9.0%. The indium concentration for HRL sample C010 is $1.11 \times 10^{17}/cm^3$ with an RMS error of 3.7%. Sample C010 was used in the fabrication of our MOSFET and resistor device structure.

A mobility variation of $T^{-1.5}$ is obtained from the boron doped sample data. The assumption was made that the mobility temperature dependence of the indium doped sample should be the same. This assumption is made based on the fact that the boron doped sample has a comparable ionized impurity concentration. Both results were also computed using a mobility variation of $T^{-1.0}$. The indium concentration for sample C005 is $5.4 \times 10^{15}/cm^3$ and for sample C010 is $8.44 \times 10^{16}/cm^3$.

A degeneracy factor, $g_{in} = 4$ has been used. A smaller degeneracy factor will result in a lower indium concentration. This is due to the larger percentage of indium being ionized.

(d) Resistance Versus 1000/T at Low Temperatures

The bulk resistance versus a 1000/T is shown plotted in Figure 12. The dependence of resistivity with temperature can be obtained from this plot. This calculation requires a knowledge of device geometry. We estimate the relationship between resistance and resistivity in our resistors using the device geometrics and measured data. Resistivity at room temperature was found to be .5Ω-cm. The bulk resistor structure is shown in Figure 1. The front and back contacts are about .08 mil deep. The circular front contact is calculated from mask dimensions to be 20 mils in diameter. The wafer thickness after processing measured 20 mil $\pm$ .5 mil. Since the contacts are highly doped compared to
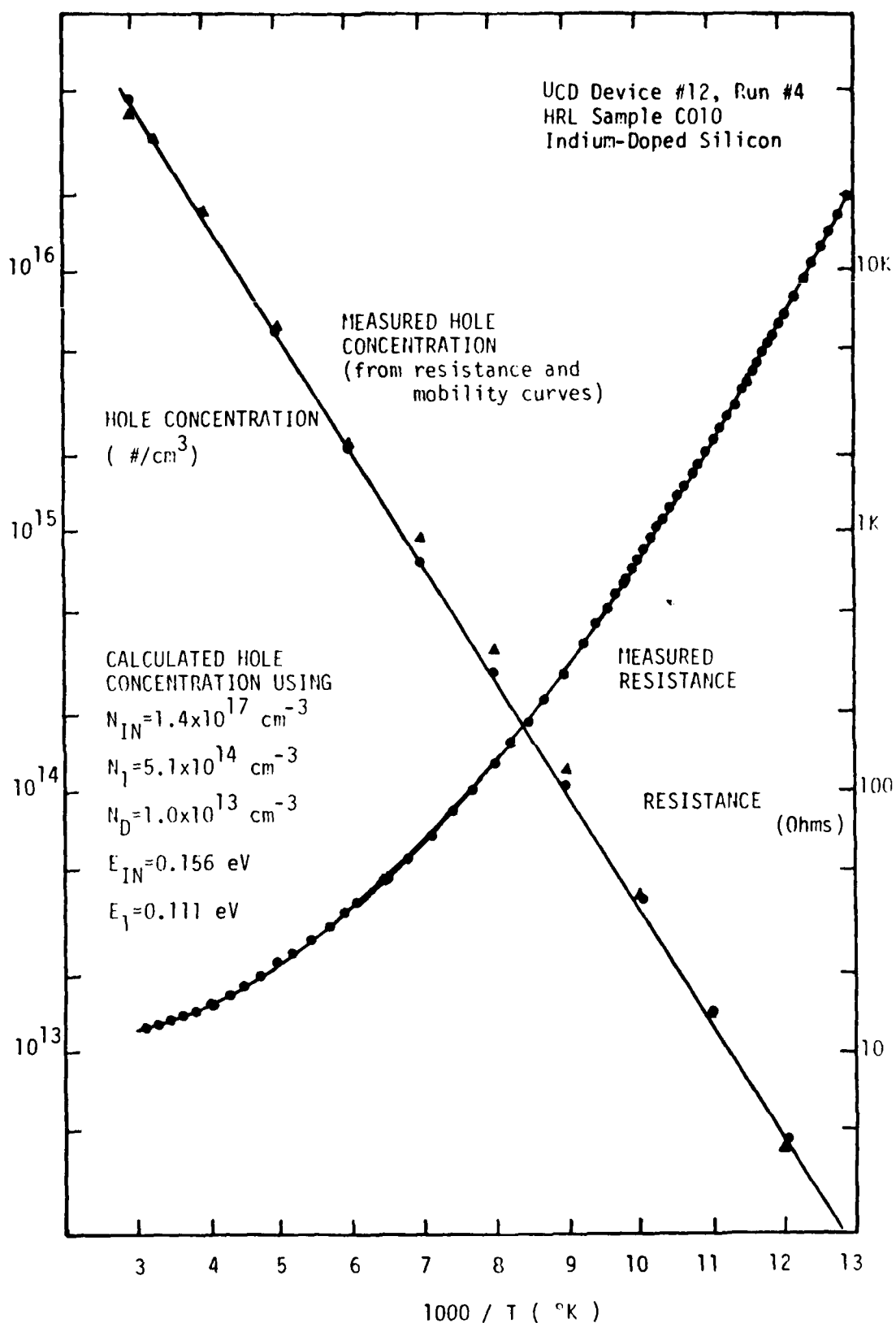
Fig. 12 Resistance and Hole Concentration of a Photoconductor at Low Temperature and Illustration of Curve Fitting to Determine, N_{IN}, N_1, and N_D.

substrate dopings, their resistance is negligible.

The ratio between resistance and resistivity can be determined
from the expression

$$R = \rho \int_0^{\ell} \frac{d\ell}{\int area\ dA} \quad . \tag{30}$$

The resistivity ρ is assumed constant. The effective geometry for
this resistor is estimated to be a truncated right circular cone. The
radius is estimated to be between .77 and .68 times the depth beneath
the surface contact. The ratio R/ρ is found to be approximately 18;
consistent with initially measured R and ρ values. Thus, the relation-
ship between resistance and resistivity used in our data fitting is not
precise and is a source of some error.

Curve fitting techniques using a least squares fit were used to
determine a plot of resistivity and hole concentration versus tempera-
ture. The parasitic series resistance of the measurement system is
typically .25Ω and never more than 1Ω at room temperature. Curve fit-
ting results with this 1Ω subtracted were essentially the same as those
found ignoring this series resistance.

The expression for the resistivity of p-type silicon is

$$\rho_p = \frac{1}{pq\mu_p} \quad , \tag{31}$$

where, p is the hole concentration, q the electronic charge and μ_p is
the hole mobility. The hole concentration versus temperature can be
determined using this equation and knowledge of the hole mobility. The
hole mobility has been obtained from Hughes Research Labs as a function
of temperature by Hall measurements and conductivity measurements. The
hole mobility as a function of temperature for indium doped silicon is
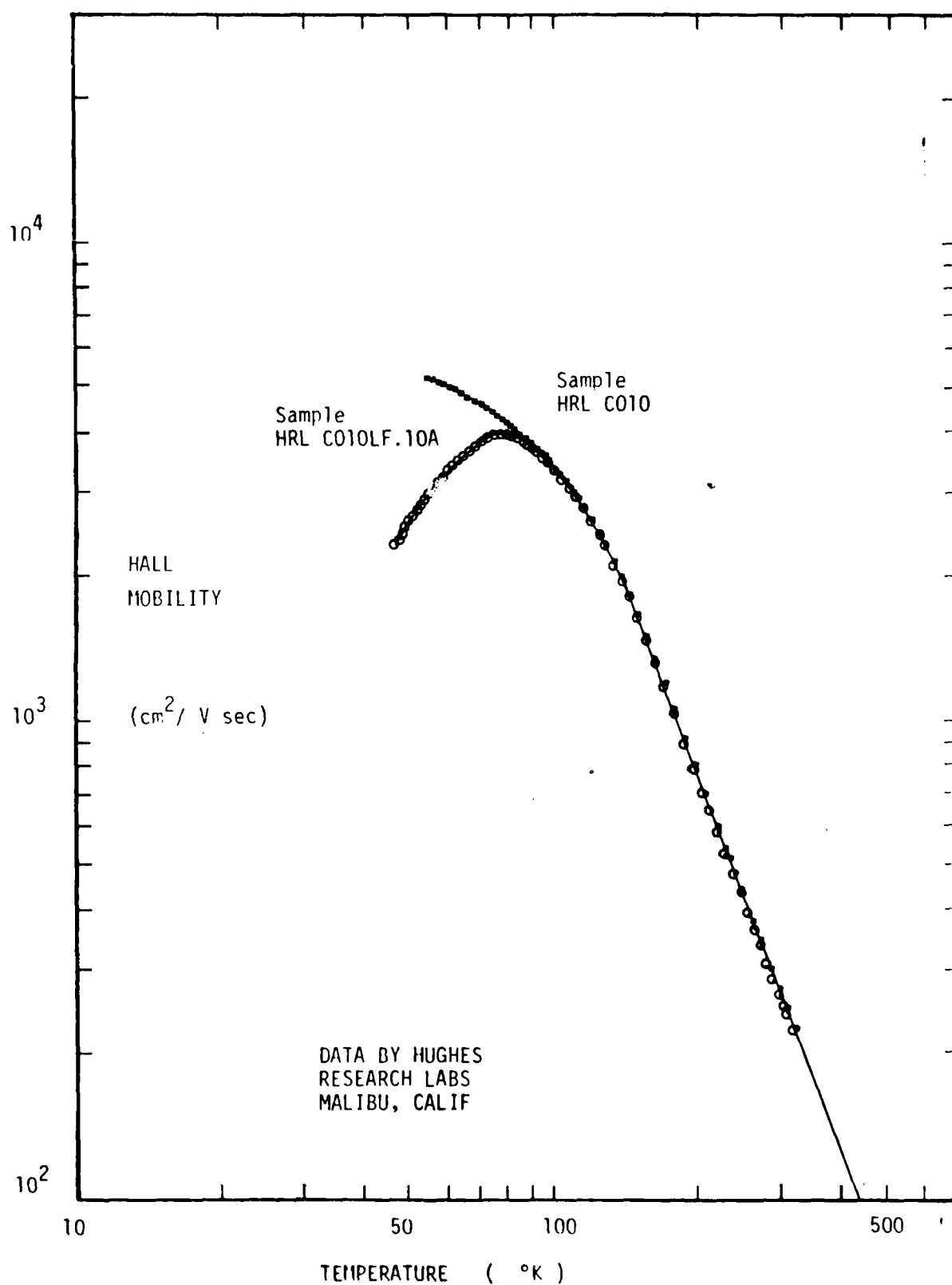shown in Figure 13. The values obtained from this plot were used in

Fig. 13 Hall Mobility for Holes in Indium Doped Silicon

the calculation of the hole concentration versus temperature.

Impurity dopant concentrations were calculated from the charge balance equation

$$p + N_D - N_A = \cfrac{N_{IN}}{1 + \cfrac{pg_{IN}}{N_V} \exp(E_{IN}/KT)} + \cfrac{N_1}{1 + \cfrac{pg_1}{N_V} \exp(E_1/KT)} \quad . \quad (32)$$

A least-squares, relative error curve fitting technique was used. N_1, g_1, E_1, are the density, degeneracy, and energy level of the .111eV acceptor. The .156eV slope of the indium dopant appears to be replaced by a .111eV slope at higher temperatures characteristic of the new indium level reported by Baron, et al. [22]. The degeneracies g_{IN} and g_1 were set equal to 4 [22], and the temperature dependent effective mass of Barber as implemented by Baron [22] was used in calculating the density of states N_V. Typically, N_{IN}, N_1, and (N_D-N_A) were found to be $6.0\times10^{16}/cm^3$, 4×10^{15} and 6.0×10^{13} respectively. This indium concentration corresponds well with those found in sections IV a, b, and c. In Table I dopant concentrations are shown for several devices.

If the higher temperatures (near 300°K) are omitted from our data sets, indium concentrations comparable to the $2\times10^{17}/cm^3$ reported by HRL [22] are obtained upon fitting of the charge balance equation. But, since at high temperatures the contribution of indium to the hole concentration should dominate, we should not neglect these data points in computing impurity concentrations.

In the least squares analysis of our data we assume a known constant set of impurity energy levels and solve the linear system equations obtained for a least squares fit of N_{IN}, N_1, and N_A-N_D to the charge balance equation. The function actually fit is the percentage error

HRL SAMPLE C010: UCD DEVICE RUN #4

E_{IN} = 0.156 eV ; E_1 = 0.111 eV

Device #	$N_I(10^{16} cm^{-3})$	$N_1(10^{15} cm^{-3})$	$N_D-N_A(10^{13} cm^{-3})$	RMS ERROR IN FIT (%)
4	8.11	2.31	2.86	18.1
6	8.32	0.797	1.14	13.4
12	14.0	0.51	1.01	11.3
13	8.78	1.71	1.59	10.6
14	14.4	1.13	1.75	11.8
15	8.84	4.26	3.21	23.9
p vs. T Fig. 14	15.3	0.964	5.99	13.4

E_{IN} = 0.166462 eV ; E_1 = 0.11300 eV (HRL Values)

4	11.0	3.30	2.95	20.1
6	12.07	1.44	1.44	16.2
12	18.9	1.45	1.77	16.5
13	12.82	2.59	1.73	26.1
14	21.9	2.17	2.29	13.9
15	10.75	5.81	3.19	25.7
p vs. T Fig. 14	32.72	0.787	3.49	1.3

HRL ANALYSIS OF THEIR HALL DATA ON THIS SAMPLE AFTER HIGH TEMP PROCESSING
E_{IN}=0.166462 E_1=0.11300

p vs. T Fig. 14	33.3508	0.782798	3.47940	1.02

TABLE I.   IMPURITY CONCENTRATIONS (From Resistance vs. 1000/T on HRL Sample C010)

$$\text{error } (T) = \dfrac{p(T) - \dfrac{N_{IN}}{1 + \dfrac{p(T)g_{IN}}{N_V}\exp(E_{IN}/kT)} - \dfrac{N_1}{1 + \dfrac{p(T)g_I}{N_V(T)}\exp(E_1/kT)} - (N_A - N_D)}{p(T)} \ . \tag{33}$$

After solving for N_{IN}, N_1 and N_A-N_D, Pcalc is then found and the RMS error calculated:

$$\epsilon_{RMS} = \sqrt{\frac{1}{NPTS} \sum^{NPTS} \left(\frac{Pcalc - Pexp}{Pexp}\right)^2} \ . \tag{34}$$

By trying many different energy levels and selecting the one which yields the least error, we can approximate the method used at HRL. We did experiment with conjugate gradient minimization of the error function but the seven parameters were adjusted at such a slow rate that it proved prohibitively expensive.

The results of our analysis of resistivity versus temperature are shown in Table I. The table ...cludes the energy levels used, the impurity concentrations and the RMS error in the fit to the variation of the hole concentration with temperature.

Results obtained by Hughes Research Labs (HRL) for the impurity concentrations in sample CO10 are included in Table I. These are results done using Hall measurements after high temperature processing at Davis. Figure 14 shows a plot of HRL data of hole concentration as a function of temperature. We did obtain the same impurity concentrations using their data and their energy levels with our curve fitting technique.

One obvious source of error in this test procedure lies in the measurement of temperature. The simple cold finger set-up was used for most of these measurements. This set-up doesn't allow for thermal equilibrium to be established prior to each measurement. The relatively
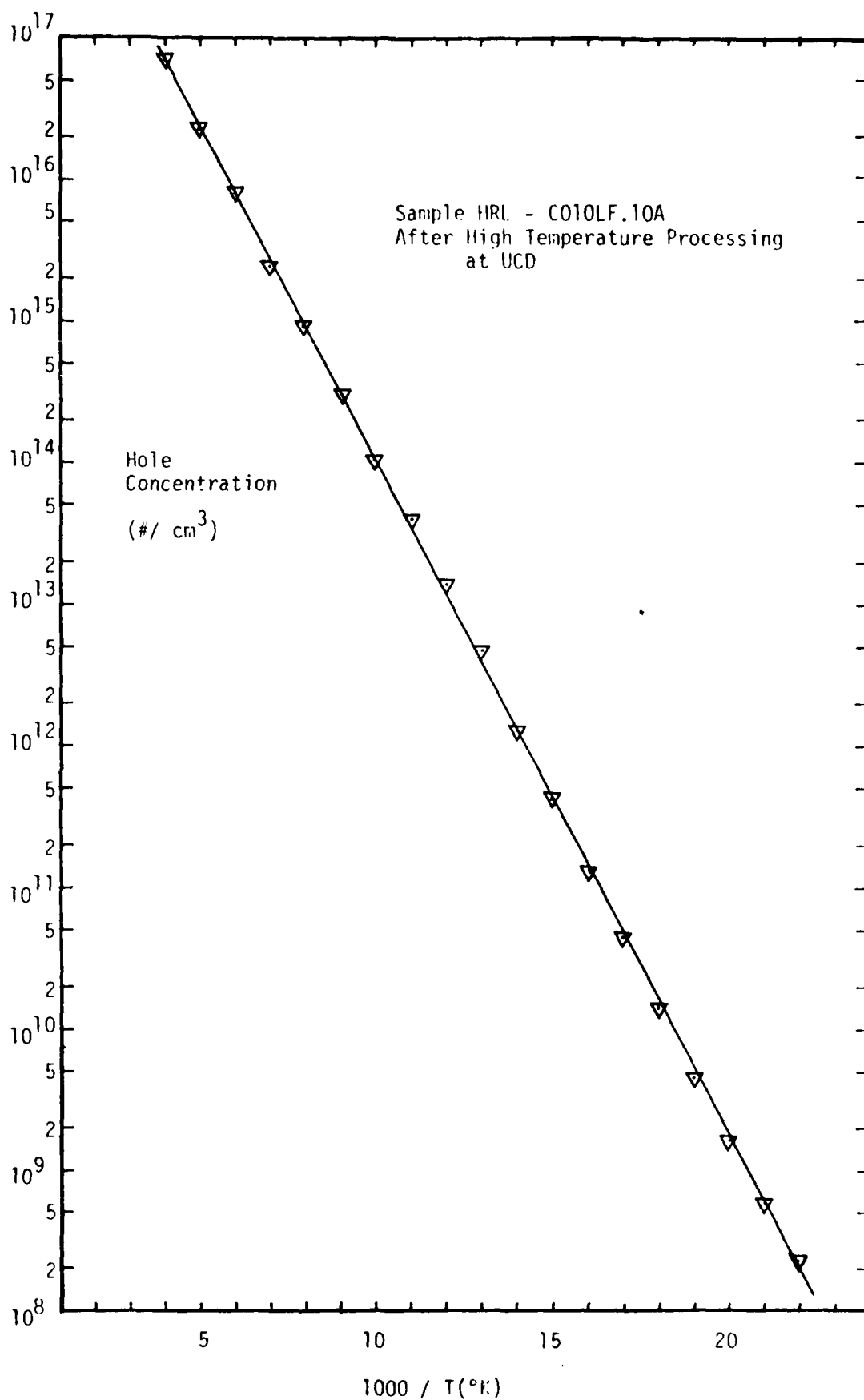
Fig. 14   Hall Measurements of Hole Concentration by Hughes Research Labs

large data fitting errors shown in Table I may be partially con-
sequence of this simple variable temperature cold finger. Since the
actual interest in this experiment lies in the 77°K data, which is
in thermal equilibrium, we estimate that the error attributable to
the gradient temperature effects (dT/dt) between T = 77°K and T = 300°K
will not seriously affect the conclusions reached.

B. Emission Rate of Holes From the Indium Sites in Silicon

The thermal emission rate of holes from the indium centers in
silicon versus temperature have been measured using backgate voltage
pulses. Backgate voltage increases the depletion region width [16].
To maintain the overall charge balance in the semiconductor the
neutral indium centers must emit holes to balance the applied negative
backgate voltage. The net effect of the backgate voltage is to
cause the indium centers to change their charge state. This change in
charge state results in a decrease in the conductivity of the MOSFET
channel region [20]. Thus, electrons from the bulk device are cap-
tured by the neutral indium center. Electron capture corresponds to
hole emission. Thus, the neutral indium centers become negatively
charged. These negative indium centers make up the increased depletion
region caused by the backgate voltage. Thus, a relation can be
obtained between the change in drain current and hole emission.

As demonstrated in a previous paper by Forbes [20], the relation-
ship of the drain current change with respect to time is approximately

$$I_{DS}(t) = [I_{DS}(0)]exp(^{-t}/\tau_{I_{DS}}) + I_{DS}(\infty) . \qquad (35)$$

Since the device is operated in the linear region and the indium con-
centration is far larger than the concentration of residual acceptors,

114

an approximation is made by Forbes [20]. This approximation states
that one half the time constant associated with the change in indium
charge state is equal to the time constant of the drain current decay.

$$\frac{1}{2} \tau_{hole\ emission} = \frac{1}{2}(\frac{1}{e_p}) = \tau_{I_{DS}} \ . \tag{36}$$

The drain current decay being exponential; a more accurate expression
of the hole emission time constant can be found using the expression

$$1 - \left(-\frac{\Delta I_{DS}(t)}{\Delta I_{DS}max} + 1 \right)^2 = exp(t/e_p) \ , \tag{37}$$

if desired rather than the approximate value [20].

The hole emission time constant from the neutral indium center
is highly temperature dependent. As explained previouSly, and in
Ref. [13], and shown in Figure 4, a change in charge state of the
indium center will result in a change in the channel current. Figure 15
shows plots of $t_{1/2}$ versus 1000/T. $\tau_{1/2}$ corresponds to the time neces-
sary to half the maximum voltage change. This voltage change was mea-
sured at the drain where the current change is 180° out of phase and
for time constants less than 10^{-2} sec. For time constants greater than
10^{-1} sec the voltage change was measured across a source resistance.
The voltage and current waveforms being in phase at the source.
Figure 16 shows a typical data waveform for both conditions. Figure 15
shows hole emission time constant versus temperature for several dif-
ferent samples. Previous results obtained by Forbes [13] are also
shown. The thermal emission time constant of holes from the neutral
indium center at 77°K was found to be $\frac{1}{e_p} = 20_{\mu sec}$. The energy level
of the indium center in the silicon band gap can be found from the
equation
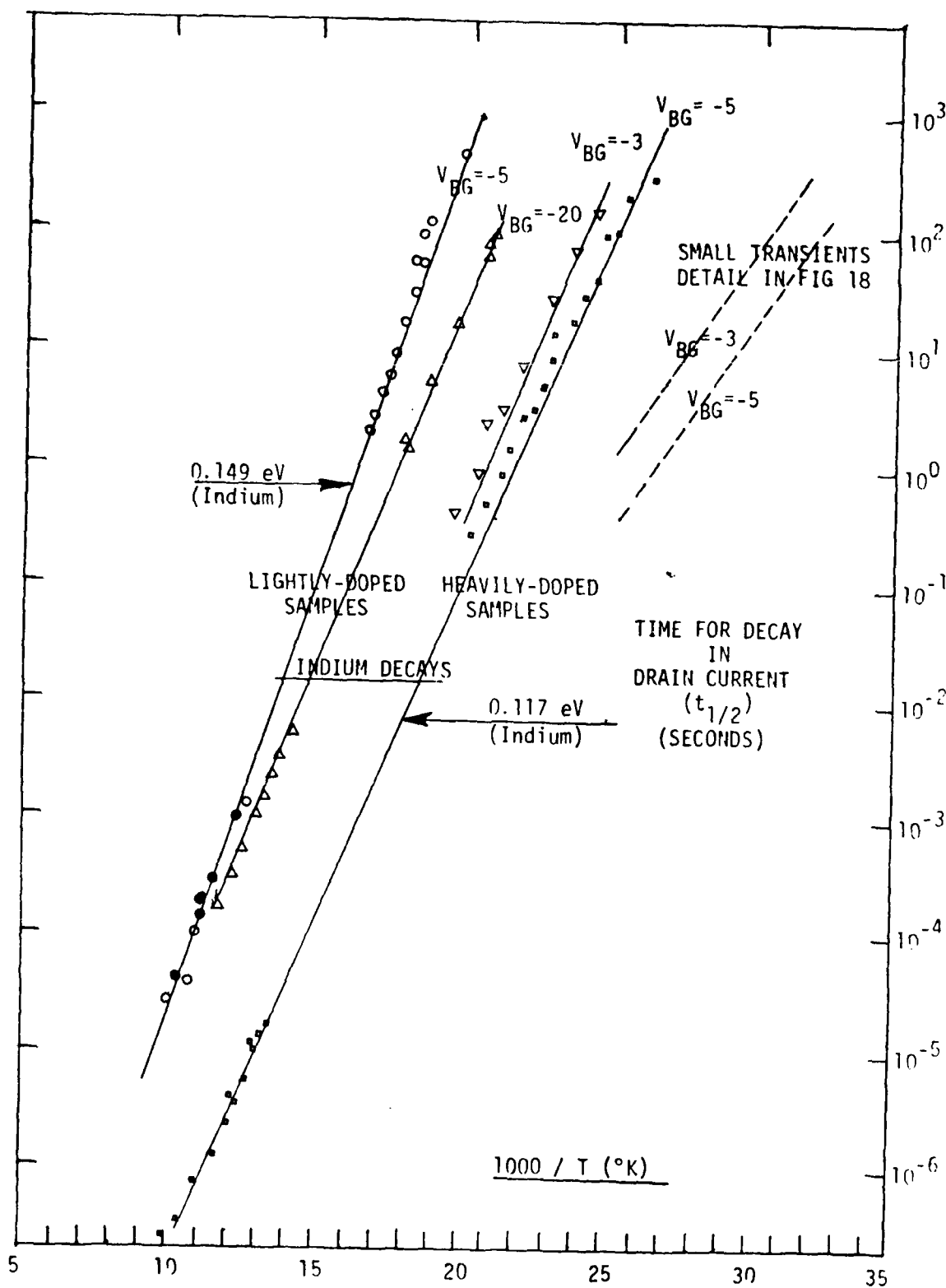
Fig.15. Emission Time Constants vs. 1000/T.

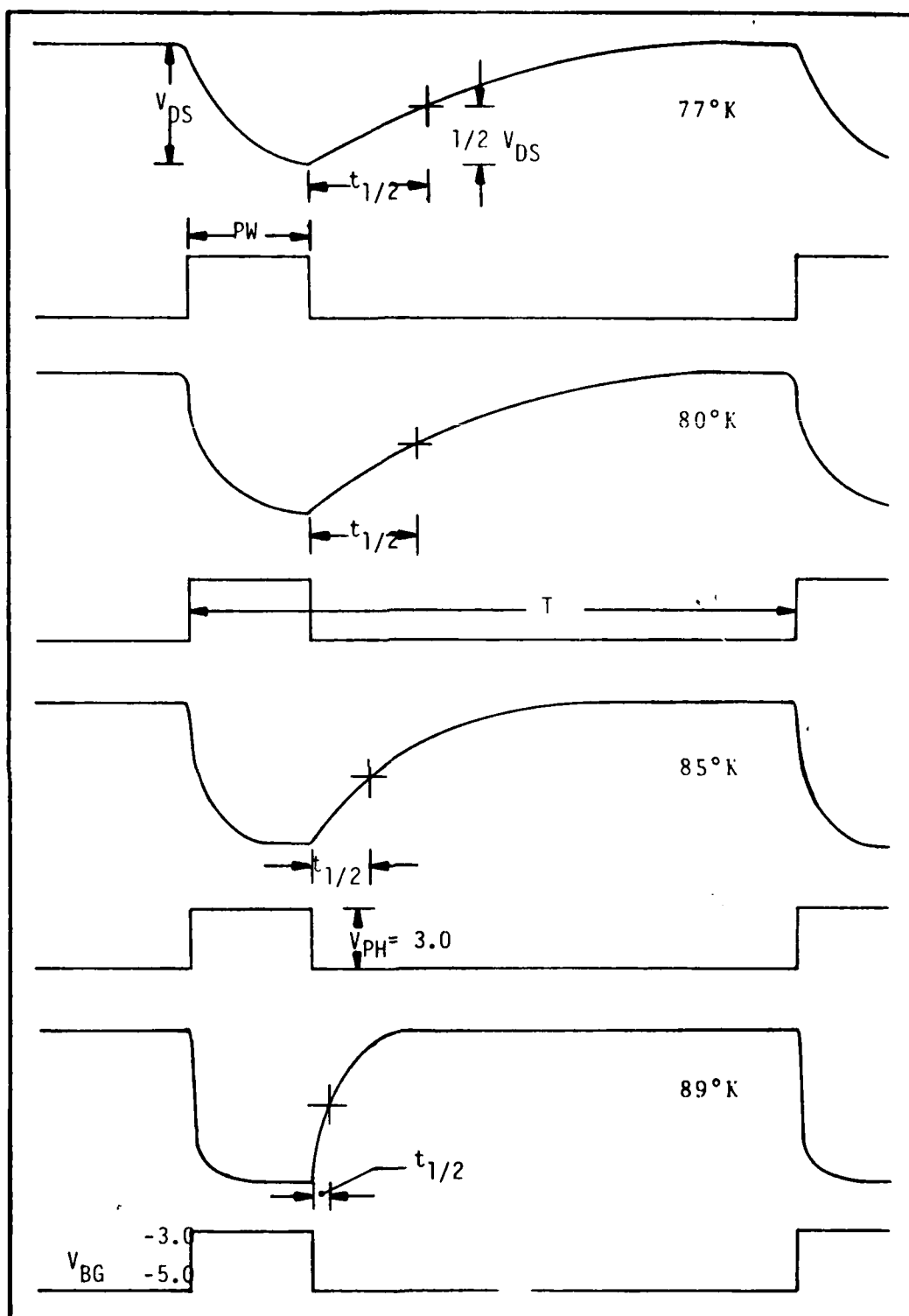Fig. 16 Typical Data Waveforms for $t_{1/2}$ Measurements for Different Temperatures.

$$\tau_{hole\ emission} = A_1 T^{-1.5} \exp(\Delta E/kT) \quad . \tag{38}$$

ΔE is the relative energy level with respect to the valence band. This equation can be found in references by C. T. Sah and others [2,20]. Thus, the slope of the line in Figure 15 can be related to the following expression to determine ΔE,

$$\Delta E = \frac{\Delta \log_e \tau + 1.5 \Delta \log_e T}{11.605 \ \Delta(1000/T)} \quad . \tag{39}$$

This method provides a unique identification of the thermal activation energy of the indium center. Results obtained on devices made from HRL sample C042 over a wide range of temperatures yield a thermal activation energy of .149eV for a 5 volt backgate voltage. These results compare favorably with those obtained from the General Diode sample [13].

The thermal activation energy level depends upon the electric field. Energy barrier lowering due to electric-field-assisted thermal ionization of trapped charge carriers in semiconductors is known as the Poole-Frenkel effect [27,28]. This effect is also found in Gallium doped silicon [14]. As shown in Figure 15, increasing the backgate voltage to 20 volts results in a smaller time constant due to field enhanced thermal emission. Sample C042 is lightly doped, therefore, the magnitude of the electric field is low. Sample C010 is heavily doped. The higher doping results in a much larger electric field amplitude in the surface depletion or space charge region. As a result, the barrier energy is reduced by the Poole-Frenkel effect and the activation energy for thermal emission is 0.117eV. The emission time constant is also much faster. Two important observations can be made from Figure 15.

1. The thermal emission time constant is reduced in addition to the barrier energy lowering as a consequence of the Poole-Frenkel effect.

2. The magnitude of the decay is proportional to the concentration of the impurity centers.

A detailed analysis has been made of the field dependence of the thermal emission rate of holes from the neutral indium centers in silicon. A plot of the thermal emission rate of holes using the $t_{1/2}$ approximation versus the quantity $((1+V_{BG})N_{IN}/10^{16})^{1/4})$ is plotted in Figure 17. Where the backgate voltage was the quantity varied, the Poole-Frenkel effect predicts that the equation relating the emission rate to the electric field is

$$e_p{}^t = A \exp(\beta\epsilon^{1/2}/kT) \quad , \tag{40}$$

where β is the Poole-Frenkel coefficient as determined by the hydrogen atom model [14,27,28], ϵ is the average electric field, k the boltzmann constant and T is the temperature. Contained in Figure 17 are data analyzed for both the lightly and heavily-doped samples C042 and C010 respectively. A value of β is calculated to be approximately $1.0 \times 10^{-4} eV/Vcm)^{1/2}$. This value is in good agreement with the value previously obtained by measurements on the gallium impurity center in silicon [14].

The field dependence and barrier lowering caused by the Poole-Frenkel effect must be taken into account when searching for the 0.11eV level. Hughes Research Labs have reported this energy level to be present in those silicon samples heavily-doped with indium. This field dependence should be considered in the analysis of the operation of photoconductive infrared detectors. The detectors have p^+ contacts on
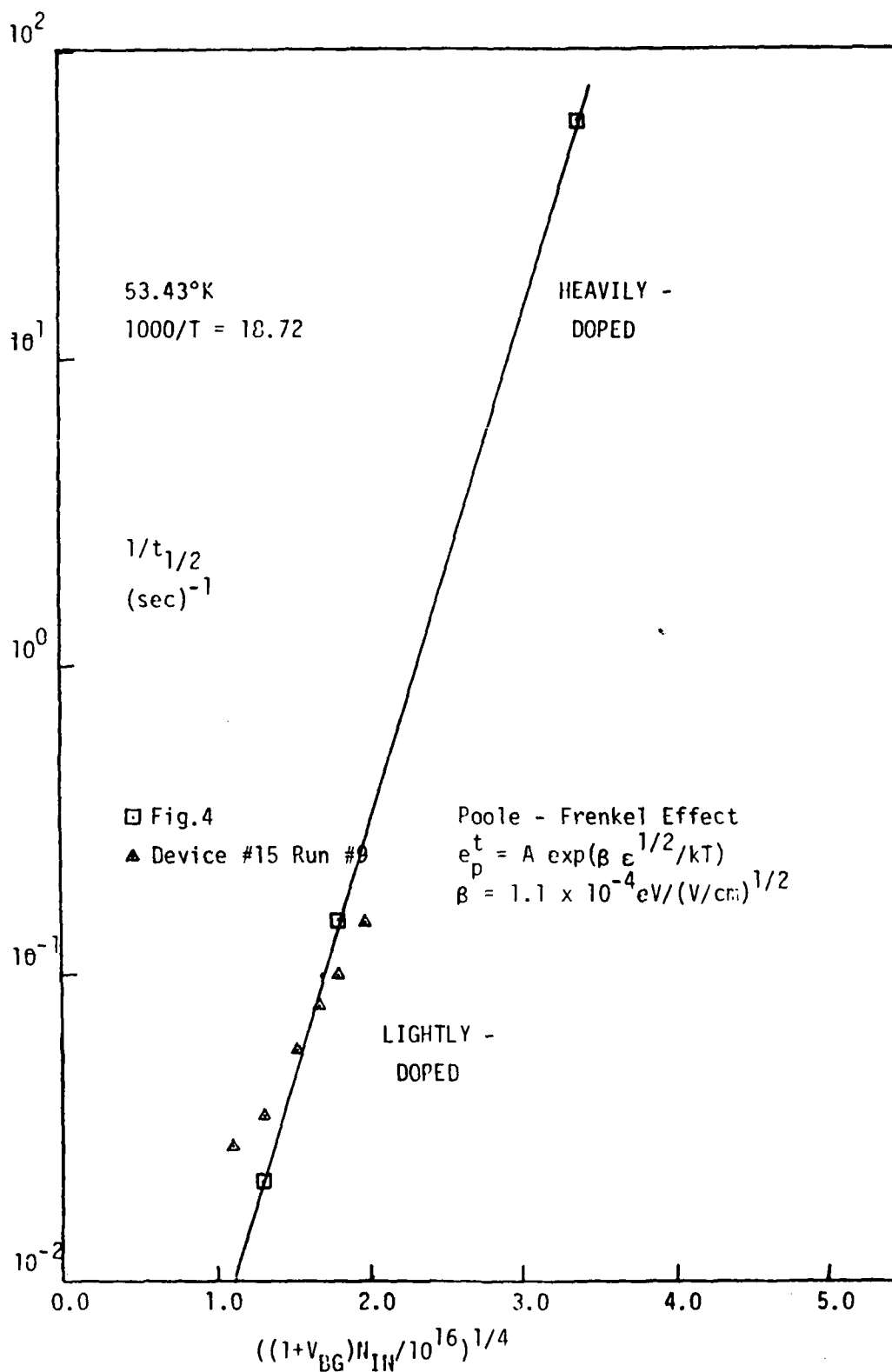
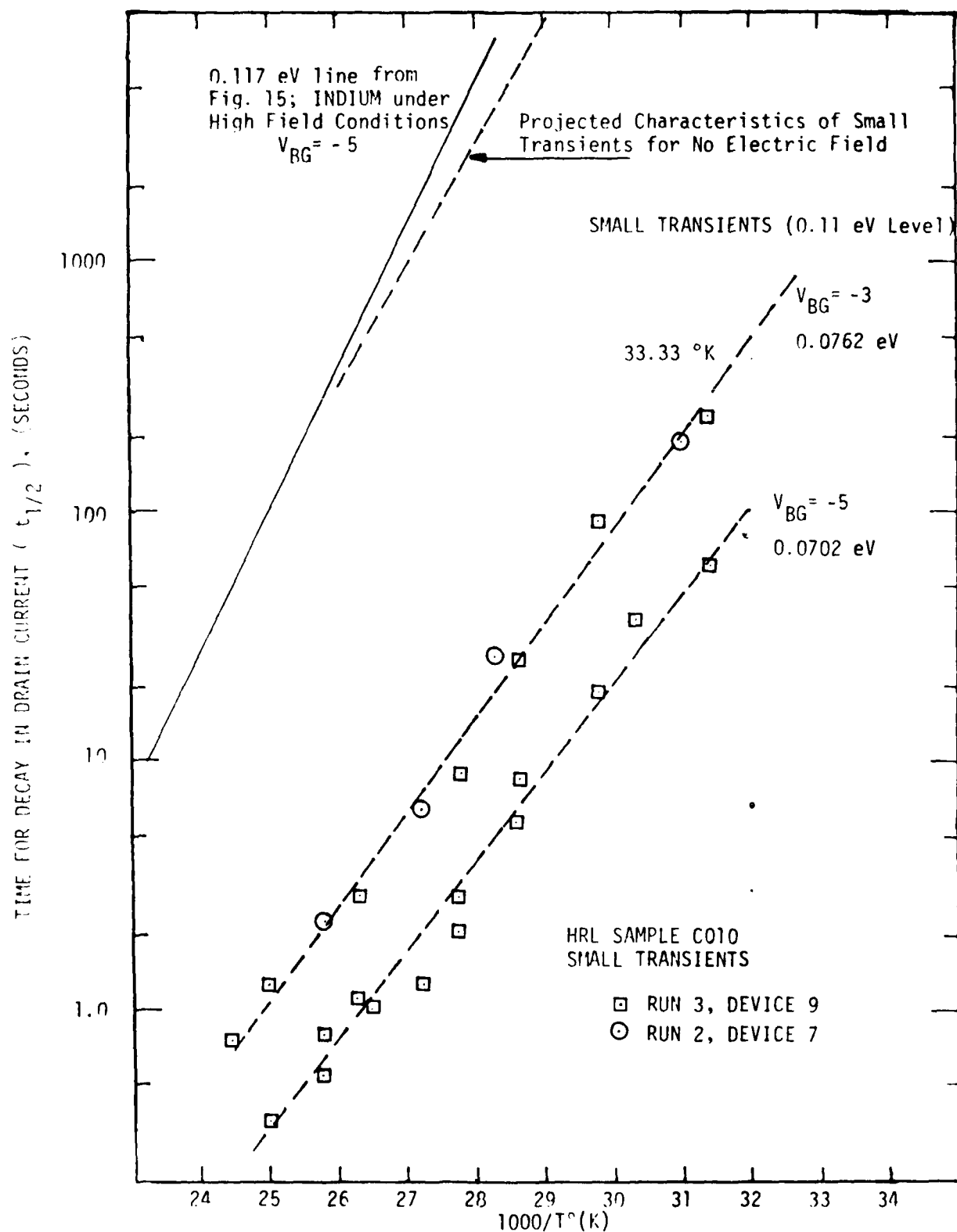Fig. 17 Field Dependence of the Thermal Emission Rate of Indium in Silicon

Fig.18. Details of Small Transient (0.11 eV Level).

the high impedance p-type indium doped material at low temperatures.

High electric fields can exist in the p$^+$, p junction and may result

in an apparent reduction in the ionization energy of the indium center

in the contact region. Possibly, application could be made of this

effect to create voltage tuning of the device response in the

infrared spectrum.

The small transients in Figure 15 which display activation energy

levels of .08eV are shown in detail in Figure 18. These transients

are associated with the 0.11eV level as reported by Hughes Research

Labs [22] after allowing for barrier lowering by the Poole-Frenkel

effect. The results in Figure 18 can be projected back to the zero

field condition. The results obtained indicate the results expected

for thermal hole emission from a 0.11eV energy level with no Poole-

Frenkel effect. Thus, this is strong proof for the existence of the

0.11eV energy level in a silicon sample heavily-doped with indium.

C.   Capture Time Constant of Holes by the Indium Centers

As in the previous section, the time constants of the change

in the indium charge state controls the time constant of the change

in drain current. In this experiment, to observe the hole capture

time constant of the indium centers, the indium centers are initially

in a negative charge state. The application of a short positive going

pulse against a fixed negative backgate bias voltage as depicted in

Figure 19, momentarily decreases the backgate voltage. This allows

the surface depletion region to collapse. The negative indium centers

capture holes from the bulk region in order to maintain charge neutrality.

Thus, the capture of a hole occurs in a region of zero applied electric

field.

If a pulse is very wide, then all of the negative indium centers

will capture holes and become neutral. When the larger backgate bias is reapplied, a large change in drain current followed by hole emission due to thermal decay will result. But if the pulse is very narrow, insufficient time will elapse for the centers to capture holes. Therefore, when the larger bias voltage is reapplied the conductivity will not change. The net effect will be the same as if the pulse had never been applied to the MOSFET. By recording the magnitude of the change in drain current versus pulse width the hole capture time constant at negative indium centers in silicon can be determined. In making these measurements the time between pulses must be long enough to allow the indium center to thermally emit holes. This time should usually be equal to five hole emission time constants at the temperature of measurement.

Note that in Figure 19, the maximum change in drain current for each device is plotted at zero pulsewidth. The plot in Figure 19 is made by finding the narrowest pulse for which the switching current is maximum. Suppose this pulse was found to be 20 μsec at 77°K, then a pulse of 40 μsec would have the same switching current such that the difference between the two switching currents would be approximately zero. Thus, by subtracting the change in current for narrower pulses from the value of maximum switching current, we would obtain δI_{DS} which is plotted in Figure 19 at 77°K.

Example:

$\Delta I_{DS}\text{max} = .6\times10^{-2}$ amps at 77°K for a 20 μsec pulse

$\Delta I_{DS} = .2\times10^{-2}$ amps at 77°K for a 1 μsec pulse

then $\delta I_{DS} = \Delta I_{DS}\text{max} - \Delta I_{DS} = .4\times10^{-2}$ amps for a 1 μsec pulse at 77°K.

$$\text{Time Constant of Capture, } \tau$$
$$\tau = 1/(c_p p + e_p)$$
$$1/e_p = 20\mu sec$$
$$\tau \cong 1/c_p p$$

10^{-2}

log

$\delta I_{DS}(t)$

10^{-3}

(amps)

10^{-4}

■ Device #12 Run #4
▲ Device #14 Run #4
⊙ Device #13 Run #4

0   1   2   3   4   5

Pulse Width (µsec)

-2

-5

Variable   Pulsewidth

V_{DS}

$\delta I_{DS}(t)$
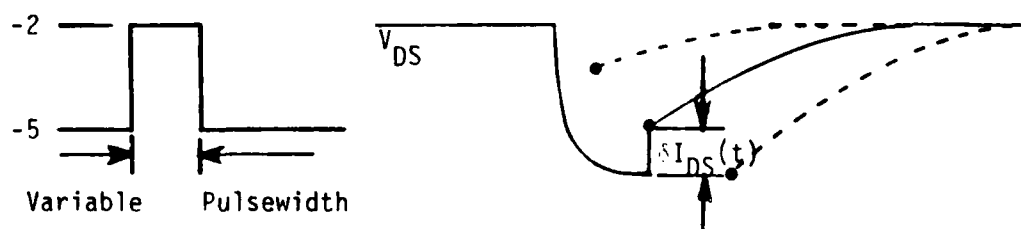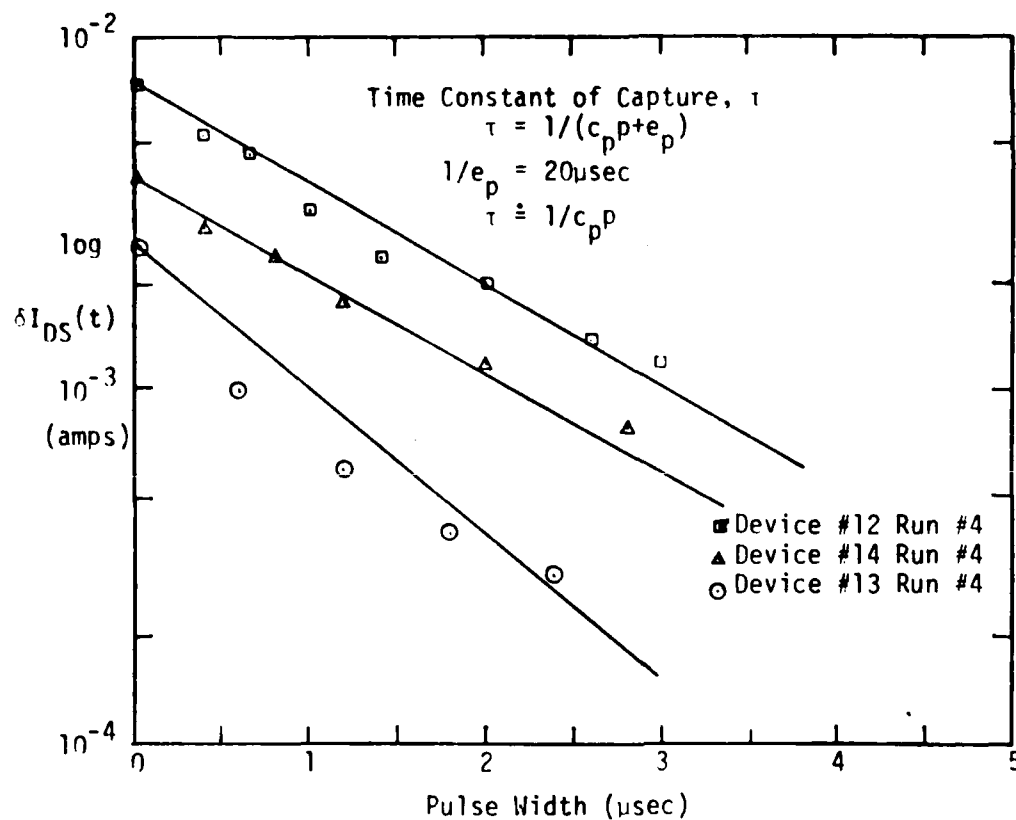
Table II. Capture Experimental Results for HRL Sample C010.

Device # (Run 4)	Hole Concentration At 77°K ($\times 10^{12}/cm^3$)	Time Constant (µsec)	c_{p} ($\times 10^{-7} cm^3/sec$)
14	1.46	1.7	4.03
13	2.16	1.2	3.86
12	1.26	1.7	4.67
6	1.60	3.2	2.20

Fig. 19. Illustration of Determination of the Capture Coefficients and Table of Values.

124

The hole time constant can be determined from the plot in Figure 19 by finding the time at which δI_{DS} has decreased to e^{-1} of its original value obtained for a pulse of zero width. Table II gives a list of the hole time constant for several devices at 77°K.

The relation between the hole capture time constant and the capture cross section c_p, the hole concentration p, and the hole emission rate e_p is

$$\tau_{hole\ capture} = 1/(c_p p + e_p) \ . \tag{41}$$

The hole emission rate must be included since both capture and re-emission can occur in the zero field region. The experiment can be done at temperatures such that $e_p \ll c_p p$ and therefore,

$$\tau \simeq \frac{1}{c_p p} \ . \tag{42}$$

The capture coefficient can be determined since the hole concentration was calculated in section 4.A d. Using our results for the hole concentration c_p is found to be $3.7 \times 10^{-7} cm^3/sec$ at 77°K. Using the Hall data at 77°K for the hole concentration determined by HRL, we found c_p to be $3.2 \times 10^{-7} cm^3/sec$. The most reliable technique previously used to determine c_p has been photoconductive, for which Milnes [21] has tabulated results. Blakesmore obtained a value for c_p of $10. \times 10^{-7} cm^3/sec$ at 77°K in 1956 [21]. Table II gives a value of some of the quantities mentioned for several samples at 77°K. Measurements have been made of the temperature dependence of the hole capture coefficient of negative indium centers. This is shown plotted in Figure 20. The capture time constant and resistance of the sample are measured as function of temperature. The hole concentration in the sample can be calculated as a function of temperature. This can
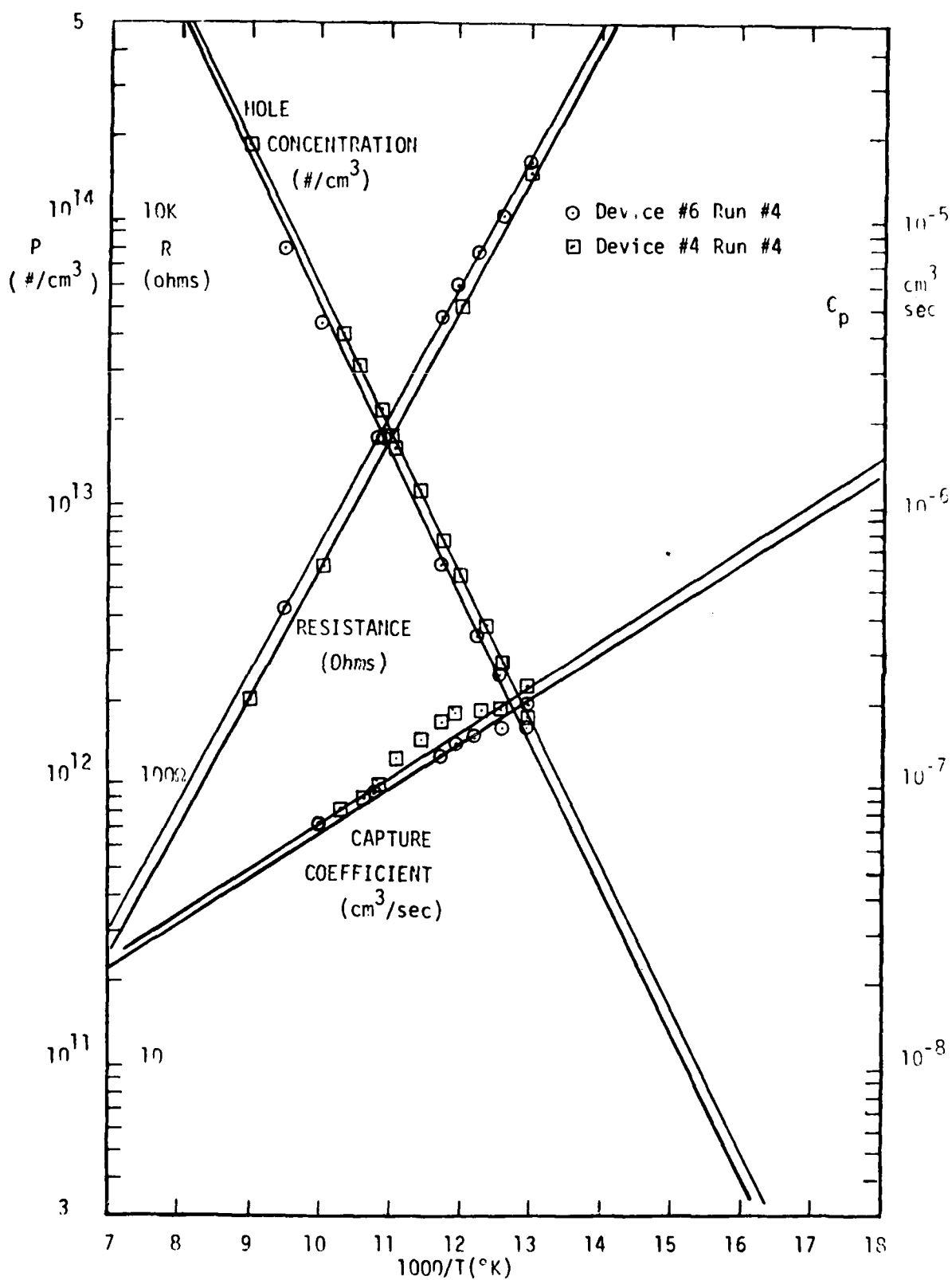
125

Fig. 20. Illustration of the Technique to Determine the Temperature Dependence of Capture Coefficients.

be done from the resistance and the mobility data as explained in section 4.A d. The capture coefficient at different temperatures can be calculated from the hole capture time constant and hole concentration at respective temperatures. Figure 20 demonstrates that the capture coefficient has a T^{-4} temperature dependence corresponding to the theory of cascade capture [3].

D. Capture Time Constant of Holes at "X-Level"

The same technique as applied previously to the indium center to determine the capture coefficient for holes can now be applied to the "x-level". In this case however the temperature must be low enough so that the indium center will not discharge or emit holes and will remain in the neutral charge state.

This is accomplished by operating the device at very low temperatures in the range 30 K to 37 K. The emission rate for holes from indium is very small or the emission time constant very long. Once holes are allowed to come towards the MOSFET channel indium centers will capture these holes and remain essentially neutral for all times of interest and *not interfere* in the observation of emission and capture at the "x-level" in indium doped silicon.

Fig. 21 demonstrates an application of this technique. The hole concentration in the bulk of the sample is determined from the resistance of the photoconductor device structure. The hole concentration is calculated, as in the previous section, by a least square fit of the experimental points. The results have been extrapolated to lower temperatures, as indicated by the broken lines in Fig. 21, where it is impossible to measure the hole concentration. As in the previous section this hole concentration is required in the calculation of the capture coefficient of holes at the x-level.

The experimental procedure is the same as in the previous section. The device is taken to a low temperature of less than 37 K and the "x-level" allowed to emit holes and change to its most negative charge state in the space charge region in the MOSFET device structure, with
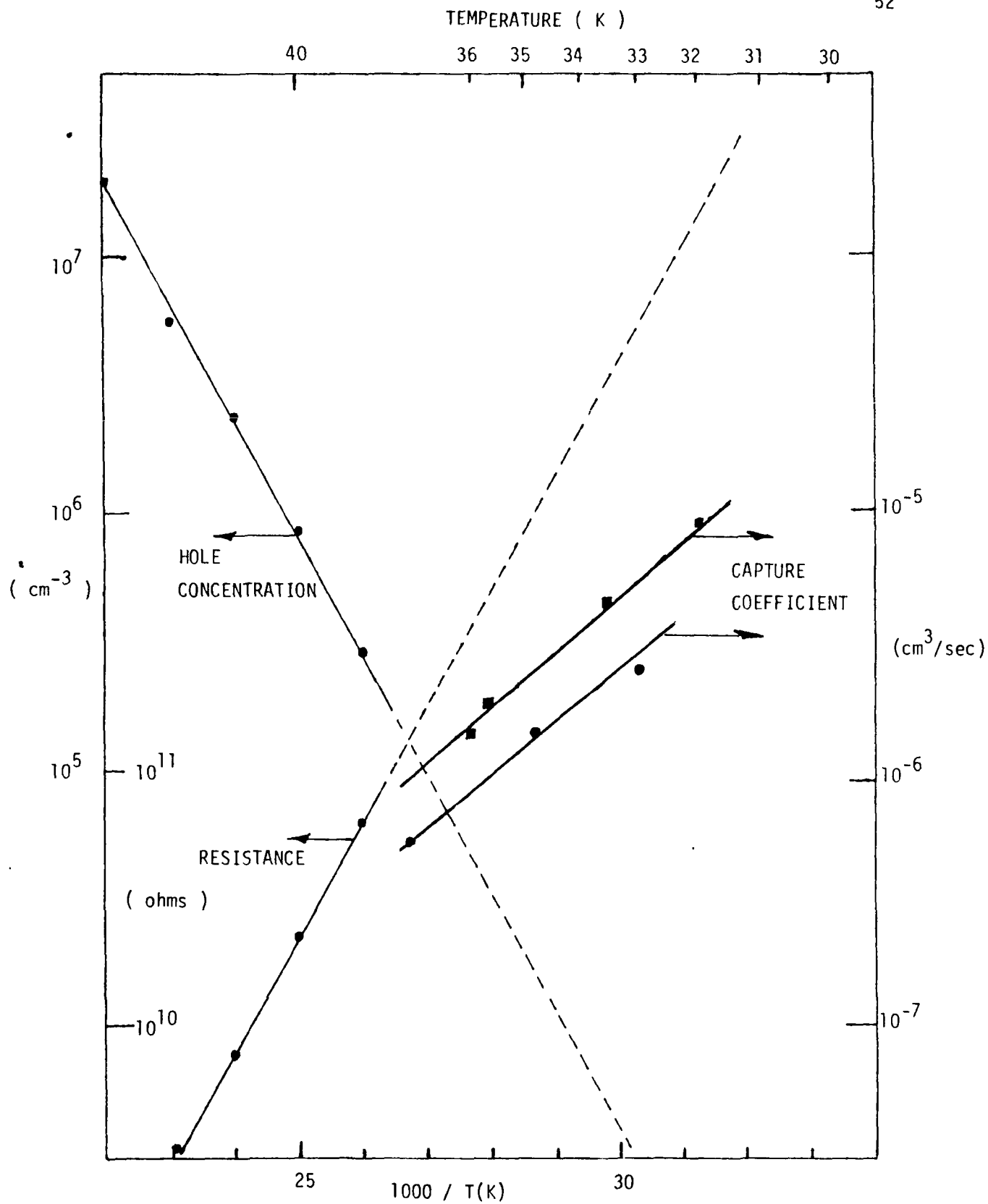
128

Fig. 21. Determination of the Hole Capture Coefficient at the 0.11 eV Level

structure, with a fixed backgate bias of 5 Volts applied. Holes are then allowed to return to the surface region by removing this backgate bias, for different periods of time. Following reapplication of the full backgate bias, one can again observe emission of those holes which have been captured at the "x-level". The magnitude of this latter emission transient is proportional to the number of x-level centers which have captured holes. If the backgate bias is removed for long time periods all of the "x-level" centers will have sufficient time to capture holes. As in the previous section, one can then determine the capture coefficient for holes at the "x-level" in indium doped silicon and this is shown in Fig. 21 as being around $1.5 \times 10^{-6} cm^3/sec$, at 35 K.

In this case however, the hole concentrations in the bulk are very low and the time constants long so that the transients were recorded by an x-y plotter rather then an oscilloscope. In addition, while the time constant associated with the indium center emission are very long at these temperatures the indium concentration is much larger than the "x-level" concentration so at the higher temperatures in this experiment a slight base line drift can be observed due to the emission of holes from the indium centers. The faster transients due to capture and emission at the "x-level" are superimposed upon this base line drift and can be separated from this effect.

The magnitude of the "x-level" capture coefficient or cross section suggests that the "0.11eV-level" is a singly charged acceptor-like center. There may however be other shallower levels associated with this center which this experiment might possibly resolve at lower temperatures but which were not searched for in detail. The measurement

of the capture coefficient for holes at the 0.11eV level in indium-
doped silicon is to our knowledge a new result. This parameter is
of some consideration in determining the frequency response
and responsivity on indium doped silicon photoconductive infrared
detectors as will be shown in the next section.

V. PHOTOCONDUCTOR CHARACTERIZATION

Photoconducting infrared detectors were fabricated in the heavily-doped Silicon:Indium sample C010. Concentrations of indium, .111-eV level acceptors, and excess donors were taken from Table I to be about $1.4 \times 10^{17} \mathrm{cm}^{-3}$, $.51 \times 10^{15} \mathrm{cm}^{-3}$, and $1.01 \times 10^{13} \mathrm{cm}^{-3}$, respectively. The device structure is similar to the bulk resistor shown in Figure 1, except larger.

Dark and irradiated ("ON") resistances were measured versus temperature and an example is shown in Figure 22. The infrared source utilized was a Spectronics SE5751 InSb emitting diode producing infrared emissions of $6 \mu m$ wavelength. We can see from the figure that significant dc photocurrents are not generated until a temperature of about 40°K is reached. Calculated hole concentrations, and hole mobility extrapolated from Figure 13 are also shown in Figure 22. The photon flux per unit area, ϕ, actually exciting the detector and providing the input energy may be estimated as

$$\phi = \frac{c_p (\Delta p)^2}{\sigma_0 N_{TT}} \text{ photons/cm}^2\text{-s} \quad .$$

where c_p is the hole capture coefficient discussed in Section IV-C, and found to be about $3 \times 10^{-7} \mathrm{cm}^3/s$ for Indium; σ_0 is the photoionization cross section, about $10^{-16} \mathrm{cm}^2$; N_{TT} is the total number of Indium centers, about $1.4 \times 10^{17} \mathrm{cm}^{-3}$; and Δp is the change in hole concentration due to incident infrared radiation. We may estimate Δp by examining the "OFF" and "ON resistances at 40°K, for example. At this temperature with no
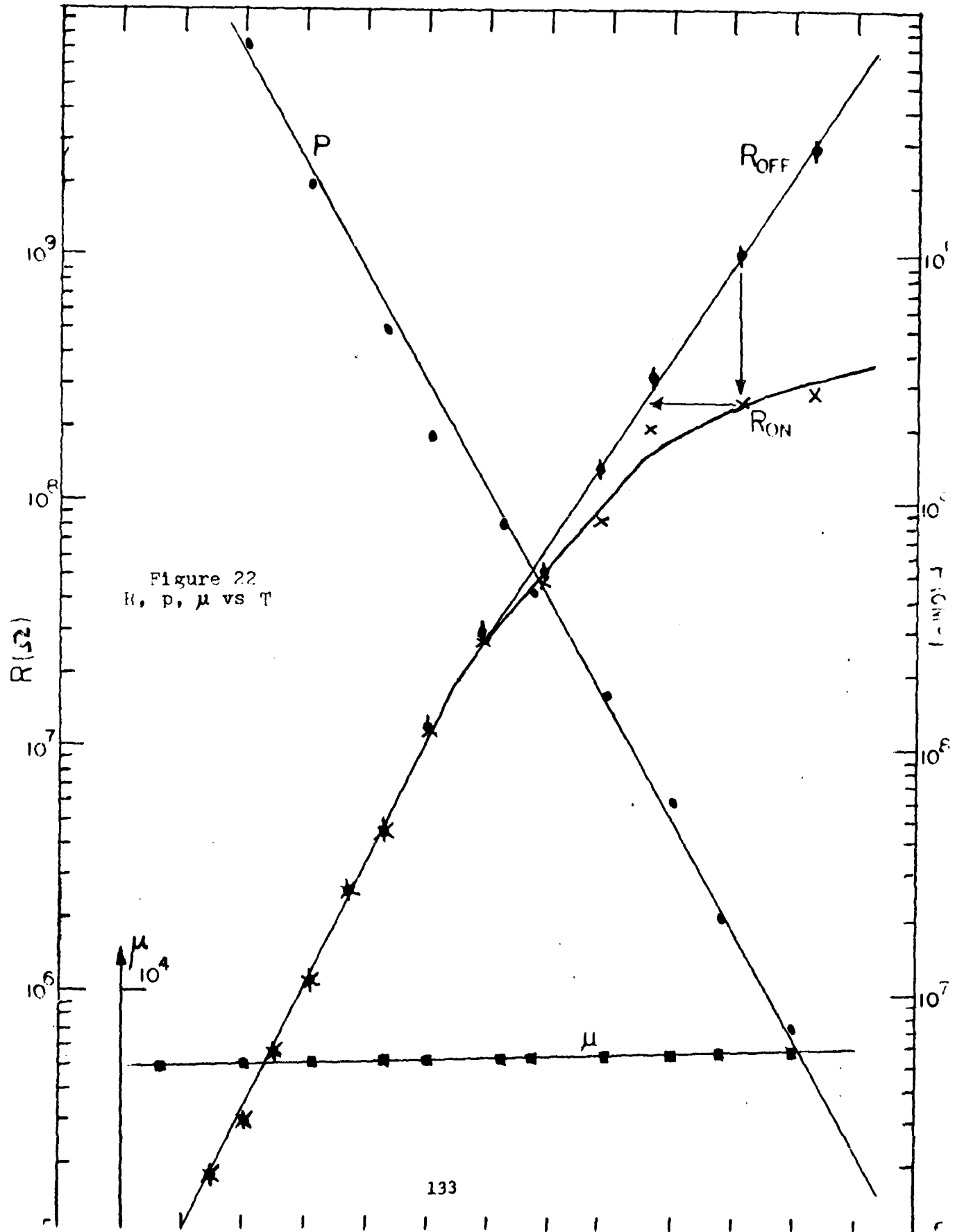
Figure 22
R, p, μ vs T

background flux, we get a hole concentration of about $2 \times 10^7 \text{cm}^{-3}$. With
infrared incident upon the detector we see a reduction in resistance to
a value equivalent to the dark resistance of 42.8°K. Thus, the hole
concentration at 42.8°K with no flux is equal to the hole concentration
at 40°K with the photogeneration of carriers, and $\Delta p \sim 5.9 \times 10^7 \text{cm}^{-3}$.
With these data we estimate ϕ to be $7.33 \times 10^7 \text{photons/cm}^2\text{-s}$.

Responsibility, R_I, may now be estimated

$$R_I = \frac{I\lambda}{\phi Ahc} \frac{A}{W}$$

where λ is the peak wavelength, ϕ is the photon flux per area of detector,
A is the detector area, h is the Planck's constant, c is the velocity of
light, and I is the measured dc current change due to the change in carrier
concentration with the incidence of infrared photons. We obtained a dc
responsivitity of about 30 mA/μw for the data shown.

Frequency domain behavior of these photoconductors was predicted
by examining the dielectric relaxation time constant τ_{RC}, and the time
constant associated with the capture of holes by the indium and .111-eV
level centers τ_p. For dielectric relaxation the RC time constant for the
bulk material is estimated to be

$$\tau_{RC} = RC = \frac{\ell}{pq\mu A} \cdot \frac{\epsilon A}{\ell} = \frac{\epsilon}{pq\mu} \quad .$$

τ_{RC} versus temperature is shown in Figure 23. Hole capture at an indium
or .111-eV center has a characteristic time constant

$$\tau_p = \left(\frac{1}{C_p N_{IONIZED}} \right)_{INDIUM} + \left(\frac{1}{C_p N_{IONIZED}} \right)_{.111-eV} \quad .$$

Capture coefficients for indium and the .111eV levels were shown previously

Figure 23
τ_{RC}, τ_p vs T
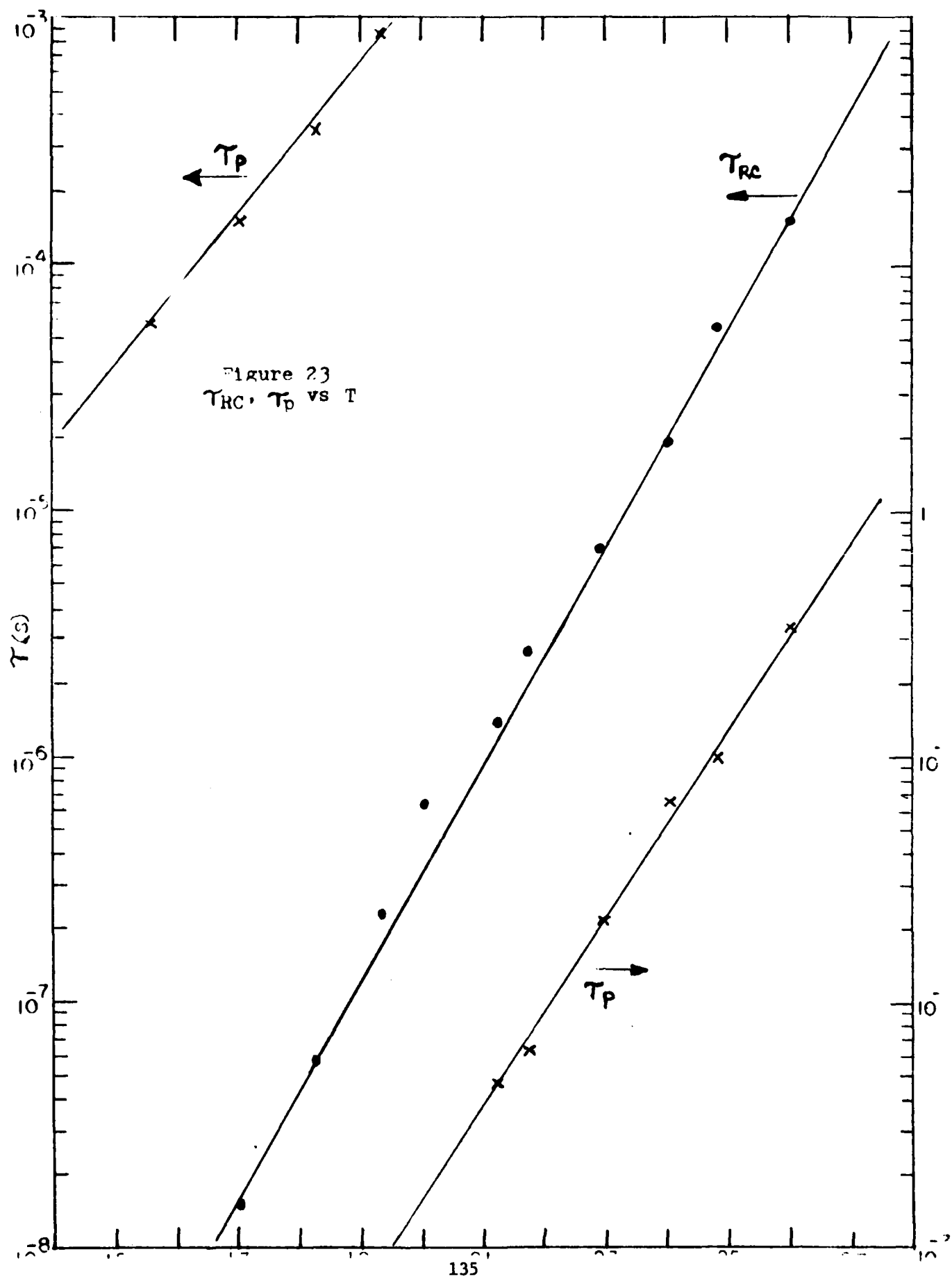
to be about $3 \times 10^{-7} cm^3/s$ for indium and $10^{-6} cm^3/s$ for the .11eV level. The number of centers ionized at any given temperature will be

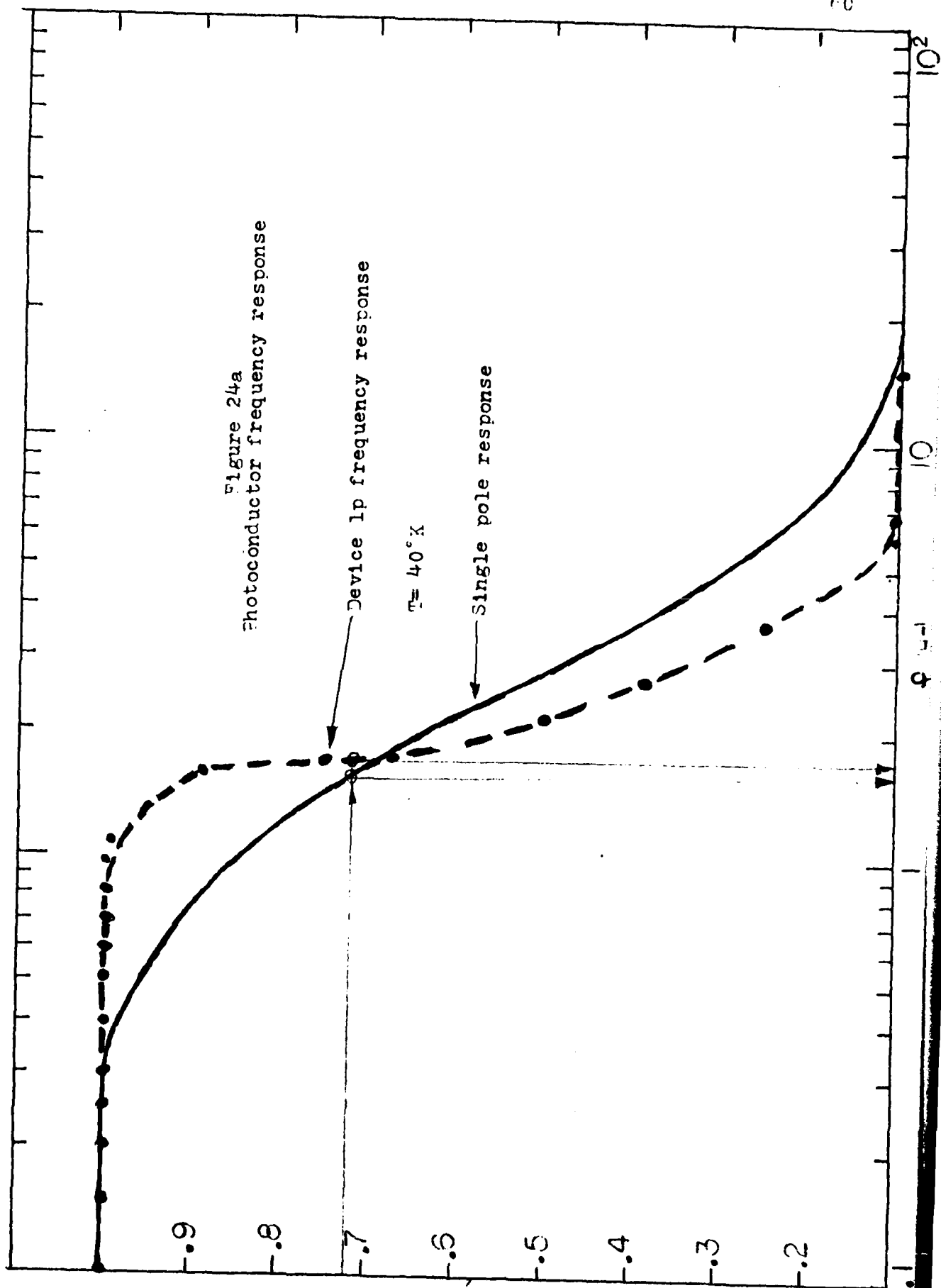$$\frac{N_{IN}}{1 + P(T)\frac{g_{IN}}{N_V(T)}\exp(E_{IN}/kT)} \quad \text{for indium}$$

and

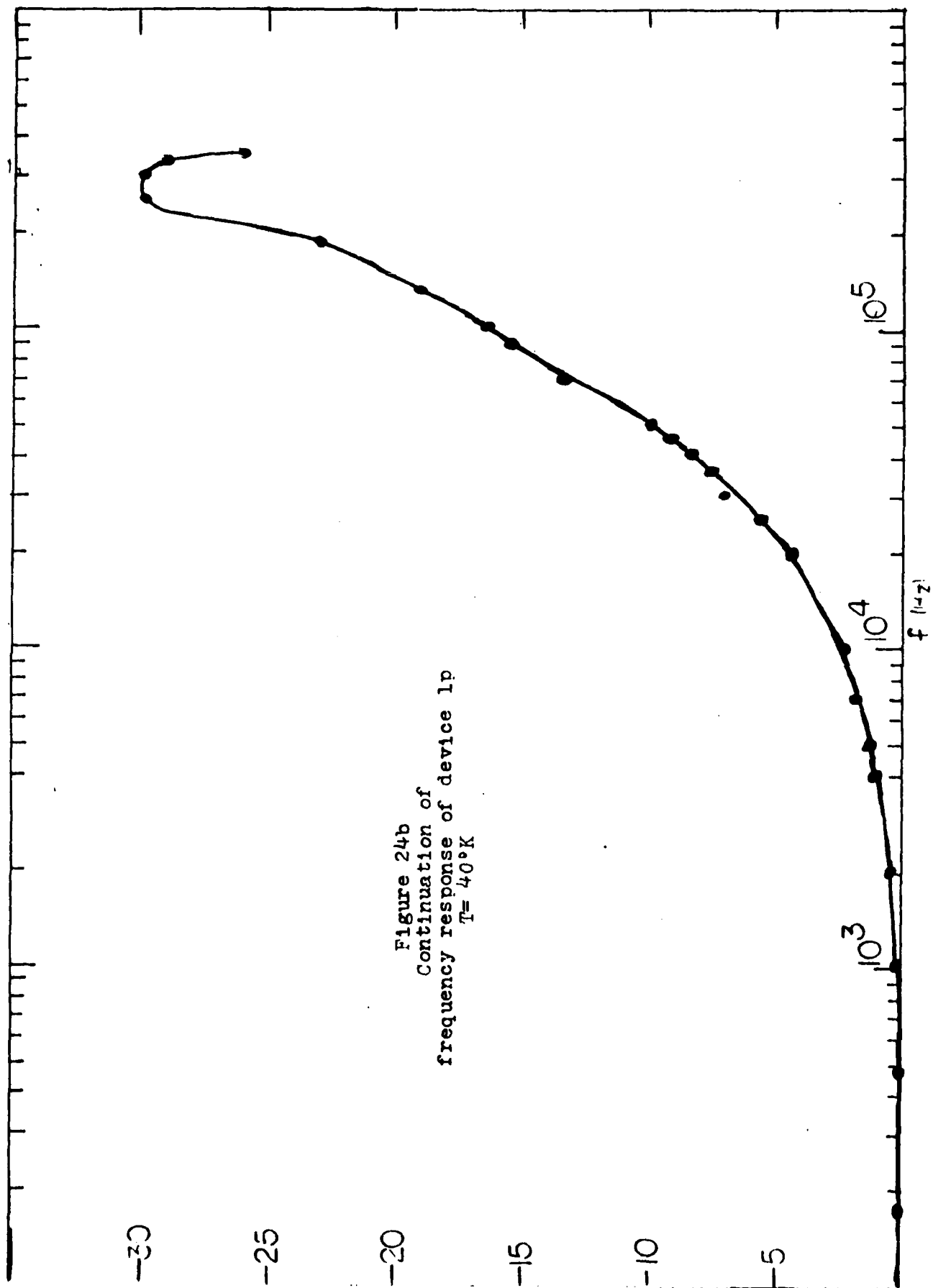$$\frac{N_1}{1 + P(T)\frac{g_1}{N_V(T)}\exp(E_1/kT)} \quad \text{for the .11eV level center.}$$

The function τ_p versus temperature is shown in Figure 23. Comparing these time constants, we see that at 40°K where acceptable dc photoconduction effects are expected, the limiting time constant is $\tau_p = 10^{-1}$ sec. Assuming this to be the dominant effect, a single pole frequency response

$$\left|\frac{I_{OUT}(f)}{I_{OUT}(0)}\right| = \frac{1}{\sqrt{1 + (\tau 2\pi f)^2}}$$

$$= \frac{1}{\sqrt{1 + (.395f^2)}}$$

can also be expected. The expected and actual frequency responses are shown in Figure 24a. Here the expected response's smooth single pole roll-off with a 3-dB cutoff frequency of about 1.6Hz is contrasted by our experimental response's rather sharp roll-off. The cutoff frequency obtained for this photodetector at 40°K is about 1.75Hz.

The detector frequency response is continued on Figure 24b over the interval 100Hz to 3.5K Hz. The increase in response with frequency is thought to be the effect of parasitic capacitive coupling in the circuit wiring within the cold tip.

Figure 24a
Photoconductor frequency response

Device lp frequency response

$T = 40°K$

Single pole response

Figure 24b
Continuation of
frequency response of device 1p
T= 40°K

VI. Conclusions

The MOSFET device has been demonstrated to be a powerful tool for the characterization of imperfection centers in high impedance semiconductor material. The experimental equipment necessary for use with the MOSFET structure is simple and provides data which can be more readily understood than results obtained from previous methods. The relation between the MOSFET conductance and the impurity charge state has been explained.

A detailed study has been made of the thermal emission rate of indium in silicon including both the temperature and field dependence. A unique determination has been made of the relative energy level of indium impurity in silicon. These results have been found to correspond well with previous results by Forbes [13] on a single sample under a single field condition. Evidence has been found to support the existence of the .11eV level of indium-doped silicon as reported by Pines and Baron [29]. These results are on a large number of different samples operated under different conditions. The thermal activation energy was found to be field dependent in correspondence with the Poole-Frenkel effect. As such the majority of these results represent new information which has not been available or reported in the literature.

The capture coefficient has been investigated for the indium centers in silicon and its temperature dependence determined. Experimentally obtained values of the capture coefficient coincides well with the value obtained by Blakesmore [21]. Measurements have also been made of the capture coefficient for holes at the "x-level"

in indium-doped silicon. The MOSFET device structure has been demonstrated to be useful for the determination of capture cross-sections. The application of these techniques using the MOSFET device structure to other impurity centers in semiconductor materials can be easily done.

Application of the results in determining and describing the frequency response of indium-doped silicon photoconductive infrared detectors has been shown.

REFERENCES

1. M.T. Ludwick, Indium, The Indium Corporation of America, 1950.

2. C.T. Sah, "Bulk and Interface Imperfections in Semiconductors,"
    Solid State Electronics, Vol. 19, pp. 975-990, 1976.

3. D.V. Lang, "Deep Level Transient Spectroscopy: A New Method to
    Characterize Traps in Semiconductors," J. Appl. Physics, Vol. 45,
    No. 7, pp. 3023-3032, July 1974.

4. D.V. Lang, "Fast Capacitance Apparatus: Application to ZnO and O
    in GaP p-n Junctions," J. Appl. Physics, Vol. 45, No. 7, pp. 3014-
    3022, July 1974.

5. D.V. Lang and C.H. Henry, "Nonradiative Recombination at Deep
    Levels in GaAs and GaP by Lattice Relaxation Mutiphonon Emission,"
    Phys. Rev. Lett., Vol. 35, pp. 1525-1528, Dec. 1975.

6. K. Nagasawa and M. Schulz, "Fast Transient Capacitance Measurements
    for Implanted Deep Levels in Silicon," Appl. Phys., Vol. 8, pp. 35-
    42, 1975.

7. H. Lefevre and M. Schulz, "Double Correlation Technique (DDLTS) for
    the Analysis of Deep Level Profiles in Semiconductors," Appl. Phys.,
    to be published.

8. M. Schulz, "Determination of Deep Trap Levels in Silicon Using Ion
    Implantation and C V Measurements," Appl. Phys., Vol. 4, pp. 225-
    236, 1974.

9. C.T. Sah, L. Forbes, L.L. Rosier, and A.F. Tasch, "Thermal and
    Optical Emission and Capture Rates and Cross Sections of Electrons
    and Holes from Photo and Dark Junction Current and Capacitance
    Experiments," Solid State Electronics, Vol. 13, pp. 759-788, 1970.

10. A.S. Grove, Physics and Technology of Semiconductor Devices, John
    Wiley and Sons, New York, 1967.

REFERENCES (continued)

11. C.T. Sah, "The Equivalent Circuit Model in Solid State Electronics
    Part I.: The Single Energy Level Defect Centers," Proceedings of
    the IEEE, Vol. 55, No. 5, May 1967.

12. W.C. Parker and L. Forbes, "Experimental Characterization of Gold
    Doped Infrared Sensing MOSFETs," IEEE Trans. on Electron Devices,
    Vol. ED-22, No. 10, pp. 916-924, October 1975.

13. L. Forbes, L.L. Wittmer, and K.W. Loh, "Characteristics of the
    Indium Doped Infrared Sensing MOSFET (IRFET)," IEEE Trans. on
    Electron Devices, Vol. ED-23, No. 12, pp. 1272-1278, Dec. 1976.

14. K.W. Loh, H. Elabd, B.M. Hawkins, and L. Forbes, "Characteristics
    of the Gallium Doped Infrared Sensing MOSFET," IEEE Trans. on
    Electron Devices, Vol. ED-24, No. 8, August 1977.

15. R.N. Hall, W. Schockley, and W.T. Read Jr., "Statistics of Recom-
    binations of Holes and Electrons," Phys. Rev., Vol. 87, pp. 835-
    842, Sept. 1952.

16. R.H. Crawford, MOSFET in Circuit Design, McGraw-Hill Book Company,
    New York, 1967.

17. S.M. Sze, Physics of Semiconductor Devices, Wiley - Interscience,
    New York, 1972.

18. R.S.C. Cobbold, Theory and Applications of Field Effect Transistors,
    John Wiley and Sons, New York, 1970.

19. W.N. Carr, and J.P. Mize, MOS/LSI Design and Application, McGraw-
    Hill, New York, 1972.

20. L. Forbes, J.R. Yeargan, K.W. Loh, W.C. Parker, L.L. Wittmer, H. ELabd,
    and B.M. Hawkins, "Infrared Response of Impurity Doped Silicon MOSFETs
    (IRFETs)," Rome Air Development Center Air Force Systems Command,

REFERENCES (continued)

20. Grissfiss Air Force Base, New York 13441, RADC-TR-76-357, November 1975.

21. A.G. Milnes, Deep Impurities in Semiconductors, John Wiley and Sons, New York, 1973.

22. R. Baron, M.H. Young, K.K. Neeland, O.J. Marsh, "A New Acceptor Level in Indium Doped Silicon," Appl. Phys. Lett., Vol. 30, pp. 594-596, June 1977.

23. B.G. Streetman, Solid State Electronic Devices, Prentice Hall, 1972.

24. W.C. Parker, L.L. Wittmer, J.R. Yeargan, L. Forbes, "Experimental Characterization of the Infrared Response of Gold Doped Silicon MOSFETs (IRFETs)," late newspaper No. 4.8, Int. Electron Dev. Meeting, Washington D.C., Dec. 1974.

25. L.L. Wittmer, W.C. Parker, H. Elabd, K.W. Loh, J.R. Year_an, L. Forbes, "The Infrared Sensing MOSFET," presented as paper 22.5, Int. Electron Dev. Meeting, Washington D.C., Dec. 1975.

26. L. Forbes, R. Brown, M. Shiekholeslam, K.W. Current, "Application of the MOSFET Device Structure in Characterizing Imprefection Centers in Indium Doped Silicon," submitted.

27. J.L. Hartke, "The Three Dimensional Poole-Frenkel Effect," J. Appl. Phys., Vol. 39, pp. 4871-4873, 1968.

28. P.U. Calzolari, S. Graffi, C. Morandi, "Field-Enhanced Carrier Generation in MOS Capacitors," Solid State Electronics, Vol. 17, pp. 1001-101i, 1974.

29. M.Y. Pines, R. Baron, "Characteristics of Indium Doped Silicon Infrared Detectors," Proc. Int. Electron Dev. Meeting, 446, Washington D.C., 1974.

REFERENCES (continued)

30. D.K. Schroder, T.T. Braggins, H.M. Hobgood, "The Doping Concentrations of Indium-Doped Silicon Measured by Hall, C-V and Junction Breakdown Techniques," Westinghouse Research and Development Center, Pittsburg, PA 15235, 1977.